The University of Nottingham

UNITED KINGDOM · CHINA · MALAYSIA

MECHANISMS OF SOOT TRANSFER TO OIL OF AN HPCR DIESEL ENGINE

Gianluca Di Liberto

Thesis submitted to the University of Nottingham

for the degree of Doctor of Philosophy

October 2016

Abstract

High levels of soot-in-oil can cause an increase in engine wear and oil viscosity, thus reducing oil drain intervals. The mechanisms by which soot particles are entrained into the bulk oil are not well understood. The research reported in this thesis addresses questions on the mechanisms of soot transfer to the lubricating oil in light-duty diesel engines with high pressure EGR systems. Deposition as a result of blow-by gas passing the piston ring pack and by absorption to the oil film on the cylinder liner via thermophoresis are soot transfer mechanisms that have been considered in detail. The investigations are based on analytical and simulation studies, and results based on complementary experimental studies are used to validate these.

The experimental investigations aimed at evaluating the typical rate of accumulation and size distribution of soot agglomerates in oil. The oil samples analysed were collected during regular services from light-duty diesel engine vehicles. These were representative of vehicles meeting Euro IV and V emission regulation standards driven under real-world conditions. The rate of soot-in-oil was determined by thermogravimetric analysis and results showed a concentration of approximately 1 wt% of soot-in-oil after 15,000 km. The particle size distribution was determined using a novel technique, Nanoparticle Tracking Analysis (NTA), applied for the first time to soot-laden oil samples by the author [1, 2]. Results showed an average particle size distribution of 150 nm, irrespective of oil drain interval. Almost the totality of the particles were between 70 and 400 nm, with micro particles not detected in any of the samples analysed. For the samples investigated in this work, the Euro standard did not influence either the rate of soot deposition or the particles size distribution. To the author's best knowledge, this is the first time that rate of soot deposition and particles size distribution from oil samples collected from vehicles of different Euro standard driven under real-world conditions are analysed and compared.

Exhaust Gas Recirculation (EGR) is a common technique used in diesel engines in order to reduce NO_x emissions. However, it has the drawback that it increases the production of soot. In this work, particular attention has been given to its effects on the rate of soot deposition in oil. Both its influence on the soot produced during the combustion process and on the soot re-introduced in the combustion chamber by the EGR gas has been investigated through CFD simulations using Kiva-3V. Examining the relative importance of near–surface transport of soot by thermophoresis to the oil film on the liner and from blow-by gases to surfaces in the ring pack shows the former to be the dominant mechanism of soot transfer. EGR increases the rate of deposition of soot on the liner not only by increasing net production of soot, but also through the re-cycled particles. At EGR levels higher than 20%, the contribution of the Re-cycled soot becomes the major source for soot-in-oil.

The study of soot deposition was evaluated during the entire engine cycle, including compression stroke and post-Exhaust Valve Opening (EVO) period. Existing deposition models found in the literature typically limit the domain to only from the Start of Injection (SOI) to (EVO) period [3-5]. Results from this thesis indicated that compression stroke and post-EVO period can contribute up to 30% of the total rate of soot deposition into oil.

List of Publications Resulting from this Work

- Di Liberto, G., La Rocca, A., Shayler, P., *Computational Analysis of the Influence of Exhaust Gas Recirculation on the Rate of Soot Transfer to Lubricating Engine Oil.* Fisita World Automotive Congress, Busan, Korea, September 2016.
- La Rocca, A., Campbell, J., Di Liberto, G., Fay, M. W., *Electron Tomography of Carbon Generated Nanoparticles.* 19th ETH- Conference on Combustion Generated Nanoparticles, ETH Zentrum, Zurich, Switzerland, 2015.
- La Rocca, A., Di Liberto, G., Shayler, P., Parmenter, C. D. J., Fay, M. W., *Application of Nanoparticle Tracking Analysis Platform for the Measurement of Soot-in-Oil Agglomerates from Automotive Engines.* Tribology International, 2014. 70: p.142-147.
- La Rocca, A., Di Liberto, G., Shayler, P., Parmenter, C. D. J., Fay, M. W., *A Novel Diagnostic Tool for Measuring Soot Agglomerates Size Distribution in Used Automotive Engine Oils.* SAE Int. J. Fuels Lubr., 2014. 7(1): p.301-306.
- La Rocca, A., Di Liberto, G., Shayler, P., Fay, M. W., *The Nanostructure of Soot-in-Oil Particles and Agglomerates from an Automotive Diesel Engine.* Tribology International, 2013. 61: p.80-87

Contents

Acknowledgements

Firstly, I would like to thank Professor Paul Shayler, Head of the Engines Research Group at the University of Nottingham for his support and patience throughout my PhD. I am also extremely grateful to Dr Antonino La Rocca, who has been much more than just my supervisor. I would not be in the position I am today without his guidance throughout the past four years.

I would also like to thank all the colleagues and members of staff I have met during this period for all the encouragements and support I received from each of them. My special thanks go to James, Rich and Yousuf who over the past four years became more than just colleagues.

I wish to acknowledge the financial support I have received through the Vice-Chancellor's Scholarship for Research Excellence provided by The University of Nottingham.

I am indebted to my grandmother, Mario and Nadia, for giving me the courage and opportunity to be here writing these acknowledgments. To my parents and my brother who always encouraged me throughout my life and academic career, I am simply lucky to have you. Finally, to my Maria who has shared with me every single day of this long path. I am sure that without her love, patience, support, and much more, this work would have never came to an end.

Abbreviations

AFR	Air Fuel Ratio
ASOI	After Start of Injection
ATDC	After Top Dead Centre
BDC	Bottom Dead Centre
BMEP	Brake Mean Effective Pressure
BTDC	Before Top Dead Centre
CA	Crank Angle
CCD	Charge-Coupled Device
CFD	Computational Fluid Dynamics
CI	Compression Ignition
CO	Carbon Monoxide
CO_2	Carbon Dioxide
CR	Compression Ratio
DC	Direct Current
DI	Direct Injection
DLS	Dynamic Light Scattering
DOC	Diesel Oxidation Catalyst
DPF	Diesel Particulate Filter
EC	Elemental Carbon

EGR	Exhaust Gas Recirculation
EVO	Exhaust Valve Opening
FTIR	Fourier Transform Infrared Spectroscopy
GDI	Gasoline Direct Injection
HC	Unburned Hydrocarbons
HPCR	High Pressure Common Rail
HP-EGR	High Pressure EGR
ID	Ignition Delay
IDI	In-Direct Injection
IMEP	Indicated Mean Effective Pressure
IVC	Inlet Valve Closing
IVO	Inlet Valve Opening
LNT	Lean NO_x Trap
LP-EGR	Low Pressure EGR
LRP	Lower Reference Point
MAF	Mass Air Flow
MOFT	Minimum Oil Film Thickness
NEDC	New European Drive Cycle
NO_x	Oxides of Nitrogen
NSC	Nagle and Strickland-Constable
NTA	Nanoparticle Tracking Analysis
OCR	Oil Control Ring

PAH	Poly-Aromatic Hydrocarbons
PFI	Port Fuel Injection
PM	Particulate Matter
PN	Particle Number
SCR	Selective Catalytic Reduction
SEM	Scanning Electron Microscopy
SOF	Soluble Organic Fraction
SOI	Start of Injection
StD	Standard Deviation
TAB	Taylor-Analogy Breakup
TCR	Top Compression Ring
TDC	Top Dead Centre
TEM	Transmission Electron Microscopy
TGA	Thermogravimetric Analysis
TWC	Three-Way Catalyst
URP	Upper Reference Point
VGT	Variable Geometry Turbocharger
ZDDP	Zinc DialkylDithioPhosphate

Nomenclature

γ	Ratio of specific heat capacities	[-]
λ	Gas mean free path	[m]
ν	Kinematic viscosity of the gas	[m^2/s]
μ	Dynamic viscosity of the gas	[Pa·s]
ϕ	Fuel-air equivalent ratio	[-]
ϱ_{cyl}	Spatial-averaged in-cylinder soot concentration	[g/cm^3]
ϱ_{liner}	Soot concentration at near-liner region	[g/cm^3]
ρ_g	Gas density	[kg/m^3]
ρ_{OH}	Concentration of OH	[kg/m^3]
ρ_s	Soot particle density	[kg/m^3]
τ_p	Particle relaxation time	[s]
A	Heat transfer surface	[m^2]
A_f	Calibration factor for soot formation model	[-]
A_O	Piston ring gap area	[m^2]
A_{O2}	Calibration factor for soot O_2 oxidation model	[-]
A_{OH}	Calibration factor for soot OH oxidation model	[-]
a	Crank radius	[m]
C_c	Cunningham slip correction factor	[-]
Cd	Discharge coefficient	[-]
C_m	Momentum exchange coefficient	[-]
C_s	Thermal slip coefficient	[-]

C_t	Temperature jump coefficient	[-]
D10	Tenth percentile	[m]
D90	Ninetieth Percentile	[m]
D	Diffusion Coefficient	[m^2/s]
D_h	Hydrodynamic Diameter	[m]
D_{max}	Maximum soot-in-oil particle size from NTA	[m]
D_{min}	Minimum soot-in-oil particle size from NTA	[m]
D_p	Soot particle diameter	[m]
$\frac{dm_{sf}}{dt}$	Rate of soot formation	[g/s]
$\frac{dm_{so}}{dt}$	Rate of soot oxidation	[g/s]
$\frac{dm_s}{dt}$	Rate of soot production	[g/s]
ds	Piston displacement every 1° crank angle	[m]
dt	Time step	[s]
dT/dy	Temperature gradient normal to the surface	[K/m]
E_{sf}	Reaction activation energy for soot formation	[J/mol]
F_d	Drag Force	[N]
F_{th}	Thermophoretic force	[N]
f_{exp}	Fraction of liner contributing to soot-in-oil build up	[-]
f_{BB}	Fraction of blow-by	[-]
f_{swept}	Fraction of liner-border CFD cell involved with thermophoresis	[-]
hc	Convective heat transfer coefficient	[W/(m^2·K)]
K_A	Oxidation model constant	[g/(cm^2·s·atm)]

K_B	Oxidation model constant	[g/(cm^2·s·atm)]
K_b	Boltzmann Constant	[m^2 · kg/(s^2· K)]
Kn	Knudsen number	[-]
K_T	Oxidation model constant	[g/(cm^2·s)]
K_{th}	Thermophoretic constant	[-]
K_Z	Oxidation model constant	[atm^{-1}]
k_g	Thermal conductivity of air	[W/(m K)]
k_p	Thermal conductivity of soot	[W/(m K)]
L	Stroke length	[m]
$L_{p\infty}$	Particle stopping distance	[m]
L_{th}	Distance travelled by the particle at the thermophoretic velocity	[m]
l	Connecting rod length	[m]
Mc	Molecular weight of carbon atom	[g/mol]
M_{fv}	Fuel vapour mass	[g]
M_{OH}	Molecular weight of OH	[g/mol]
$\dot{m}_a$	Mass of air inducted	[g/h]
$\dot{m}_{BB}$	Mass flow rate of blow-by gas	[g/h]
m_{EGR}	Mass of exhaust gas recirculated	[g/h]
$m_{exh\_blowdown}$	Mass of charge exhausted during blowdown	[g]
$\dot{m}_f$	Rate of mass of fuel injected	[g/h]
$\dot{m}_i$	Rate of mass of in-cylinder charge inducted	[g/h]
$m_{i,BDC}$	Mass of in-cylinder charge at the end of the expansion stroke	[g]

$m_{i,TDC}$	Mass of in-cylinder charge at the end of the exhaust stroke	[g]
$m_{oil\ sump}$	Mass of lubricating oil in oil sump	[g]
m_s	Net amount of soot	[g]
$m_{s,BB}$	Mass of soot entering the piston ring pack	[g]
$m_{s,bottom}$	Net amount of soot near the piston head-liner corner	[g]
$m_{s,dep@lin}$	Soot deposited via thermophoresis contributing to soot-in-oil	[g]
$m_{s,EGR}$	Mass of soot re-cycled with EGR	[g]
$m_{s,EGR@liner}$	Mass of Re-cycled soot near the cylinder liner	[g]
$m_{s@EVO}$	Amount of in-cylinder soot at EVO	[g]
$m_{s,lin}$	Amount of soot deposited on the oil film at the cylinder liner	[g]
$m_{s@liner}$	Net amount of soot near the cylinder liner	[g]
$m_{sInc@liner}$	Mass of In-cycle soot near the cylinder liner	[g]
$m_{s,TGA}$	Mass of soot estimated from TGA	[g]
m_{TDC}	Mass of charge at end of exhaust stroke	[g]
N	Engine speed	[rpm]
N_A	Avogadro's number	[mol^{-1}]
p	Gas pressure	[Pa]
$p_{@EVO}$	In-cylinder gas pressure at EVO	[Pa]
p_{exh}	Gas pressure in exhaust manifold	[Pa]
p_O	Downstream pressure	[Pa]
p_{O2}	Oxygen partial pressure	[atm]
p_u	Upstream pressure	[Pa]
$\dot{Q}_w$	Heat flux through cylinder walls	[W]

R	Universal gas constant	[J/(mol·K)]
R_g	Specific gas constant	[J/(kg·K)]
$\dot{R}_{NSC}$	Net reaction O_2 oxidation rate	[g-atom/(s·cm^2)]
$\dot{R}_{OH}$	Net reaction OH oxidation rate	[g-atom/(s·cm^2)]
$\bar{S}_p$	Average piston velocity	[m/s]
S_p	Instantaneous piston velocity	[m/s]
T_g	Gas temperature	[K]
T_0	Mean gas temperature in the vicinity of the particle	[K]
T_w	Cylinder liner temperature	[K]
U_{th}	Thermophoretic deposition velocity	[m/s]
$u_{p(0)}$	Initial particle velocity	[m/s]
$u_{p(t)}$	Instantaneous particle velocity	[m/s]
V_{BDC}	In-cylinder volume at BDC	[m^3]
V_{cyl}	In-cylinder volume	[m^3]
V_{lin}	Near-wall liner volume considered by the CFD	[m^3]
V_{swept}	Swept volume due to thermophoretic effect	[m^3]
V_{TDC}	In-cylinder volume at TDC	[m^3]
wt%	Percentage in mass of soot from TGA	[%]
x	Fraction of carbon surface covered by a more reactive type	[-]

1 Introduction

1.1 Introduction

The Particulate Matter (PM) produced by the combustion process in a diesel engine is mainly carbon soot. Most of this soot is expelled from the cylinder with the exhaust gas, but a small proportion is transferred to the lubricating oil. The amount of particles in oil is not restricted by any standards, but as soot builds-up it degrades the performance of the lubricating system, accelerating engine wear and increasing oil viscosity and friction [6-8]. Soot-in-oil also has an indirect effect on CO_2 emissions, as adulteration of the oil worsens fuel economy. Although these consequences are well recognised, there is a lack of understanding in how soot transfer takes place and what factors influence this.

This thesis addresses the need for a better understanding and prediction of soot-in-oil deposition on light-duty diesel engines, via a combination of computational and analytical tools. Specifically, the pathways from combustion system to bulk oil have been investigated. The questions considered include how soot production and distribution depend on engine running conditions and the mechanisms of near-surface movement of soot particles into the oil film by thermophoresis. These have been addressed by evaluating the effects of engine load and speed and Exhaust Gas Recirculation (EGR) levels on the rate of soot deposition. The effect of EGR on soot-in-oil deposition has been taken into account not only by studying its influence on the soot particles produced during the combustion process (In-cycle source of soot), but also by considering the soot recirculated with the EGR gas in the combustion chamber (Re-cycled source of soot). The two sources were considered as two independent sources so that their relative importance on deposition could be investigated.

Soot production and distribution in the regions of interest for soot-in-oil have been investigated computationally by employing Computational Fluid Dynamic (CFD) code and post-processing computational results. The rate at which these particles are transferred into oil has been studied analytically by applying the thermophoretic model proposed by Talbot et al. [9]. Its application was extended to the entire engine cycle, including also periods typically considered of no interest for deposition into oil such as compression stroke and post-Exhaust Valve Opening (EVO) period.

Together with the computational and analytical works, experimental investigations on fifteen diesel engine oil samples collected at the oil change service interval have been conducted. Techniques to measure soot-in-oil particle size distribution and concentration are described and applied to the fifteen oil samples. The former is measured by using Nanoparticle Tracking Analysis (NTA), a novel technique applied for the first time by the author [1, 2] to soot-laden oil samples. Particle size results from NTA are used as input data for the soot deposition model via thermophoresis discussed in Chapter 5. The concentration of soot-in-oil is determined by using Thermogravimetric Analysis (TGA). Results are used to provide a typical rate of deposition range for light-duty diesel engines. The ambition is to compare this experimental-derived rate of deposition with those obtained from the deposition model presented in this work. This is of particular importance as a direct validation of the proposed soot-in-oil deposition model was not possible as the diesel engine used as a model for the CFD simulations was not available at the time of the investigation.

1.2 Background

1.2.1 Soot Particles in Diesel Engines

Through most of the 20th century, diesel engines were predominantly used in heavy-duty vehicles, marine and power generation applications. Only a small proportion of light-duty vehicles had diesel engines. Since the adoption of technologies such as common rail fuel injection, turbocharging, alongside

economic and political factors there has been a dramatic increase in the market share of diesel vehicle light-duty sales. In 2011, as shown in Figure 1.1, the market share of diesel cars in the UK exceeded that of gasoline vehicles for the first time [10].

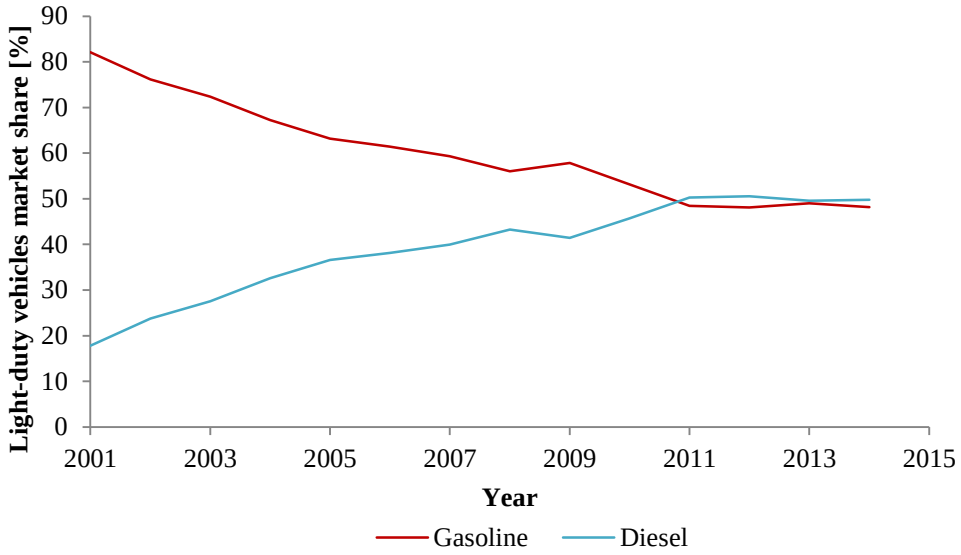

Figure 1.1: Percentage of market share for gasoline and diesel light-duty engines in the UK [10].

Diesel engines compared to gasoline engines produce less CO_2 as a direct result of lower fuel consumption due to typically higher efficiency for the same output power. However, they produce higher amounts of NO_x and PM. The legislative definition of PM is everything that may be trapped when exhaust gases are passed through a filter. As shown in

Figure 1.2, PM can be divided into *soluble* and *insoluble*, depending on their ability or not to evaporate upon heating or to dissolve in specific solvents. The soluble particulates can be further divided into sulphates, nitrates and Organic (SOF) fractions. Typically 15 to 30 mass percentage of PM is soluble [11]. The insoluble fraction consists of carbonaceous material, here referred as soot, and ash. The correct term for soot is carbonaceous material rather than carbon black or Elemental Carbon (EC) as sometimes confused in literature. This emphasises the fact that although carbon is its main constituent, other elements such as hydrogen, oxygen and nitrogen may be present in the particle [12]. With ash contributing for

approximately 1 percent in mass of total PM, soot particles in diesel engines are the larger contributors of PM [13].

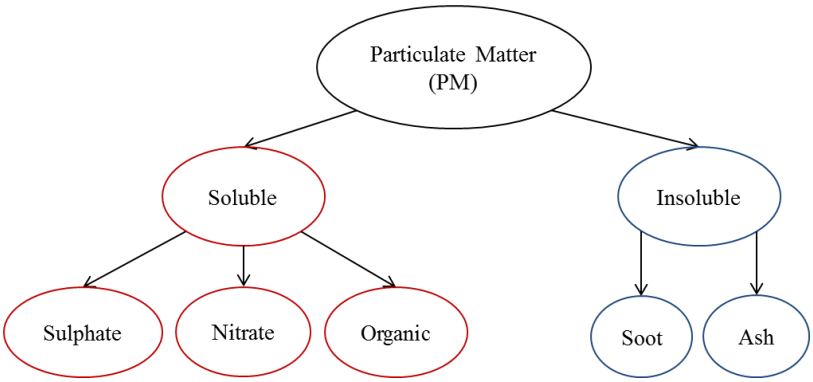

Figure 1.2: Schematic for Particulate Matter composition [13].

Diesel engines, compared to Port Fuel Injection (PFI) gasoline engines, are more prone to produce soot due to the differences in the combustion process. In diesel or Compression Ignition engines (CI), fuel is injected in the combustion chamber at the end of the compression around Top Dead Centre (TDC), finding the in-cylinder charge at high temperature and pressure. Despite the global fuel-air lean composition, due to the short time available for the fuel and air to mix together, the charge is heterogeneous with some regions experiencing a lack of oxygen. The local absence of oxygen and high gas temperature and pressure cause pyrolysis reactions which break down the fuel molecules into soot precursors. These precursors undergo nucleation in which the first nuclei of soot are formed, followed by surface growth and particle growth. A detailed description of the soot formation and oxidation processes is given in Chapter 2.

In PFI gasoline engines, the fuel is mixed with air prior to induction, leading to a much more homogeneous fuel-air stoichiometric mixture, which limits the formation of fuel rich areas during the combustion process. Furthermore, the ignition process is aided by the spark plug and therefore, temperatures and pressures at the end of the compression stroke are not as high as in CI engines where the combustion starts via autoignition. Recently, in order to improve the overall efficiency of gasoline-powered vehicles, engines with Direct Injection (GDI) have been introduced on the market. As the injection process occurs

directly within the combustion chamber, the time available for fuel evaporation and mixing with the in-cylinder charge is reduced. This, similarly to what happens with diesel engines, can lead to local fuel-rich areas promoting the formation of soot particles [14, 15].

1.2.2 Tailpipe Emission levels and Soot-in-Oil

The development of light-duty diesel engines is mainly driven by the emission standards, such as the current Euro VI in Europe and the Tier 2 in the United States of America. In Figure 1.3 the evolution from Euro I to VI of PM and NO_x emissions level is illustrated. Over the past 20 years the allowable levels of PM and NO_x have been reduced by over 90%. With the Euro 5b standard, a limit to Particle Number (PN) of $6 \cdot 10^{11}$ particles/km has been further introduced. As diesel engines run with lean air-to-fuel ratios, the emissions of Hydrocarbon (HC) and Carbon Monoxide (CO) are typically very low [16]. It is important to highlight that the emission limits do not refer to engine-out values, but to tailpipe amounts. Moreover, as PM values refer to both the soluble and insoluble fractions, its reduction can be achieved also by only reducing the amount of soluble particulate matter via the use of a Diesel Oxidation Catalyst (DOC), without reducing the amount of soot. These two aspects are of importance for the concentration of soot-in-oil, as this is mainly governed by the amount and distribution of soot inside the cylinder, which can strongly differ from tailpipe values. This implies that the trend in PM emissions over the past decades reported in Figure 1.3 could significantly differ from that of soot-in-oil concentration. This, as it will be discussed in Chapter 3 from the TGA results, is confirmed by the similar values of soot-it-oil concentrations in diesel engines meeting Euro IV and V legislations, despite the large reduction achieved in tailpipe emissions.

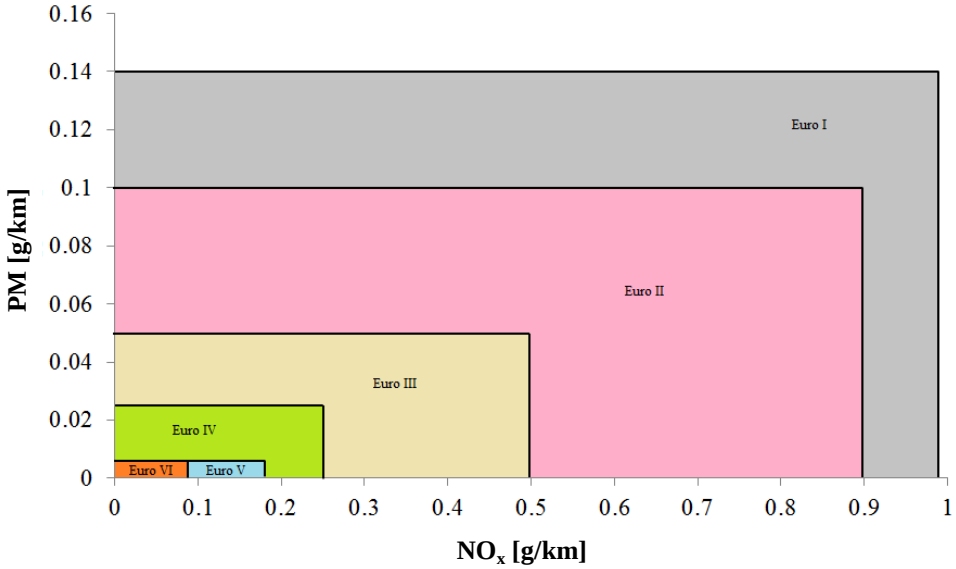

Figure 1.3: Euro Stage Limits for PM and NO_x emissions [17].

Throughout Euro I to VI, two different approaches to control PM and NO_x emissions have been followed: in-cylinder control and after-treatment systems. The Euro I and II standards led to the shift from mechanical to electromechanical injection and to the introduction of the DOC after-treatment system for limiting HC emissions and the typical diesel odour produced by the sulphur fuel component. PM limits were, therefore, obtained via reduction of the soluble fraction. As the combustion in CI engines is lean, the use of a Three-Way Catalyst (TWC) technology for reducing NO_x as in gasoline engines is precluded due to the excess of oxygen in the exhaust stream [11]. The main challenge of reducing NO_x emissions through in-cylinder control, without the use of a TWC, gives rise to the typical trade-off between NO_x and soot particles [11].

Euro III engines have seen the shift from In-Direct Injection (IDI) to Direct Injection (DI), allowing for lower fuel consumption and better mixture preparation [18]. They were also characterised by the introduction of high pressure electronic-controlled fuel injection systems, with pressures up to 1,300 bar. This allowed a better fuel atomisation and air-fuel mixing, reducing PM emissions, including the soot fraction. The introduction of High Pressure Common Rail (HPCR) systems also facilitates finer control and more complex injection strategies compared to cam-controlled injectors, with the possibility of

shifting from single to multiple injections. For example, post-injection allowed lowering in-cylinder gas peak temperature, reducing NO_x formation. However, by retarding the end of injection the fuel spray can escape the piston bowl region, with soot formation occurring directly on the squish region, close to the liner, rather than in the piston bowl. This influences the in-cylinder soot distribution, directly affecting the amount of soot available for deposition into oil [3-5]. Under Euro III, NO_x emissions were also typically controlled with cooled EGR. The downside of EGR is that it lowers the amount of oxygen available in the combustion chamber as well as the peak gas temperature, promoting thus the formation of soot particles [19-21]. Furthermore, as the re-cycled gas is typically unfiltered, a fraction of exhausted soot is re-introduced in the combustion chamber, with direct consequences on the amount of soot deposited into oil.

Tzamkiozis et al. [16] compared the total PM and soot emissions from Euro II to III diesel engines. They reported an increase in the amount of engine-out soot, despite a decrease in total PM value. The overall PM reduction is explained by the reduction in the soluble fraction via the DOC system. They explained the increase in soot emissions despite the higher fuel injection pressures as a consequence of the use of high levels of EGR [16]. Although a search of the literature did not identify a comparison of soot-in-oil amounts between Euro II and III engines, the use of EGR and post-injection strategies, suggest a potential increase of soot-in-oil amounts despite the reduction in the legislated PM values.

In order to achieve the reductions imposed by the Euro IV standard, improved fuel injection technology with higher pressures and better metering strategies were introduced, together with systems to improve the air-fuel mixing such as turbocharging with intercooling. Also, in 2005 the allowable sulphur in fuel concentration was reduced to 10 ppm (0.001%). This resulted in a reduced sulphur fraction of PM in addition to better efficiencies of the DOC system. In order to control NO_x emissions, a better control of the EGR system was achieved via a Direct Current (DC) motor.

The 80% reduction in PM from Euro IV to Euro V required the introduction of an after-treatment system able to limit soot tailpipe emissions, the Diesel Particulate

Filter (DPF). Although the use of the DPF allowed to comply with the more stringent regulations, it caused further potential problems from an oil contamination point of view for two reasons. Firstly, as soot particles are trapped in the filter, the DPF clogs increasing the exhaust backpressure, causing increasing pumping work, cylinder scavenging and turbocharger problems. Secondly, to remove the accumulated PM particles, a process called regeneration has to be performed, typically every 500-1,000 km [18]. A spontaneous regeneration in diesel engines is made difficult by the typically high Compression Ratio (CR) values, which result in low exhaust gas temperatures at the DPF (200-300°C), well below the onset soot oxidation temperature (above 500°C). The common method to unblock the filter is by dynamic regeneration, where the vehicle has to be driven at high engine loads conditions in order to increase the exhaust gas temperature. To further increase the exhaust gas temperature, the injection strategy is modified allowing for late injections [22]. As mentioned above, late injection can cause the soot cloud to be formed directly in the squish region, with direct consequences on the distribution of the carbonaceous particles, leading to a detrimental effect on soot-in-oil.

With the introduction of Euro VI and Particle Number (PN) limit, an even better combination of in-cylinder and after-treatments measures had to be achieved. Typically, the injection pressure is raised to values up to 2,000 bar with multimode injection strategies. The Variable Geometry Turbocharger (VGT) is used to better control momentum and direction of gas through the turbocharger turbine during transient operational conditions and through the EGR loop. NO_x values 66% smaller than during Euro V can require the use of either a Lean NO_x Trap (LNT) or a Selective Catalytic Reduction (SCR) after-treatment system. In the SCR urea is used to produce ammonia which then reacts with NO_x to produce water and nitrogen [23]. Theoretically, due to the high conversion efficiency of the NO_x after treatment systems, the engine could be calibrated towards high NO_x engine-out emissions values, i.e. with less or without the use of EGR, allowing for higher engine efficiencies and lower PM production. This, however, would increase the costs related to the after-treatment systems, and in the case of the SCR, would require for the vehicles' owners to periodically refill the urea tank.

The review presented in this section highlights how the emission standards that have driven the automotive industry towards complying with the imposed tailpipe limits, may have had a detrimental effect on the amount of soot entrained into oil. From Euro I to Euro IV, before the introduction of the DPF systems, the technologies for reducing PM focused on reducing the soluble fraction of PM, with values of solid particles, soot, remaining essentially unchanged over the two decades [16]. The introduction of the DPF aimed at reducing the tailpipe values of soot particles, rather than engine-out values. Furthermore, technologies and strategies applied to reduce NO_x emissions such as EGR and multiple injections can result in higher levels of soot-in-oil.

1.2.3 Accumulation of Soot in the Crankcase Oil

Accumulation of soot in the crankcase oil is a critical factor limiting engine oil life. Soot concentrations in oil of over 3 % to 4 % in weight can lead to severe engine wear, compromising the lifetime of the engine itself [24]. Oil filters and anti-dispersant oil additives are commonly used to reduce oil degradation. However, soot primary particle agglomerates are of the order of few hundred nanometres in size [25], about an order of magnitude smaller than any common filter mesh size, which makes them very difficult to remove. On the other hand, the role of anti-dispersant additives is to avoid further aggregation once particles are already entrained in the oil sump, rather than reducing the amount of soot contained in the oil.

The common method for eliminating the problems caused by high levels of soot-in-oil is to drain the used lubricant and refill the engine with new oil. Car manufacturers' recommendations are based on oil age or vehicle mileage. This method, however, is not cost effective for the vehicle owner and also represents a problem from an environmental point of view. For instance, a typical oil change requires approximately 4 litres of new lubricant every 13,000 km of vehicle use. In 2011, there were 28.5 million diesel cars licensed for use on the roads in the United Kingdom [10]. Based on these figures, 114 million litres of oil have to be regularly replaced and disposed of as waste. If the concept of 'sealed for life'

engines is to become a reality, rates of soot transfer to oil must be reduced substantially and a better understanding of the transfer mechanisms will aid this.

An alternative solution for limiting soot-in-oil and extending the lubricant lifetime would be to prevent the transport of soot from the combustion chamber to the oil sump. However, there is a need to expand the limited knowledge of the nature and factors contributing to the transport of soot into oil. This is of paramount importance when engine operating conditions, calibration controls, technologies and strategies such as EGR play an important part in the amount of soot- in-oil.

1.3 Project Aim and Objectives

The aim of this project is to understand and predict the mechanisms that govern the deposition and transport of soot particles from the combustion chamber to the crankcase oil. To achieve this, the following objectives have been set out:

- To estimate the relative contribution of deposition in the piston ring pack during blow-by and in the oil film at the cylinder liner via thermophoresis as the main transfer mechanisms of soot-in-oil. This has been achieved with the aid of Kiva-3V and analytical calculations.
- To investigate the influence of engine speed, load and EGR levels on soot-in-oil deposition rates. The effect of EGR is investigated by considering both its influence on the amount of soot formed during the cycle (In-cycle source of soot), and on the soot re-entered in the combustion chamber during the induction stroke (Re-cycled source of soot).
- To apply the soot deposition model to the entire engine cycle, including also compression stroke and post-EVO period.
- To experimentally measure the typical amount of soot and particle size distribution from light-duty diesel vehicles meeting Euro IV and V legislations.
- To validate the proposed deposition model against the typical amount of soot experimentally obtained from used light-duty diesel engine oils.

1.4 Thesis Layout

The thesis consists of seven chapters:

Chapter 2 covers a review of soot formation and oxidation processes, factors influencing soot production, pathways by which soot is deposited into the lubricant, effects and characterisation of soot-in-oil.

The analysis of used engine oils from a range of light-duty diesel vehicles driven under typical real-world driving conditions is reported in Chapter 3. This included measurement of the typical concentration of soot particles in oil via TGA, and particle size distribution via NTA. TGA results are used as benchmark value for the results obtained in the deposition model proposed by the author. NTA results are used to provide typical values for particle size distribution in the deposition model discussed in Chapter 5.

Results on the amount and distribution of soot available for deposition at the near-liner and piston head-liner corner regions can be found in Chapter 4. These two regions are of interest for deposition in the oil film at the liner and in the piston ring pack during blow-by, respectively. The amount and distribution of soot were calculated from a CFD model representative of a light-duty diesel engine meeting to Euro IV legislation [26].

Chapter 5 is focused on the soot deposition mechanisms at the cylinder liner via thermophoresis. As the CFD code did not include for a thermophoresis sub-routine, this transfer mechanism was analytically evaluated using the model proposed by Talbot et al. [9]. The work aimed at evaluating the influence of engine parameters and EGR level on the thermophoresis deposition velocity.

The availability of soot in the regions of interest, and the study on particle deposition mechanisms discussed in Chapters 4 and 5, allowed in Chapter 6 the calculation of the rate of soot in oil deposition from both the pathways investigated in this work. The results obtained here, are compared with the typical amount of soot-in-oil previously obtained with TGA. Chapter 7 includes discussion, future work and conclusions.

1.5 Contribution to Knowledge

This thesis contributes to the knowledge of soot transfer mechanisms to lubricant oils from light-duty diesel engines. As part of the understanding of the typical scenario of soot-in-oil deposition from light-duty diesel engines, several soot-laden oil samples representative of real world driving conditions were analysed. This allowed the characterisation of several samples of different sources, which would not have been possible from laboratory tests. To the author's best knowledge, this is the first time that oil drains from light-duty vehicles from engines meeting Euro IV and V standards are characterised and compared in terms of soot in oil concentration and agglomerates size distribution. Moreover, it is the first time that the NTA technique is used to determine the size distribution of soot particles entrained into oil [1, 2].

Previous computational studies estimated the rate of soot deposition into bulk oil by considering the SOI-EVO period and only taking into account the particles produced during the combustion process, here referred to as In-cycle source [3-5]. The analysis undertaken in this research has been extended to the entire engine cycle, including compression stroke and post-EVO period. Furthermore, the role of EGR on rates of accumulation in oil has studied by considering its effects on both the In-cycle source and the particles re-cycled with EGR gas during the induction stroke.

2 Literature Review

2.1 Introduction

This literature is divided into five sections, the first of which covers the main steps of the soot formation and oxidation processes. The second is a review of the typical combustion model used to describe the production of soot in diesel engines, together with factors affecting the formation of soot. The third section is a review on the studies conducted on the soot transfer pathways to engine oil. In the last two sections the effects of soot-in-oil with particular focus on oil viscosity and engine wear, and the current methods to characterise soot-in-oil in terms of concentration and size distribution are discussed.

2.2 Soot Production

Soot is generally accepted to be the insoluble fraction of Particulate Matter (PM). In the automotive field, the formation of soot particles in Direct Injection (DI) engines is a concern due to its impact on both environment and human health [27]. Soot particles are formed in both diesel and DI gasoline engines, but the first are particularly prone to produce particulate material as a consequence of the differences in fuel injection and ignition modalities and gas conditions [28]. High gas temperature and pressure, and the presence of fuel-dense pockets, typical of diesel engines, enhance the pyrolysis of the fuel and hence the formation of soot.

Soot particles are mainly composed of carbon, oxygen and hydrogen. Other elements such as nitrogen, sulphur, zinc, phosphorous, calcium, iron, silicon and chromium are also detected [29, 30]. Sulphur and traces of calcium, iron, silicon and chromium can be attributed to the diesel fuel, while typical elements from the lubricating oil additives are zinc, phosphorous and calcium [29]. In Table 2.1 the typical constituents of the soot exhausted and of the soot contained in the

lubricant oil are shown [12]. Their composition is quite different, with the soot-in-oil having a much higher carbon content. This is partially due to the different oxidation process that they undertake.

Soot Constituent	Soot-in-oil content [%]	Exhaust soot content [%]
Carbon	90	>50
Oxygen	4	<30
Volatile Content	6	20

Table 2.1: Main constituents of soot-in-oil and exhausted soot [12].

In diesel combustion, the main path for the carbon molecules is to react with the oxygen to form combustion products such as carbon monoxide and carbon dioxide. Despite the overall lean Air to Fuel Ratio (AFR), typically well above 18 [11], local fuel-rich areas exist during the early stages of the combustion process. As a consequence, some of the carbon molecules will fail to bond with oxygen, forming solid carbon. Heywood reported a critical carbon/oxygen ratio of 1 in order to determine soot formation [11]. Soot production, in simple steps, can be divided into soot formation, responsible for the growth in terms of both mass and number, and soot oxidation which acts as a surface-burning. Particle formation can be further schematised into: particle nucleation, surface growth and agglomeration [31, 32]. The net amount of soot produced within the combustion chamber is given by the competition between the soot formation and oxidation processes.

2.2.1 Particle Nucleation/ Inception

The available fuel can undertake either pyrolytic or oxidation reactions, depending on the availability of oxygen. During pyrolytic reactions, unsaturated hydrocarbons, polyacetylenes and other aromatic compounds are produced, growing then together to form Poly-Aromatic Hydrocarbons (PAH) [33]. The combination of large PAH forms two-dimensional PAH molecules, which merge together to form three-dimensional particles. In this later stage mass is converted from a molecular to a particulate system.

While the process of conversion from fuel to two-dimensional molecules is widely accepted, the conversion from a molecular to a particulate system is still not well understood. Graham et al. [34] proposed a method for nucleation for low and intermediate temperatures, typical of diesel engines. At low temperatures, soot nuclei can be formed from the condensation of the aromatic rings into a graphitic layer structure. At temperatures above 1800 K, soot nuclei are formed following an indirect path that involves ring breakup into smaller hydrocarbon fragments, which then polymerise to form larger unsaturated molecules. Finally, these are responsible for the production of soot nuclei.

Another model is that of Haynes and Wagner [32] who described nucleation as formed from the first condensed phase material produced from the pyrsolisation products of the fuel molecules, such as PAH. In their model, the condensation reaction of these gas species is considered as the most likely precursor of soot nuclei in flames, leading to the appearance of nuclei of $d<1.5$ nm with about 100 carbon atoms.

2.2.2 Surface Growth

Once the nascent soot particles are formed, their mass is increased by the aggregation of gas-phase species such as acetylene and PAH, including PAH radicals. The surface growth involves the gas-phase deposition of the hydrocarbon intermediates on the surfaces of the spherules developed from the nucleation process, forming the outer shell which surrounds the inner core. The typical inner core-outer shell structure of a diesel engine soot primary particle is shown in Figure 2.1. That causes a significant increment of soot mass compared to the nucleation phase, although the number of soot particles does not decrease. Unlike the particle nucleation, surface growth occurs also at lower temperatures [35].

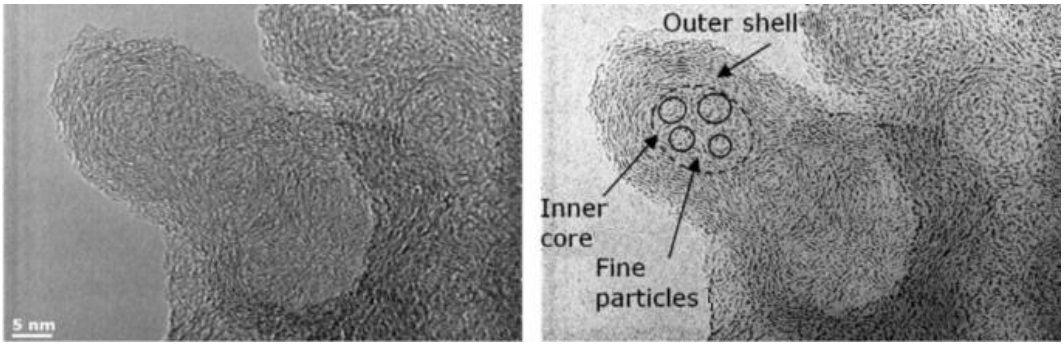

Figure 2.1: Primary particle at a high level of magnification using Transmission Electron Microscopy (left-hand side). Contrast enhanced using ImageJ to show inner core-outer shell structure (right-hand side) [25].

2.2.3 Agglomeration

Agglomeration does not affect the total mass of soot. The number of soot particles is reduced while particle size is significantly increased. This step in the soot formation process can be divided into two phases [29]. The first occurs when soot particles are small or young; collisions lead particles to fuse with each other forming a larger single spheroid particle. The second phase occurs when particles before colliding have the time to mature and solidify. Consequently, during collisions, particles maintain their structure and individual characteristics, growing simply by sticking to each other forming agglomerates with cluster shapes [29]. This leads to the appearance of particles with chain-like shapes of discrete size. The chain-like shape, suggests that agglomeration occurred via electrostatic activity [36, 37].

2.2.4 Soot Oxidation

Unlike the previous step of the soot formation, soot oxidation does not occur only at a specific phase, but it occurs throughout the entire soot formation process. It is a heterogeneous process that takes place on the surface of soot particles at temperatures above 1300 K [31]. During oxidation, the particle is destroyed by the oxidising agents which deplete the carbon atoms accumulated on the particle, reducing thus the mass of soot present within the combustion chamber. The main oxidation reactants are OH, O, and O_2. The largest contributor is O_2 under fuel-lean conditions and OH under fuel-rich conditions. However, it is reported that

only 10 to 20% of the collision between OH and soot are able to gasify a carbon atom [32]. Other possible oxidants are H_2O, CO_2, NO, N_2O, and NO_2 [35].

In this thesis the soot formation and oxidation processes are studied using semi-empirical models. Details on the models used are provided in Chapter 4, where these are applied.

2.3 Combustion Model in Diesel Engines

In typical diesel engines, combustion strategies involve one or more pilot injections and a main injection. The role of the pilot injection is to promote the combustion process of the main injection by increasing in-cylinder gas temperature and pressure. Combustion after the main injection can be divided into pre-mixed and mixing-controlled or diffusion flame combustions. The main quantity of fuel is injected during the compression stroke close to TDC. The time between injection and start of the combustion is the Ignition Delay (ID), in which the fuel mixes with air before the pre-mixed combustion starts. During this stage combustion is characterised by high rates of heat release and short duration. The mixing-controlled phase starts when the fuel previously mixed with air is consumed. During this second stage, the rate of the combustion is determined by the air-fuel mixing, and as a consequence, the heat release rate is slower and lasts over a longer period of time during the expansion stroke.

The conceptual combustion model proposed by Dec [38], schematised in Figure 2.2 has been widely accepted to describe the initial stages of the soot formation and oxidation processes. The model is based on experimental results from a Cummins DI diesel engine, with the Start of Injection (SOI) occurring at 11.5° Before Top Dead Centre (BTDC) and injection duration of approximately 20° CA.

By 3° After Start of Injection (ASOI) the fuel spray has reached its maximum penetration and the hot in-cylinder air has vaporised all the fuel beyond this location. At 5° ASOI and 1,000°C fuel breakdown commences, forming large PAH in the leading portion of the fuel jet. During this stage more air is entrained

within the yet enhancing oxidation reactions, with temperatures arising up to 1900-2,000°C.

After 1°CA, the first small soot particles are observed on a large portion of the fuel spray, arising from the first part of the fuel-rich premixed combustion. Continuing, at 6.5°ASOI a thin layer on the periphery of the jet is observed, representing diffusion flame. This delimits the fuel-rich premixed burn products and the surrounding fresh air, which at this stage has reached temperatures of approximately 3,000°C.

The jet continues to grow and the soot concentration increases, mainly in the periphery region of the jet, where mixing-controlled burn and high temperatures are achieved. At approximately 9°ASOI, premixed combustion ends and combustion continues only via mixing-controlled. At 10°ASOI the head vortex is well developed, containing a large concentration of soot particles with larger size compared to those in the central region of the jet formed from the premixed combustion. The (b) part of Figure 2.2 illustrates the remainder of the mixing-controlled combustion in which the soot distribution does not change significantly, except for the increase in soot concentration and size within the head vortex.

Soot oxidation is expected to occur throughout the combustion process, mainly at the jet periphery and outside the head vortex where a high concentration of oxidants, such as O_2 and OH is observed.

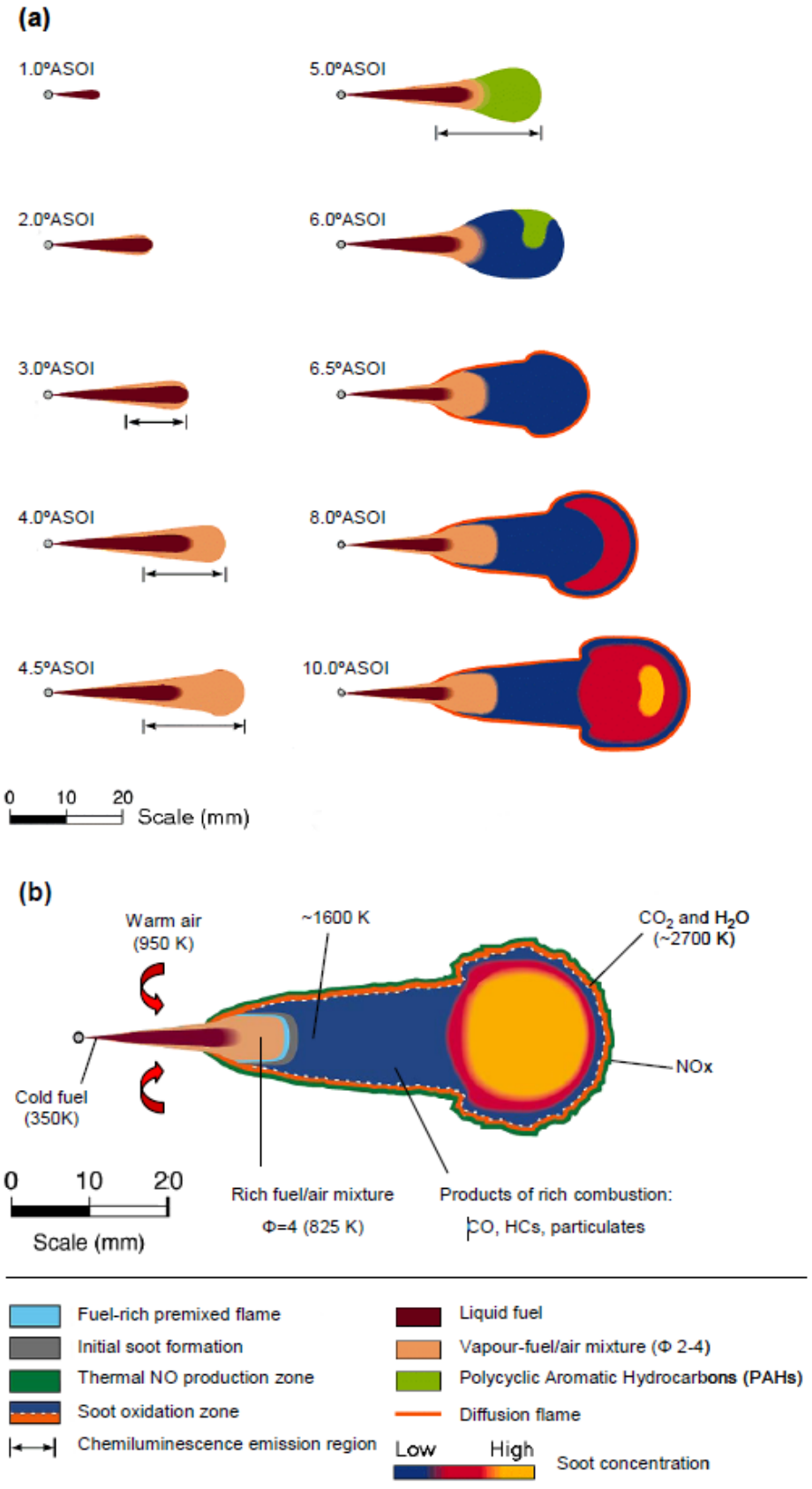

Figure 2.2: Schematic of temporal sequence during early stages of DI diesel combustion [38].

2.3.1 Factors Influencing Soot Production

Soot formation, which mainly occurs within the fuel spray during the combustion process, strongly depends on engine conditions. Soot production can be reduced by increasing the concentration of oxygen in the regions where soot formation occurs. This can be achieved by either increasing the entrainment of oxygen within the fuel jet spray or with fuel-borne oxygen. More oxygen within the jet plume will increase local flame temperature, increasing the oxidation of soot. This results in a more complete combustion and hence less soot produced, as well as less unburned Hydrocarbons (HC) formed [20]. Increasing the air swirl ratio is an effective way to increase the local air-fuel mixing and therefore reducing local fuel richness areas, i.e. soot formed [39]. On the other hand, in-cylinder temperature and oxygen availability are the factors governing NOx production. High combustion temperatures cause oxygen molecules to dissociate into monoatomic oxygen, initiating the formation chain reactions of nitric oxide [40]. This is of particular concern for diesel engines as NOx emissions cannot be removed with the use of a three-way catalyst as in gasoline engines, due to the excess of oxygen in the exhaust gas [11]. Oxygenated blends can reduce soot emissions in terms of both mass and number, as well as HC and CO [41]. Again, the drawback is that with fuel-borne oxygen an increase in NOx formation is observed [41].

Another effective way to reduce soot production is to increase fuel injection pressure. Nowadays fuel injector pressures have achieved values of 2,500 bar and above. Higher injection pressure improves fuel atomisation, reducing fuel droplets diameter and resulting in a better air-fuel mixture [42, 43]. Other techniques followed by researchers to reduce soot formation are increasing boost pressure and controlling mixing [44], optimising piston bowl shape, injector hole length to diameter ratio and direction of the injection spray [45].

High engine load levels have a strong influence on the amount of soot produced. This is a direct consequence of the higher amount of fuel injected in order to achieve the required cylinder power [46]. Increase in engine speed enhances the

overall in-cylinder turbulence level, which results in a better air-fuel mixing and hence soot oxidation [47].

Effective ways to reduce NOx emission are EGR technique, and retarding the start of injection. With EGR a portion of the exhaust gas is recirculated into the inlet manifold, displacing fresh air. However, due to the lower amount of oxygen available for the combustion as well as to the reduced flame temperature, the soot oxidation rate is reduced, increasing the net amount of soot formed [19-21]. Similarly, retarding SOI causes an increase in soot emissions due to the reduction in soot oxidation as a consequence of the global lower gas temperatures [44].

2.4 Possible Soot Pathways to Crankcase Oil

Soot particles produced during the combustion process, are firstly formed in the piston bowl region when the piston is near TDC. As the piston moves downwards during the expansion stroke, the expanding squish volume is occupied by the combusted gas previously delimited in the bowl region. As a result, soot particles, that closely follow the gas motion, may also reach the squish volume and the near-wall regions of the combustion chamber. In these regions, a large temperature gradient between the cold cylinder liner and the hot combusted gases exists. Particles present within this temperature gradient are subjected to a process called thermophoresis. This is defined as the motion of particles due to the more vigorous gas collisions from the hot side of the particle which results in a net force towards the cold side [48, 49]. Particles travelling at the thermophoretic velocity may be entrained into the oil film at the liner and then transferred to the crankcase oil via the scraping action of the piston rings.

Moreover, due to the pressure difference between combustion chamber and crankcase regions, a fraction of gas escapes the combustion chamber passing through the piston ring pack. This mechanism is referred to as blow-by. The mass of blow-by, which strongly depends on engine speed, engine load and piston ring pack configuration, is approximately 1-2% of the total charge mass [50]. As soot particles may be carried within blow-by gas, they may be deposited into the oil

while passing through the piston ring pack. These two pathways are well recognised as the only possible routes for soot entrainment into oil [12].

Previous computational studies on soot-in-oil deposition of light-duty diesel engines concluded that deposition via thermophoresis at the cylinder liner is the dominant soot pathway to oil. Deposition in the piston ring pack during blow-by was accounted for over two orders of magnitude smaller compared to the main transfer mechanism [3-5]. In these studies, the main focus was given to the role of injection strategies on soot-in-oil deposition. The role of EGR, investigated in this thesis, was not taken into account. Furthermore, they limited their period of investigation to the closed part of the cycle, from SOI to EVO, neglecting compression stroke and the post-EVO period.

The potential role of EGR on soot-in-oil deposition was investigated experimentally by Tokura et al. [51] in a study published in 1982. Experiments were conducted on a light-duty IDI LD20 diesel engine, at conditions of 2,400 rpm and 29.4 N·m. The role of EGR was investigated by considering both the soot produced during the combustion process and that brought into the combustion chamber by EGR. Furthermore, they investigated the contribution from both blow-by and cylinder liner courses. Results shown in Figure 2.3, clearly highlighted the role of EGR on soot-in-oil accumulation, and in particular, the role of the re-cycled source of soot. They reported that for moderate-high levels of EGR, the contribution from the Re-cycled source of soot was equal or above that produced during the combustion process. A limitation of the work was that the role of the Re-cycled soot was taken into account only between induction stroke and end of the compression stroke. This was due to the fact that the two sources of soot were not distinguishable after the combustion generated particles were formed and both sources were available in the combustion chamber. Deposition caused by blow-by, due to the Re-cycled source of soot, was approximately 10% of the total deposition at high levels of EGR, much higher than that reported by other authors who did not take into account the contribution of EGR [3-5]. Despite the engine used for the investigation not being representative of current engine technologies, i.e. fuel injection pressure, in-direct injection, piston bowl

shape, compression ratio, results showed the need for further investigation into the role of EGR on soot-in-oil deposition.

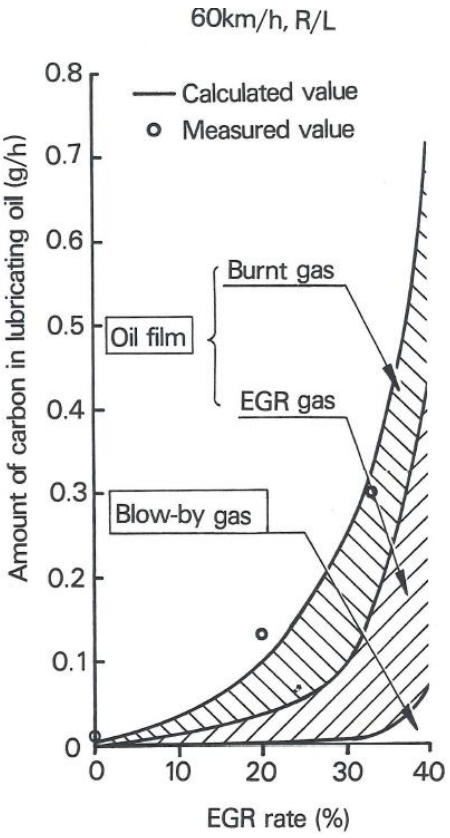

Figure 2.3: Relationship between amount of soot-in-oil and EGR rate [51].

2.5 Effects of Soot-in-Oil

The presence of soot into the lubricating oil is for the automotive industry a sub-problem if compared with the focus given to reducing soot tailpipe levels. High level of soot-in-oil, however, can create secondary problems that are not acceptable due to consequences on engine performances or even more on the engine life itself.

The interest on the effects of soot-in-oil is further growing due to the fact that nowadays lubricating oils are experiencing an even higher concentration of soot compared to former times, with reported values on heavy-duty diesel engines of up to 5 wt% [52]. This is a consequence of several factors, all linked to the

necessity to reduce engine out soot emissions. The first factor is related to the strategies adopted in order to reduce NOx emissions: High levels of EGR cause a sootier combustion as well as a sootier in-cylinder charge due to the recirculation of the exhaust gas; retarded fuel injection timing displaces the combustion event to later during the expansion stroke, lowering gas temperature. However, the soot cloud formed during the combustion process may escape the piston bowl region exposing the oil film on the liner to higher levels of soot amounts. The second factor is that, nowadays, piston rings scrape more oil in order to reduce oil consumption. This is achieved by reducing the top piston land height. Reduced levels of oil consumption have also an indirect impact on the lubricant oil stress, as the necessity of adding fresh oil is decreased, consequently reducing the dilution of soot-in-oil. Finally, with the introduction of turbocharged diesel engines, in-cylinder pressure has increased, promoting the blow-by of soot-laden gas.

Among all the potential implications of soot entering the crankcase oil, the two main consequences are the increase in engine wear and increase of the oil viscosity, as discussed in the following sections.

2.5.1 Oil Viscosity

Particle size and shape are factors affecting the influence of soot-in-oil on oil viscosity. It is understood that soot agglomerates, compared to soot primary particles occupy a larger effective volume and that the oil trapped within the pores of the agglomerates are more rheological relevant than simply the mass or fraction of soot in oil [6]. Gopalakrishnan and Zukoski [53] reported an increase in oil viscosity of over several hundred percent for concentrations of soot above 5% in weight. The drastic increase was also connected to the soot agglomeration occurring in the oil itself at such high levels of soot, referred as *secondary agglomeration*. If the particles will remain well dispersed even at very high concentrations of soot, the increase of viscosity could be drastically reduced to only few percent [13].

Ryason and Hansen [6] studied the shear rate rheometry of used oils from heavy duty diesel engines concluding that oil viscosity is strongly affected by soot

concentration, especially at low temperatures. They reported a linear increase in oil viscosity for levels of soot of up to 1% in weight. On the other hand, for levels above 1% the viscosity started to increase faster. As shown in Figure 2.4, similar rises in viscosity were observed by Green et al. [54] who used formulated oil mixed with carbon black at concentrations of up to 7 wt%.

In a hydrodynamic lubricating regime, friction is approximately proportional to the square root of the dynamic viscosity [55]. Therefore, the increase in viscosity due to soot contamination can have an indirect detrimental effect on fuel consumption and exhaust emissions. On the other hand, a study conducted by Liu et al. [56] using a cylinder-in-disc reciprocating test, indicated that the friction coefficient decreased with soot. This was associated with the role of the soot acting as a friction modifier, possibly due to the action of soot as a solid lubricant.

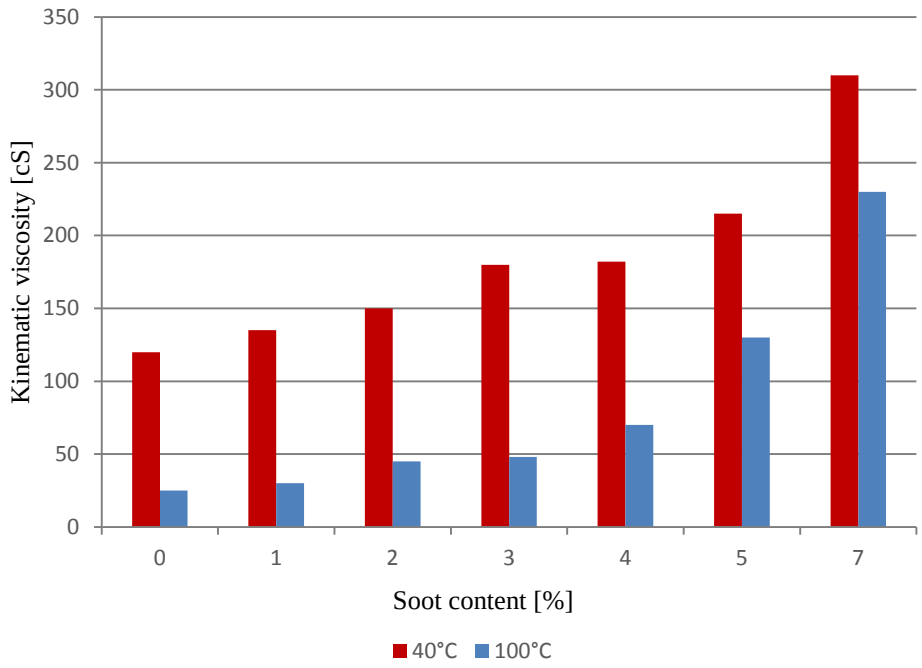

Figure 2.4: Effect of soot content on the kinematic viscosity of an engine oil at 40°C and 100°C [54].

2.5.2 Engine Wear

Engine wear is recognised as the most critical effect caused by soot-in-oil. In Figure 2.5 engine components wear is shown as a function of EGR [57]. Wear is higher in the valve train, and drastically increases with EGR of up to 10 times for all the components as a consequence of the higher concentration of soot.

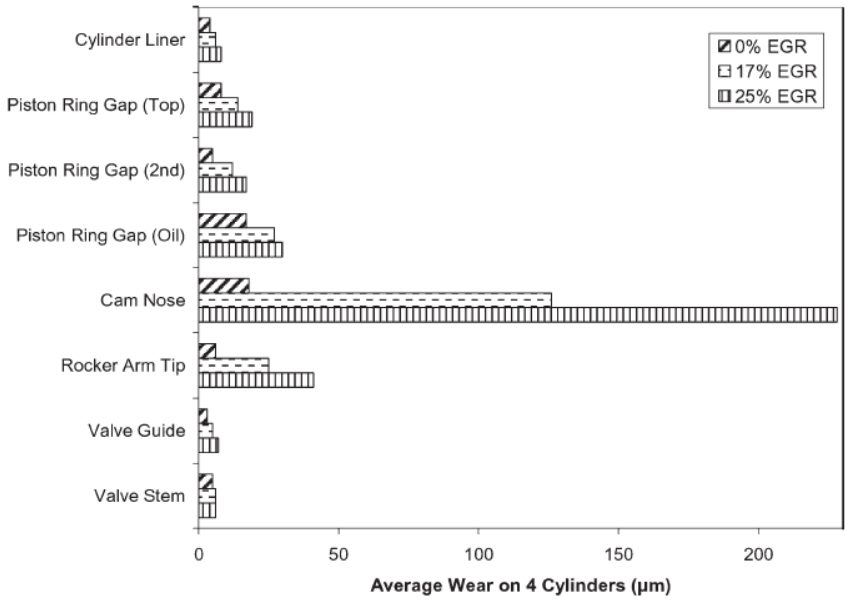

Figure 2.5: Data showing relative component wear at different EGR levels [57].

The mechanisms by which soot causes wear are not yet fully understood and the theories can be classified into three categories:

- Interference with anti-wear additives in the lubricant;
- Direct abrasion;
- Blockage and oil starvation.

Initial works ruled out direct abrasion as a potential soot-induced wear mechanism as it was believed that the hardness of soot particles was the same as that of graphite, which has a hardness much lower than steel and other engine components. For instance, one of the earliest works, conducted by Rounds [58] studied the interaction between soot and wear using a four-ball wear test machine. Rounds concluded that soot particles cause wear by absorbing anti-wear additives such as the Zinc DialkylDithioPhosphate (ZDDP). This theory, was later

contradicted by Olomolehhin et al. [59] who found that once the soot was removed from the oil, the anti-wear additive performance returned to normal levels, instead of being removed together with the particles.

Other authors [57, 60] studying wear on the valve train, showed that soot causes wear by removing the ZDDP film from the metal surfaces, rather than by absorbing the ZDDP anti-wear film as proposed by Rounds [58]. Corso and Adamo [61], found that soot interacting with ZDDP transforms the additives from anti-wear Fe_3O_4 to pro-wear FeO.

More recent studies suggest that the dominant factor causing wear is abrasion. This theory is reinforced by Li et al. [62] who showed that the soot particle hardness is higher than that of engine components such as liner, crosshead, rocker arm and top ring face, as shown in Table 2.2. The soot collected from a diesel engine equipped with EGR is harder than an engine without EGR. This is possibly due to the secondary heating and oxidation process that the particles experience.

Component	Vickers hardness [kgf/mm^2]
Soot, EGR	1302
Soot, non-EGR	988
Liner	293
Cross Head	786
Rocker Arm	732
Top Ring Face	753

Table 2.2: Vickers hardness data of different engine components and soot under EGR, non-EGR conditions [62].

Using a Scanning Electron Microscope (SEM), Li et al. [62] studied the grooves formed on the cylinder liner. They supported the theory that the grooves are caused by the soot, as their width (20-50 nm) was in the same range as the primary soot particle size, and the orientation of the grooves was parallel to the sliding direction. They described soot wear as a three-body contact mechanism, as

schematised in Figure 2.6. When the oil film thickness is larger than the soot particle size, the two sliding engine components can be separated by the oil film. However, if the oil film thickness is less than the particle size, abrasion can occur due to the soot-metal interaction.

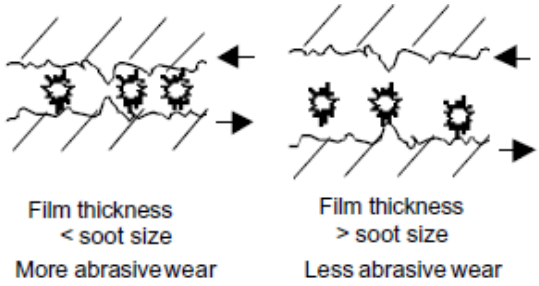

Figure 2.6: Schematic of three-body contact mechanism causing engine wear [62].

Similar conclusions were made by Berbezier et al. [63] who discovered that the particle size plays a major role on the wear rate, with agglomerates 300 nm in diameter producing approximately 60% more wear than particles of diameter 20 nm. Soot-in-oil characterisation conducted by the author together with La Rocca et al. [25], suggested that the typical agglomerate size is approximately 200 nm with primary particles of 20 nm diameter. Using carbon black and base oil, Green et al. [64] investigated the wear volume as a function of carbonaceous material concentration. They stated that below 2 wt% of contaminant in oil, wear is mainly induced by metal-to-metal sliding.

Starvation is the most extreme wear mechanisms caused by soot. For levels of soot above 4%, Green et al. [64] observed a transition from abrasive wear to starvation, due to the contaminants blocking the inlet to the contact regions. Rheology is another mechanism that may cause starvation. An increase in oil viscosity due to high levels of soot, can increase pumping losses through small channels, limiting or preventing oil flow, failing to maintain a lubricated contact, resulting thus in high levels of wear [65].

2.6 Soot-in-Oil Characterisation

2.6.1 Concentration

Determining the concentration of soot-in-oil is of particular importance as it is one of the main variables governing the oil drain interval. Furthermore, as it is strongly associated with engine wear and viscosity, it is a routine measurement for such investigations. However, in order to produce soot-laden oil samples, it is necessary to run the engine for several hours, with direct implication in terms of costs and time that a test bed has to be used for this purpose.

As a consequence, soot-laden oil samples are often produced using soot-induced tests, which dramatically increase the rates of soot build-up into oil. For example, common methods are the Cummins M11 EGR Standard Test Method for evaluating oil performance of heavy-duty diesel engines [66], and the Mitsubishi 4D34T4 which increase the concentration of soot up to 4.5 wt% via over-fuelling [67]. The two methods refer to heavy-duty diesel engines, and furthermore, they do not provide information about real-world soot-in-oil concentrations.

In both standards, the concentration of soot-in-oil is measured by using ThermoGravimetric Analysis (TGA) analysis. The TGA technique measures the percentage in mass of soot-in-oil as a function of time and temperature. It is reported that TGA is able to provide results with an error band of within 10% [68, 69]. Due to its simplicity and accuracy TGA has been also used to measure the concentration of soot by several other authors [14, 52, 68, 70]. However, none of these works provided information relative to concentrations of soot-in-oil from light-duty diesel engines. Uy et al. [71] provided values of soot-in-oil concentration for a GDI engine drain oil from customer vehicles driven under urban and extra-urban driving conditions. They reported a concentration of soot-in-oil of 0.83 wt%. However, they did not provide information about mileage at the time of the oil drain, and therefore, about the rate of soot deposition in oil. A correlation between soot-in-oil concentration and sample mileage is provided by Lockwood et al. [52], and results are shown in Figure 2.7. Three different test oils were studied under on-road conditions in five different tracks. Results show that

the amount of soot trapped in oil for a particular engine increase linearly with a correlation on the order of R^2=0.8.

In the same work, Lockwood et al. [52] measured the concentration of soot using both TGA and Fourier Transform Infrared Spectroscopy (FTIR) techniques. Although a comparison between the two techniques is not provided, FTIR is another common technique used to measure the concentration of soot-in-oil. With FTIR, the level of soot is related to the absorption of infrared light, at an absorbance wavelength of 2,000 cm^{-1} [72]. The main drawback of this technique, which has been successfully applied by several authors [52, 72, 73] on heavy-duty diesel engine oil samples, is that it requires both the used soot-laden oil and the clean oil. In fact, the amount of soot is determined by subtracting the absorbance wavelength of the clean oil to the wavelength of the used oil at 2,000 cm^{-1}. As discussed in Section 3.2, the oil samples analysed in this work were collected from several customer light-duty vehicles driven under urban and extra-urban driving conditions. Therefore, the clean oil was not available, and consequently, the FTIR method could not be applied.

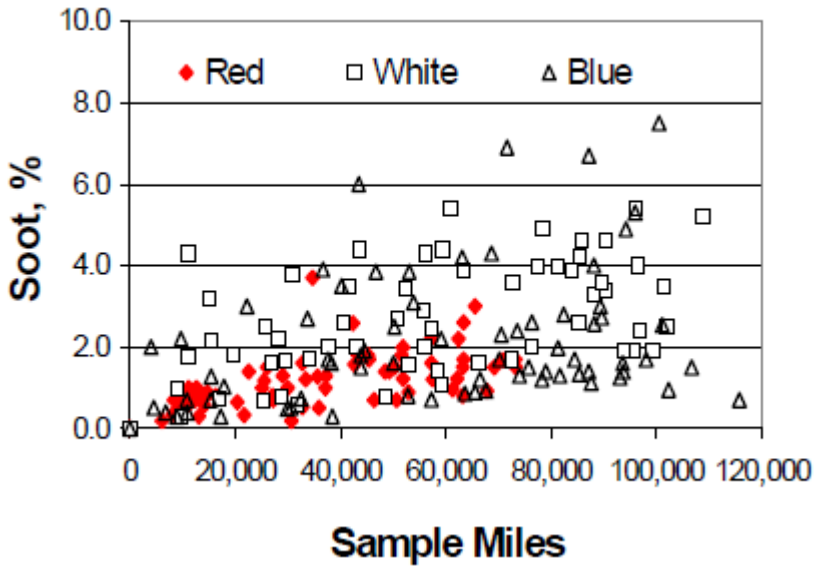

Figure 2.7: Percentage of soot-in-oil concentration from three heavy-duty diesel engines as a function of sample mileage [52].

2.6.2 Primary Particles and Agglomerates Size and Shape

Soot characterisation in terms of particle size and shape provide information regarding soot formation process, its impact on the environment, engine wear, oil lubrication and efficiency of particulate filters. Moreover, of more relevance for this work, it influences the rate at which the particles are deposited into the oil film on the liner via thermophoresis.

The most common techniques used to characterise primary particles and agglomerates dispersed in oil samples are Transmission Electron Microscopy (TEM) and Dynamic Light Scattering (DLS). Recently, a novel technique, Nanoparticle Tracking Analysis (NTA) has been applied for the first time to soot-laden oil samples by the author [1, 2]. The two works compared particle size distribution from light-duty diesel engines obtained with NTA with those from TEM and DLS. As discussed in Section 3.4, results from NTA agreed well with the other two common techniques.

The main characteristic of TEM compared to the other techniques is that it allows the study of the structure of the primary particles and the shape of the agglomerates [12, 25, 62, 74]. However, the sample preparation for soot-in-oil sample is relatively complex as used engine oil is a contaminant for electron microscopes and leads to instabilities under the electron beam; a suitable sample preparation technique has to be employed to effectively remove lubricant from the soot particles. Different sample preparation are described and applied in literature: Cryogenic vitrification and imaging by Cryogenic TEM have been used by Kawamura et al. [75] and Liu et al. [56] to visualise the soot agglomerates and their distribution in engine oil. Despite a successful demonstration of this approach, the viscosity of typically used engine oils leads to localised thick layers on the TEM grid and requires specialised preparation equipment and expertise, making it unsuitable for routine analysis such as the analysis of fifteen oil samples. Clague et al. [12] employed solvent extraction followed by centrifugation to extract soot from used engine oil and a similar technique was used by Esangbedo et al. [30]. A previous study conducted by the author on soot agglomerates showed that sample preparation can alter particle size and shape [25]. Further

drawbacks of this technique are high running costs, analysis turnaround time and the need for highly skilled operators.

On the other hand, measurements of nanoparticle suspensions size distribution with DLS are fast, user-friendly and straightforward [56]. DLS determines particle size by measuring their Brownian mobility in the suspension. The speed at which the particles are moving due to Brownian motion is detected by recording the rate at which the intensity of the scattered light fluctuates. The particle size is given as hydrodynamic diameter, D_h, defined as the diameter of a hard sphere moving at the same average diffusion coefficient of the particle being analysed. The hydrodynamic diameter is related to the Brownian particle displacement by the two-dimensional Stoke-Einstein equation [76]:

$$D_h = \frac{K_B\, T}{3\pi\, \mu\, D} \qquad 2.1$$

Where D is the diffusion coefficient, T is the temperature of the sample, K_B is the Boltzmann's constant and μ the dynamic viscosity of the solution. Despite its advantages, DLS has some downsides. Because the intensity of the scattered light is proportional to the sixth power of the particle size, the presence of large particles can result in the underestimation of small particles [77]. This is of concern for soot measurements as their typical diameter varies from few tens of nanometre to several hundred nanometres. Furthermore, as all the particles are measured simultaneously, the DLS produces results in terms of average particle size. A drawback is that DLS requires individual particle populations to differ in size by a factor of at least 3 in order to discretise them, with the consequence that DLS could fail to detect peaks on polydispersed samples [77].

Soot is found to be in the form of chain-like or cluster shapes, with typical size of the agglomerates between 150 and 500 nm [25, 30]. Soot agglomerates may contain up to hundreds of primary particles. Primary particles are spherical in shape and formed of millions of carbon atoms [35], with diameter varying between 15 and 30 nm [25, 78, 79]. The diameter of primary particles is found to be affected by engine conditions. Mathis et al. [79] found primary particles to decrease with advanced SOI, increased fuel injection pressure and engine load.

On the other hand, primary particle size was found to increase when high levels of EGR were applied. Lapuerta et al. [78] justified the increase in primary particle size with EGR due to the effect of EGR on AFR. Furthermore, they found that at high engine speed size decreased due to the reduced time available for surface growth.

2.7 Discussion and Conclusions

The review presented in this chapter highlighted that most of the studies found in the literature on soot dispersed into crankcase oil are relative to the effects that these particles have on engine wear and oil viscosity level. Almost the totality of these works applied to heavy-duty diesel engines rather than light-duty vehicles. Moreover, in these studies, soot-laden oil samples are often prepared using test methods aiming at accelerating the accumulation of soot-in-oil. This is due to the high costs and amount of time required to obtain the desired levels of soot content in oil with non-doped engine conditions.

As a result, there is a lack of knowledge regarding the rate of soot accumulation in oil, and on the effects that engine conditions have on the rate of accumulation. In particular, to the author's best knowledge, no information has been found in the literature covering the rate of soot accumulation of light-duty diesel engine vehicles driven under real-world driving conditions.

Computational studies on light-duty diesel engines have investigated the rate of soot-in-oil deposition [3-5]. These, however, did not consider the effect of EGR, which is a technique applied to reduce NO_x widely applied in current vehicles. Due to the importance that EGR has on oil degradation, [57, 62, 80], there is the need to investigate computationally the role of EGR on soot-in-oil deposition.

Tokura et al. [51] experimentally studied the role of EGR on soot-in-oil deposition, taking into account both the in-cycle and re-cycled sources of soot. Although the engine used in their investigation does not reflect the engine specifications currently encountered on the market (the study dating from 1982)

the work demonstrated the importance of EGR not only due to its effects on the soot production, but also for the soot that is re-circulated with the EGR gas.

Finally, a current limitation of the studies found in the literature on soot particle size distribution, is that these concern particles produced and collected during laboratory tests. In particular, a potential correlation between oil mileage and particle size, as well as with Euro standards or engine vehicle is currently missing.

3 Characterisation of Soot from Light-Duty Diesel Engine Oil Samples

3.1 Introduction

The aim of the work reported in this chapter was to determine the typical concentration and size distribution of soot in used engine oil. Fifteen oil samples from light-duty diesel engines meeting Euro IV or V regulations setting limits on vehicle emissions were collected from local service garages in the Nottingham area. The samples were representative of oils at the end of service intervals collected from vehicles driven under urban and extra-urban combined conditions. Details of the samples are provided in Table 3.1. Data on soot-in-oil samples from real world driving conditions was not available from the literature, as soot characterisation of light-duty vehicles during real world conditions is limited to the characterisation of the exhaust soot. Soot-laden oil samples are instead commonly produced during laboratory tests, at conditions which promote soot deposition in order to produce high concentrated samples for engine wear analysis.

Soot-in-oil concentration results are used to estimate the typical rate of soot-in-oil deposition and the fraction of fuel in oil as soot particles. The goal is to use these results to compare and validate the analytical and computational works presented in Chapters 4 and 5. The oil samples were analysed via Thermogravimetric Analysis (TGA) technique. TGA is a common method used for determining the mass of soot as a percentage by mass of sample, wt%. The technique was chosen for its simple and reliable application. To the author's best knowledge this is the first time that soot-in-oil concentration from light-duty Euro IV and V diesel engines vehicles representative of real world driving conditions has been

investigated. The instrument and the methodology used for the experiments are described in the first part of this chapter. The following sections presents the results of soot concentration and the assumptions used to estimate the rate of deposition and the fraction of fuel in oil as soot.

Results from the soot-in-oil size distribution investigation are used as input values for the thermophoretic model discussed in Chapter 5, which is sensitive to particle size. Nanoparticle Tracking Analysis (NTA) has been used for the measurements. This novel technique was applied for the first time by the author to soot-laden oil samples. A review of the NTA instrument and the methodology used for the experiments are discussed in Section 3.1. The technique is compared against two traditional techniques such as Transmission Electron Microscopy (TEM) and Dynamic Light Scattering (DLS) techniques. Details on the comparison have been published in two articles [1, 2], and main results from the two articles are also provided within this chapter. It is worth mentioning that this validation has been carried out using one oil collected from a single cylinder version of an HPCR diesel engine. After investigating the reliability of the NTA technique, the method was used to obtain the soot size distribution from the fifteen oil samples. This was then compared against soot concentration obtained during TGA investigation, to assess if a correlation between the two existed. To the author's best knowledge, this is the first time that size distribution from several oil samples of different emissions regulations representative of real driving world conditions has been investigated, permitting thus the estimation of the potential influence of emission standards on soot agglomerate particle size.

Sample [n]	Vehicle [Model]	Euro Standard [-]	Engine Capacity [L]	Oil mileage [km]	Fuel Consumption* [L/100km]	PM [mg/km]	CO_2 [g/km]	NOx [g/km]
1	Seat Leon	5	1.6	11,925	3.8	0.3**	99	0.15
2	Seat Leon	5	1.9	15,075	4.5	0.2**	125	0.17
3	Seat Leon	5	1.6	13,155	3.8	0.3**	99	0.15
4	Seat Leon	5	2	13,406	5.1	0.3**	139	0.16
5	Hyundai I30	4	1.6	23,386	4.5	10.0	119	0.18
6	Nissan Note	4	1.5	4,013	4.5	20.0	129	0.20
7	BMW 120d	4	2	11,136	4.8	0.1**	128	0.17
8	Volvo XC60	5	2.4	14,174	5.7	0**	174	0.20
9	Seat Leon	4	2	16,896	5.7	20.0	151	0.24
10	Seat Ibiza	4	1.4	13,797	4.3	20	124	0.21
11	Jaguar XF	4	2.7	14,526	6.8	0**	199	0.25
12	Toyota Avensys	4	2.2	3,320	5.4	0.001**	150	0.17
13	Toyota RAV4	5	2.2	5,805	6.0	0.001**	149	0.15
14	Toyota Avensys	4	2.2	15,933	5.4	20.0	158	0.24
15	Jaguar X-Type	4	2	15,120	5.8	20.0	149	0.22

Table 3.1: Details of the oil samples used for the TGA and NTA investigations. PM, CO_2 and NO_x obtained from NEDC [81]. (* = combined urban and extra-urban fuel consumption over NEDC; ** = with DPF) [81].

3.2 TGA Investigation

TGA is a thermal analysis technique which measures the concentration of soot from the change in weight of the oil sample as a function of temperature and time. TGA has been chosen for quantifying the amount of soot entrained in oil due to its simple and reliable application. The method is widely used in the petrochemical industry for soot analysis [2, 12, 52, 68, 70, 71]. TGA is also indicated as standard procedure for measuring the quantity of soot transferred into the oil during the Cummins M11 EGR Standard Test Method for evaluating oil performance of heavy-duty diesel engines [66]. The FTIR is another common technique for determining soot content in oil samples. However, TGA is considered to be a more accurate method for determining soot content, with an error band of within 10% [68, 69]. Furthermore, the determination of the soot content with FTIR is based on the subtraction of the clean oil spectrum to the used oil sample. Due to the source of the samples this method could not be applied.

3.2.1 TGA Methodology

The instrument used for the experiments was the TGA Q500 produced by TA Instruments. The instrument has an automated pan loading system (up to 16 pans) and is able to detect the weight loss by the sample with a sensitivity of 0.1μg and a weighting precision of 0.01%. The temperature range is ambient to 1,000^{o}C, with a maximum temperature ramp of 50^{o}C/min. The main components of the instrument are shown in Figure 3.1.

An exhaust condenser was connected to the instrument outlet in order to clean the gas prior to being expelled to the environment. The pans used for the experiments were Platinum crucibles, suitable for temperature ranges from ambient to 1,000°C. These crucibles were chosen because platinum is considered as inert during the oxidation process [82]. Furthermore, their large shape is ideal to avoid any stagnation volume and, hence, diffusion limitations [82].

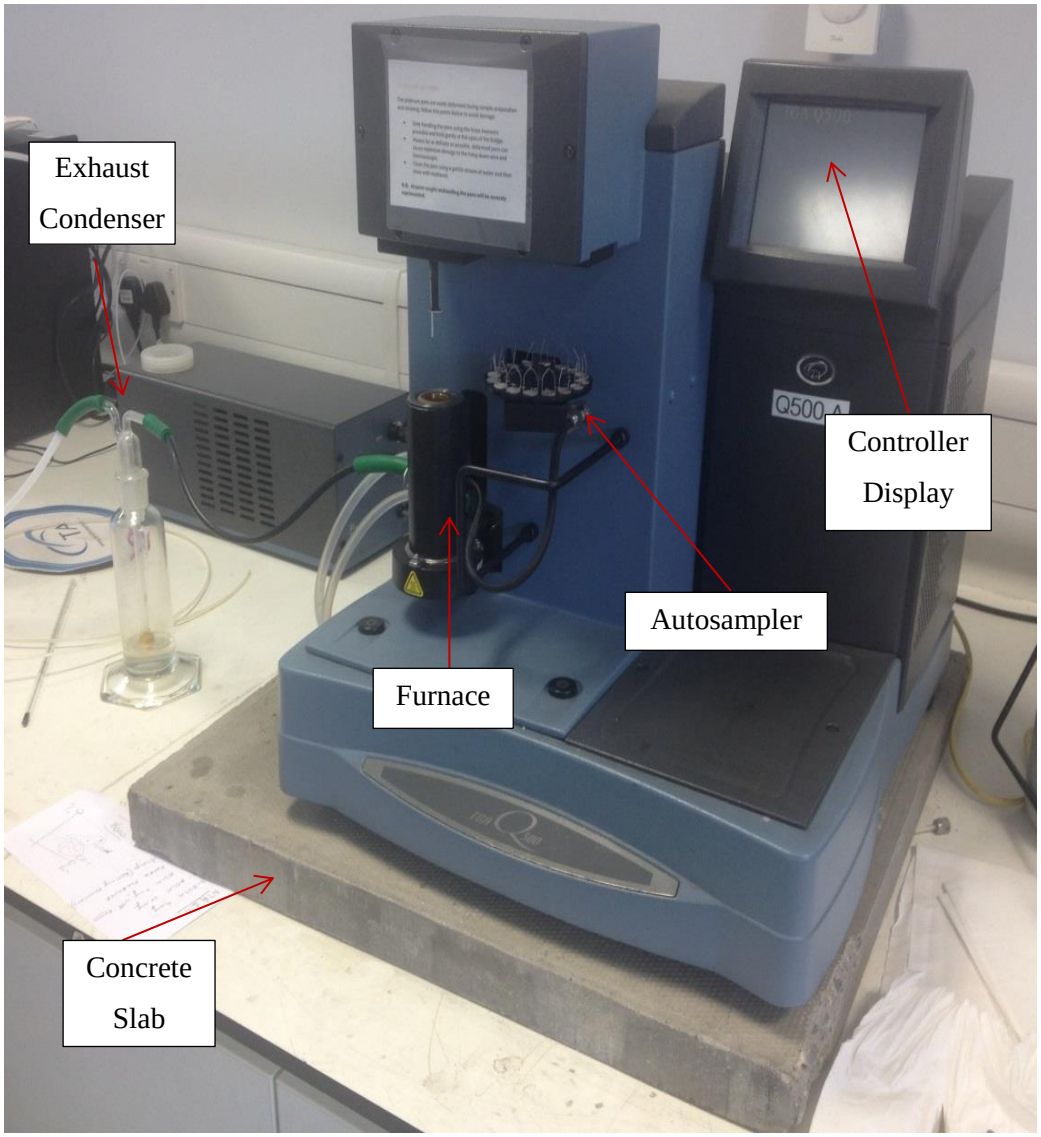

Figure 3.1: Q500 TGA machine used throughout the investigation.

In Figure 3.2 the purge gas system is shown. The gas is supplied horizontally allowing accurately metered purge gas flow directly across the sample. A portion of the gas is further directed through the chamber vertically to eliminate backflow. The gas with any sample effluent exit the chamber system by a side arm on the left-hand side of the furnace.

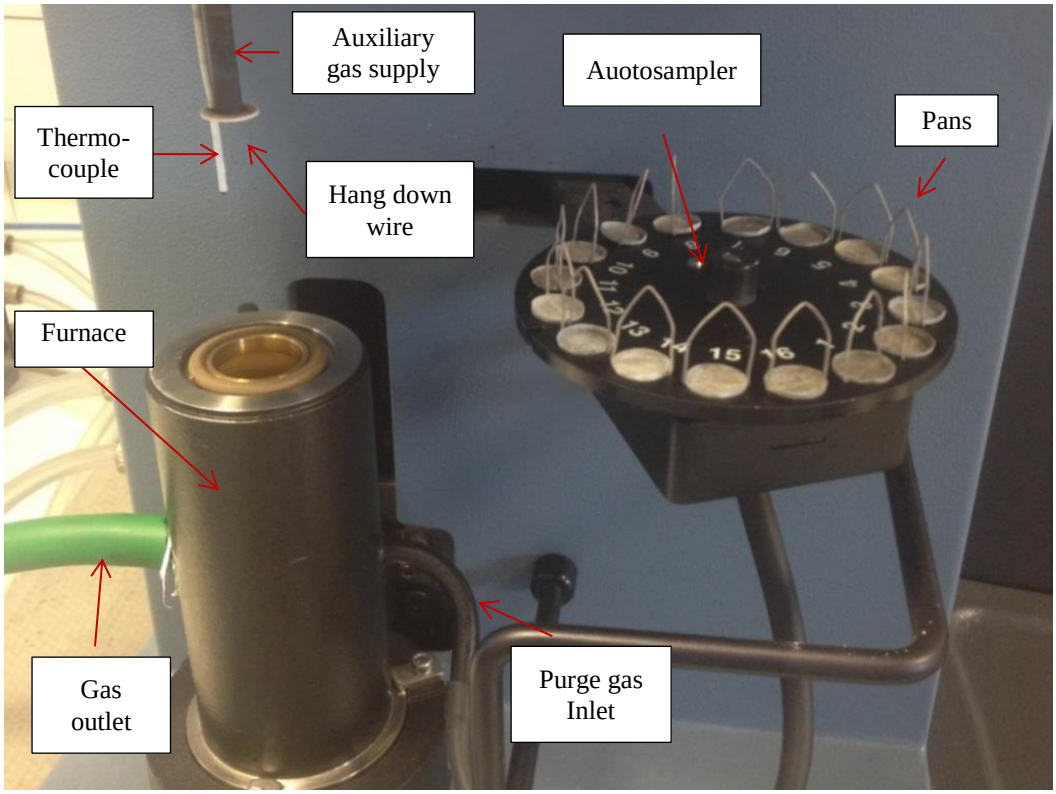

Figure 3.2: TGA details of the furnace and autosampler systems.

The quantity of soot determined by TGA measurements is obtained as a loss of mass at a calibrated temperature. A used soot-laden engine oil sample usually contains also a certain amount of water, coolant and fuel. To measure the amount of soot-in-oil, the sample must first be heated up to a temperature which allows the removal of the high (typically coolant, water and fuel) and medium-low (typically oil) volatility components contained in the used oil. During this stage it is crucial that the carbon particles do not combust or pyrolyse. To avoid this, the process was carried out in an inert environment, e.g., nitrogen. A typical temperature that allows the removal of all the volatile components is approximately 450^{o}C [70]. Above this temperature the remaining sample is composed only by the soot and ash fraction of the original oil analysed. Typical examples of ash are wear metals and non-reactive oil additives. After the removal of all the volatiles components, the sample is further heated in an oxidative environment until the complete combustion of the content of soot occurs. The mass loss during this stage is considered as the mass of soot in the sample. Typically this result is referred to as a percentage in weight of the initial sample

weight. The mass left after the evaporation and oxidation processes is referred to as ash.

The above process is standardised in the ASTM D5967 Test Method [83], listed in Table 3.2. In the D5967 standard method, 20 mg of soot-laden oil are loaded onto a platinum crucible pan. An initial isothermal purging time of one minute is performed in order to remove oxygen traces from the furnace. The sample is then heated in a nitrogen environment to 550°C, at a rate of 100°C/min and held isothermally for one minute. The gas is further heated at a rate of 20°C/min to 650°C. The gas fed is then switched to oxygen and heated to 750°C at 20°C/min to allow the complete combustion of the soot fraction. Soot is calculated as the difference in mass or in mass percentage at purge gas switching point, Upper Reference Point (URP), and after a stable mass residue is obtained from the soot combustion, Lower Reference Point (LRP).

Also shown in Table 3.2, is the methodology used in this work. This closely follows the D6597 Standard Method, and deviations have been highlighted in Table 3.2. The first variation was the use of dry air instead of oxygen, both for safety and availability reasons. However, this only has an effect on the combustion rate and not on the amount of soot oxidised [70]. Another difference, due to instrument capabilities, was the heat ramp during step *3*. In the method used by the author, this was limited to 50°C/min instead of the 100°C/min as for the standard method. Experiments at two different temperature gradients, 5°C/min and 50°C/min were performed to determine the potential effects of the heat ramp. The mass loss profiles for the two temperature gradients are shown in Figure 3.3. The curves clearly indicate how the temperature rate during step *3* only influences the rate at which volatiles components evaporates, without affecting the mass left at the end of this step. Hence, the temperature gradient during step *3* does not influence the measurement of the mass of soot.

	Step No	Methodology	
		D5967 Standard	Current Work
Temperature Program	1)	Select gas: Nitrogen	
	2)	Isothermal hold for 1 min	Isothermal hold for 15 min
	3)	Heat to 550°C at 100°C/min	Heat to 550°C at 50°C/min
	4)	Isothermal at 550°C for 1 min	
	5)	Heat to 650°C at 20°C/min	
	6)	Switch purge gas to oxygen	Switch purge gas to air
	7)	Heat to 750°C at 20°C/min	
	8)	Isothermal at 750°C for 5 min	
Sample pan		Platinum Crucible	
Sample weight		20 mg ± 2.5%	

Table 3.2: Comparison between the method used for the TGA experiments and the D5967 standard method [83].

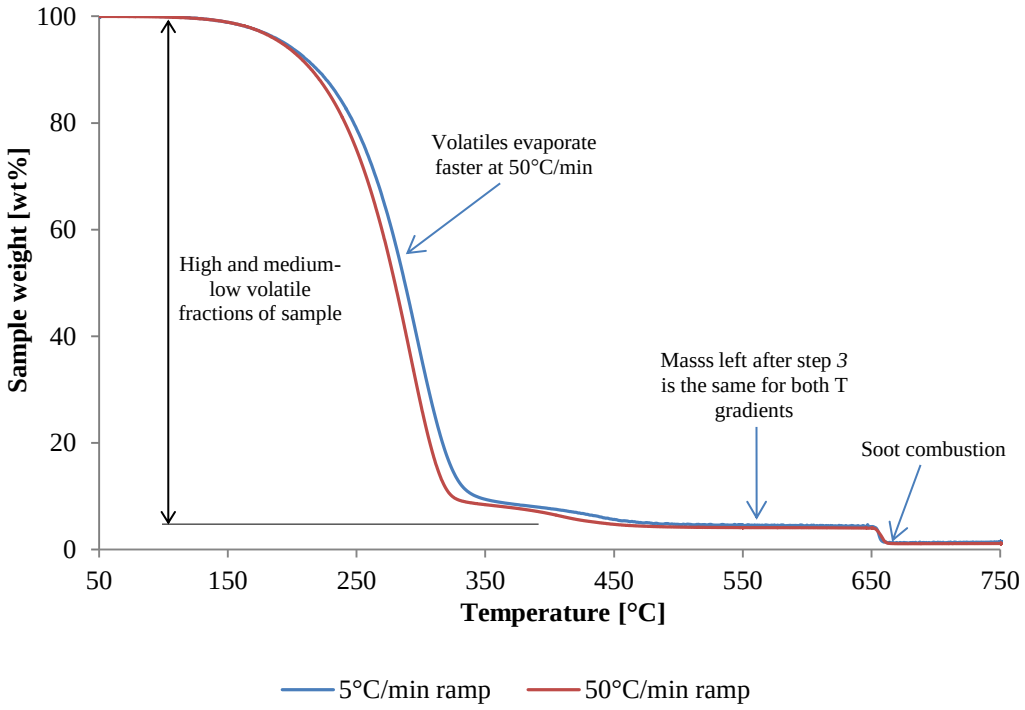

Figure 3.3: TGA mass loss profiles for sample 9 of Table 3.1, tested at two different heat ramps (step *3* from Table 3.2).

Between 320°C and 480°C a mass loss of approximately 6 wt%, with a slower mass loss gradient, was observed in all the samples analysed. As TGA is a non-specific technique which only measures the mass loss as a function of temperature and time, the nature of the compounds loss in this temperature range could not be directly identified. Instead, a clean diesel engine oil sample of Texaco Havoline 5W-30, used as test reference oil was analysed using the same methodology in order to assess if a mass loss in the same temperature range was also observed. Results shown in Figure 3.4 clearly indicate that the same mass loss is also present in the clean oil. This allowed the author considering this as due to the oil rather than due to a possible soot oxidation/pyrsolisation prior switching to air. Furthermore, analysis of the clean oil confirmed that no mass loss occurred after switching from nitrogen to air. This confirmed that the step observed on used oil is due to the oxidation of the carbonaceous soot particles.

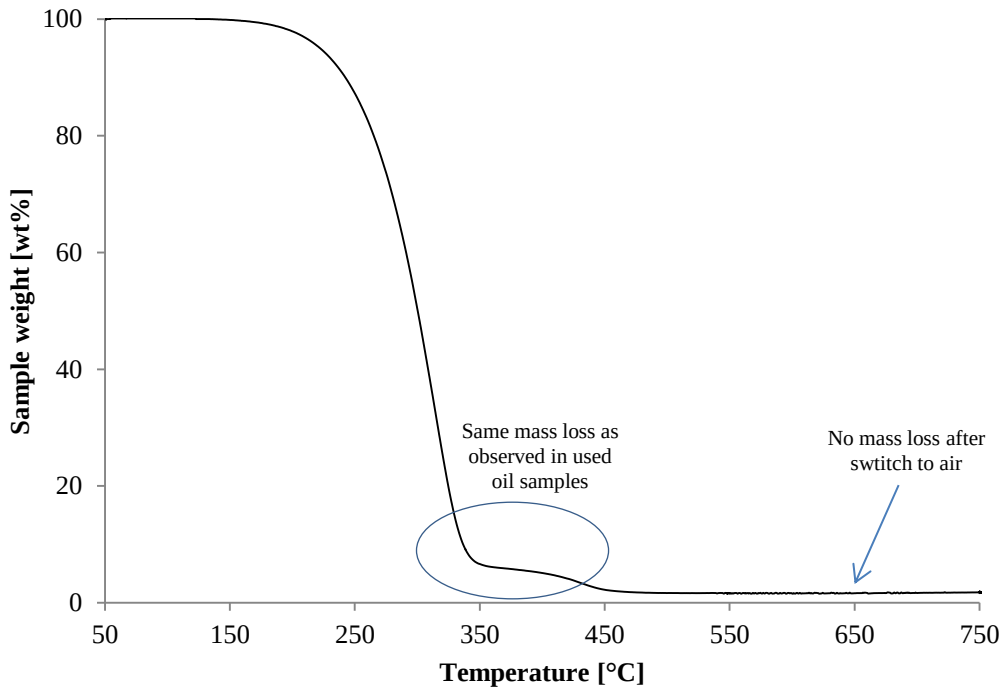

Figure 3.4: TGA mass loss profile of the clean diesel engine oil, Texaco Havoline 5W-30.

A further variation from the standard method was to increase the initial purging time in nitrogen, Step *2* from Table 3.2, from one to fifteen minutes. This was done in order to ensure an oxygen-free environment within the furnace, avoiding thus the oxidation of the soot fraction before the complete evaporation of the volatiles components. Bredin et al. [70] suggested an initial purging time of sixty minutes. The author conducted tests at two different purging times: fifteen and sixty minutes. As shown in Figure 3.5, the mass loss profiles indicated that fifteen minutes was a sufficient time to establish an oxygen free environment.

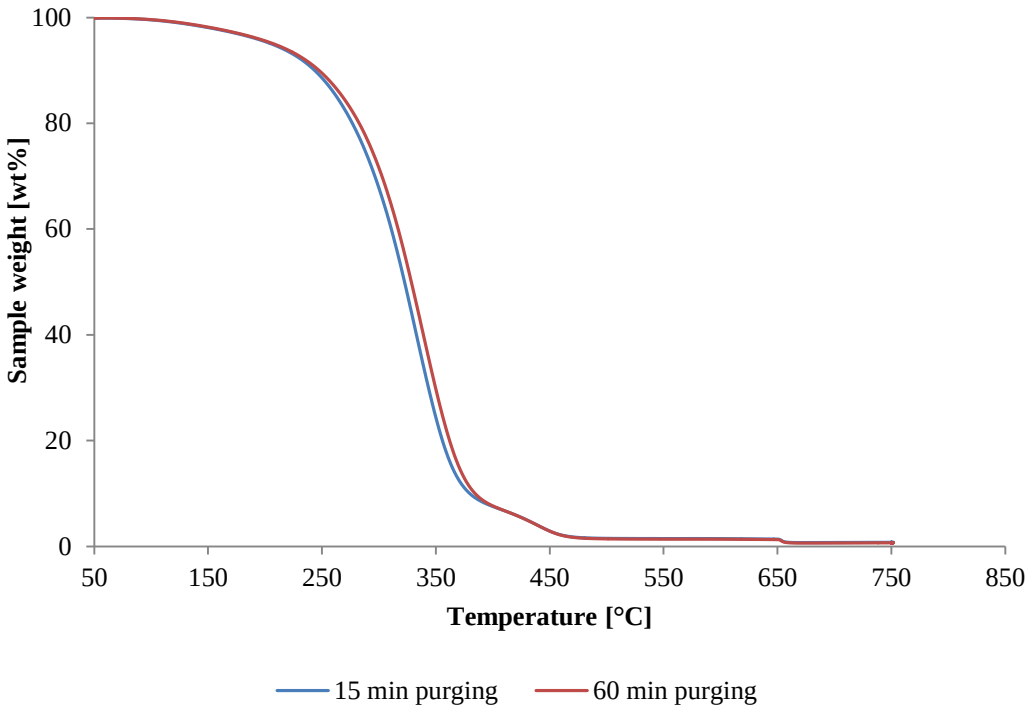

Figure 3.5: TGA mass loss profile for sample 3 of Table 3.1, tested at 15 minutes (blue) and 60 minutes (red) purging times.

To ensure that the samples analysed were representative of a homogenous oil-soot mixture within the sample container, tests at three different deep locations were conducted, i.e. bottom, middle and top. Results indicated that the difference between the three collection points was approximately 0.02 wt%. This value is of the same order of magnitude as the standard deviation obtained from the fifteen samples analysed, indicating that the samples were homogeneously distributed and that the collecting location is not likely to have affected the results.

Finally, the repeatability of the measurement was investigated by testing the same oil sample five times. In Figure 3.6 and Figure 3.7 the five thermograms for Sample two of Table 3.1 are shown. The repeatability throughout the experiment was very high. In Figure 3.7, the detail of the oxidation process indicates that the amount of soot measured is almost identical for all five repetitions: the amount of soot as a percentage in weight for Sample 2 was 0.743 wt%, with a standard deviation of 0.019 wt%. Due to the high repeatability, in order to reduce the testing time, it was chosen to test each sample three times.

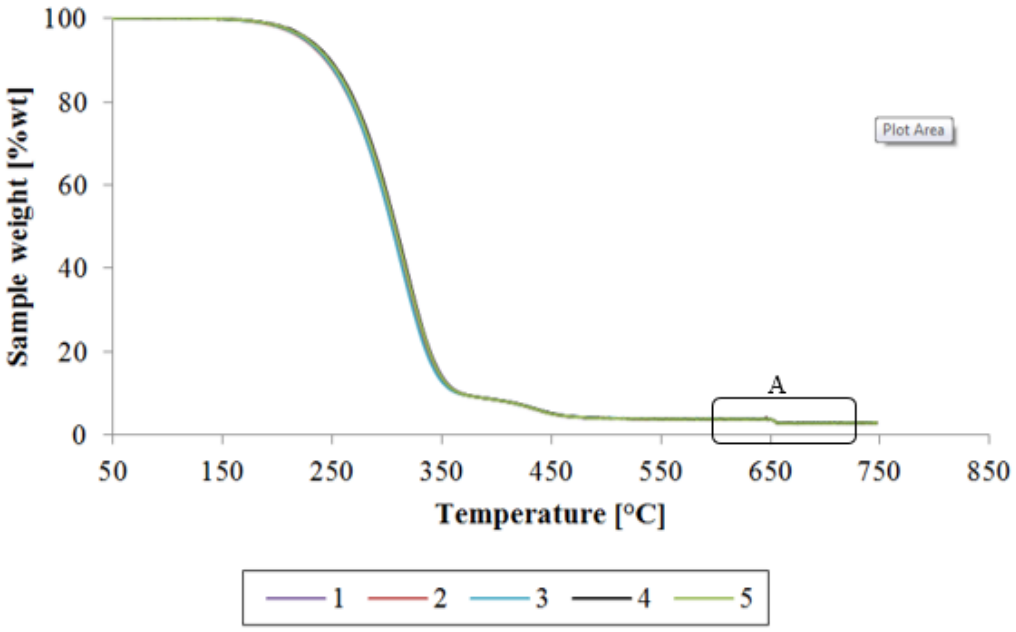

Figure 3.6 TGA mass loss profiles for sample 2 of Table 3.1, tested five times in order to assess repeatability.

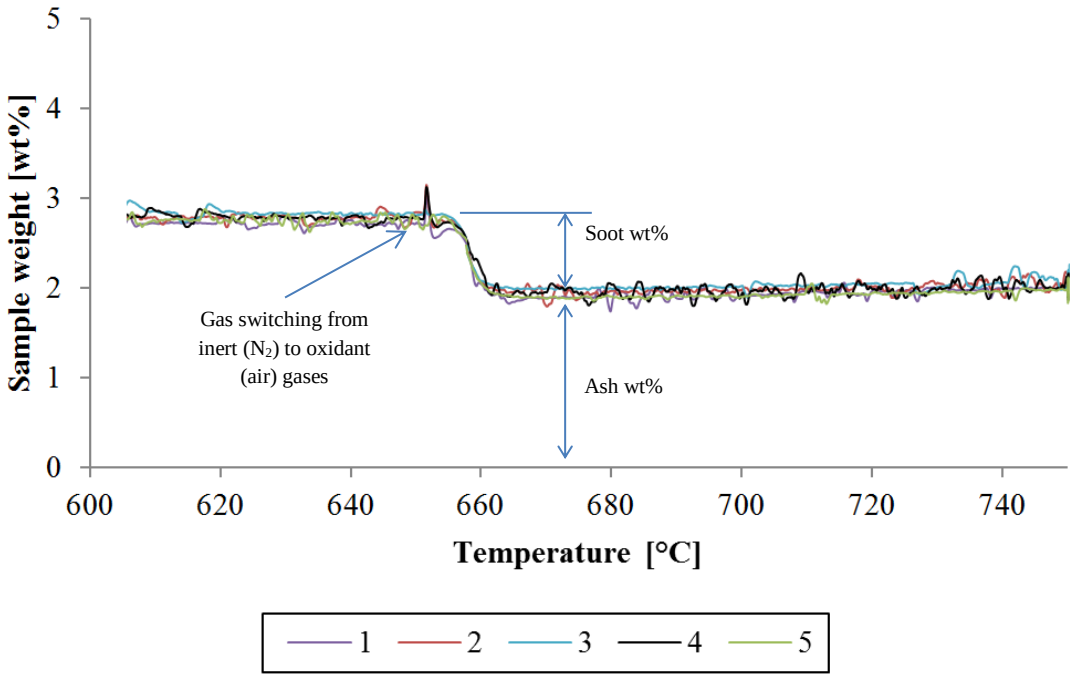

Figure 3.7: Particular A from Figure 3.6, showing details of the soot oxidation process for Sample 2 of Table 3.1.

3.2.2 Amount of Soot-in-Oil from TGA

In Figure 3.8 the concentration of soot-in-oil (wt%) is shown as a function of the oil age, as indicated by the vehicle miles travelled since the last oil change. Of the fifteen oil samples, nine were collected from engines meeting Euro IV regulation and six from Euro V engines. Oil samples from Euro VI engines were not collected as these engines were not yet introduced in the market at the time of the investigation. Results given in Figure 3.8 show soot concentration increases fairly linearly with distance travelled since oil change.

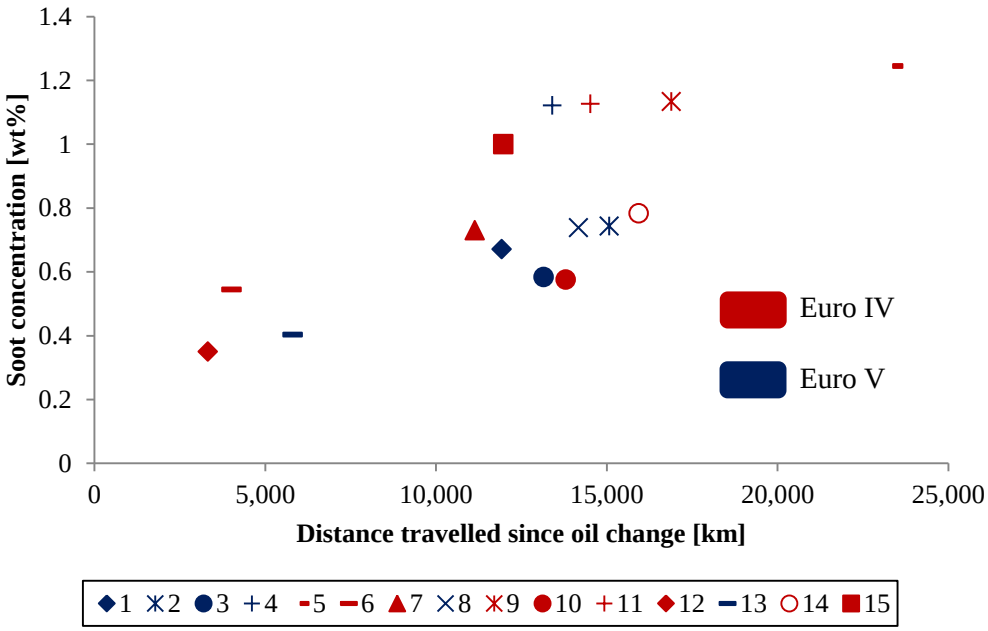

Figure 3.8: Soot concentration measured by TGA for the fifteen oil samples of Table 3.1.

In Figure 3.9, results have been normalised to define values of soot concentration after 15,000 km, which was found to be approximately the average oil drain interval period. The standardisation to a given distance, assumes that the amount of soot deposited into oil increases linearly with mileage. Lockwood et al. also reported a continuous increase of the amount of soot with time [52]. The average concentration of soot-in-oil over 15,000 km for the fifteen samples analysed is 1.0 wt% (0.4 wt% StD), with values ranging from 0.6 wt% to 2.0 wt%.

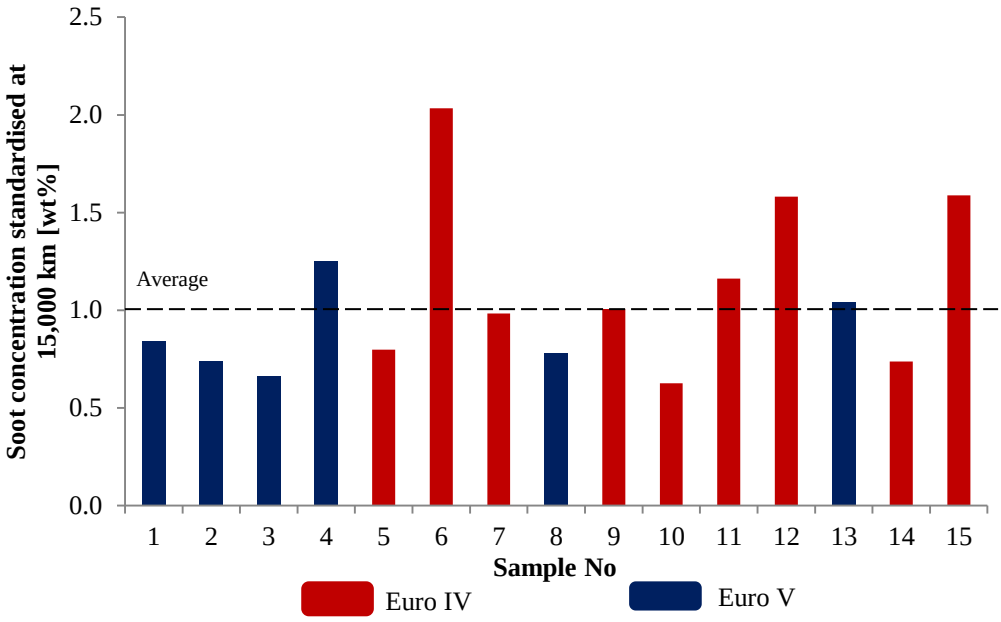

Figure 3.9: TGA results from Table 3.1 standardised at 15,000 kilometres.

The measurement of the soot concentration in oil (wt%) permits the estimation of the quantity of soot deposited into the oil sump ($m_{s,TGA}$). This can be calculated as in Equation 3.1, and results are reported in Figure 3.10:

$$m_{s,TGA} = wt\% \cdot m_{oil\ sump} \qquad 3.1$$

Where $m_{oil\ sump}$ is the mass of soot-laden oil in the sump. The sump oil capacities for the fifteen samples investigated were taken from the vehicle's specifications [84]. Equation 3.1 is based on the assumption that the soot particles, due to their small size, i.e. typical size between 100 and 200 nm as found from the investigation discussed later in the chapter, are not trapped by the oil filters. The standard oil filter equipped on light-duty diesel vehicles is a full-flow type, in which all the oil delivered to the engine passes through the filter. To ensure the required oil flow volume, these filters require relatively coarse meshes, with a typical minimum opening of 5-10 μm. This is about one hundred times larger than the typical soot particle size. Naitoh et al. [85] reported a soot trapping efficiency for a full-flow filter of approximately 5%.

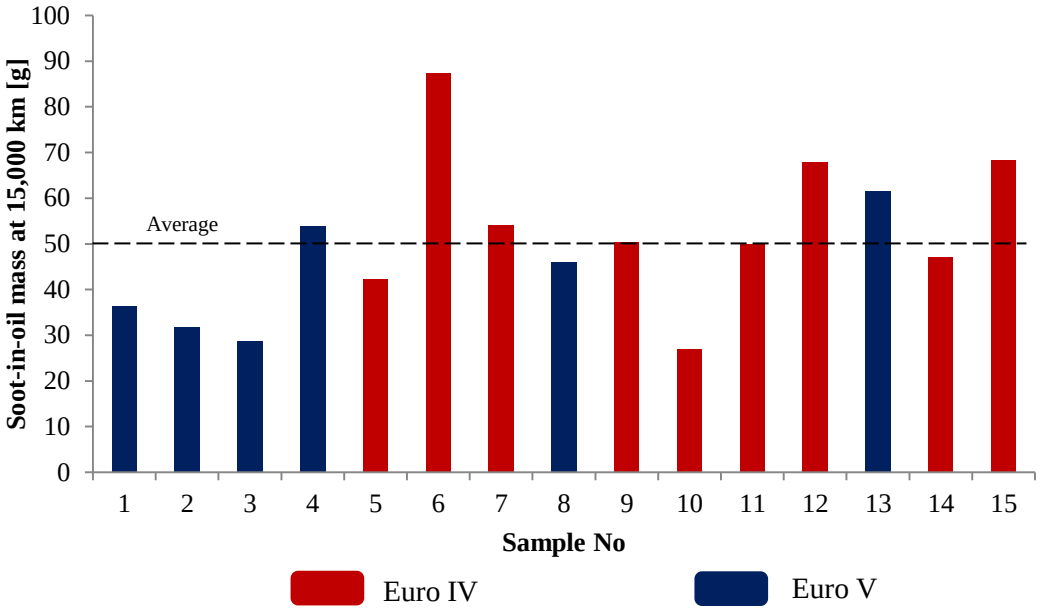

Figure 3.10: Estimated mass of soot-in-oil for the fifteen oil samples of Table 3.1 standardised at 15,000 kilometres.

Due to the similar oil sump capacity over the samples investigated, Figure 3.9 and Figure 3.10 have a similar profile. The average mass of soot entrained into oil after 15,000 km is 50 g, which leads to a rate of deposition of approximately 3.6 mg/km. The rate of deposition could not be compared with other results from the literature, as this represents the first measurement of soot-in-oil from several oil samples collected at the time of oil change from light-duty diesel engines.

3.2.3 Rate of Soot Deposition and Fraction of Fuel in Oil as Soot Particles

As mentioned earlier, the final goal of the TGA investigation is to obtain values representative of real-world driving conditions for comparison with the results from the analytical deposition work discussed in the next chapters of this thesis. Two different approaches are followed. First, via obtaining a rate of deposition expressed in terms of amount over time, and second, by estimating the fraction of fuel entrained into the oil as soot particles. The main challenge is that, due to the source of the samples analysed, information on engine conditions, driving behaviour, engine technology and calibration strategies were not available. This limits what could be drawn from the results, on what influence variables such as

engine capacity and power, Euro rating and oil mileage have on the accumulation of soot.

The rate of soot deposition, $\dot{m}_{s,TGA}$ [mg/h], from the fifteen oil samples was calculated by assuming an average vehicle speed [km/h], as shown in Equation 3.2. The vehicle speed is estimated from the New European Drive Cycle (NEDC) [86]. The vehicle speed profile over the NEDC is shown in Figure 3.11. The first part of 780 seconds is made up by four repeats of an urban driving cycle of constant acceleration and deceleration that are representative of city driving. The maximum velocity reached is 49.5 km/h, with an average speed of 14.5 km/h. The second, extra urban part of the test represents higher speed driving on motorways. It covers 6.9 km at an average speed of 62.5 km/h with a maximum velocity of 120 km/h with around 50% steady-speed driving and the rest involving acceleration. The vehicle speed used throughout the calculation, 33 km/h, is the average between the urban and extra-urban parts of the cycle, representative of combined driving condition. Although the acceleration achieved during the NEDC cycle are well below that of a typical mid-range passenger car during real world driving conditions [16, 87], the range of vehicle speeds well compared with the typical vehicle speeds in Nottingham area, which is reported to be 30 km/h [88, 89].

$$\dot{m}_{s,TGA} = m_{s,TGA} \cdot Vehicle\ Speed \qquad 3.2$$

The rates of deposition derived from the TGA investigation are shown in Figure 3.12. The average rate of soot deposition over the 15 samples tested is 110 mg/h, with a standard deviation of 35 mg/h. This value is used in Chapter 6 as reference value for the typical soot-in-oil deposition rate from a light-duty diesel engine under combined driving conditions. The average rate of deposition for the Euro IV engines was estimated to be 113 mg/h, against 100 mg/h of the oil samples collected from Euro V diesel engines. Although the number of samples tested was relatively limited, the comparison between the Euro IV and Euro V results clearly did not follow the imposed reduction in PM emissions, where the PM values were reduced by over 80%. This indicates that the more stringent PM values of the

Euro V regulation are achieved outside the combustion chamber, via the after-treatment system.

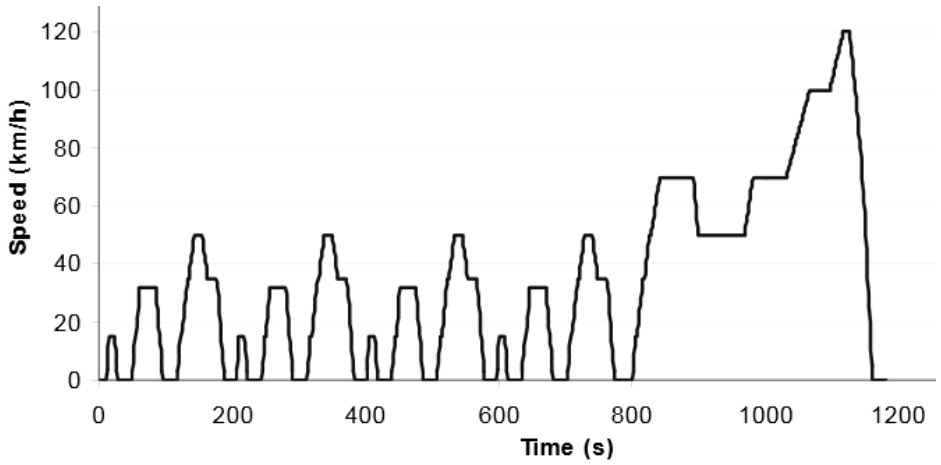

Figure 3.11: The NEDC speed profile [86].

The calculation of the fraction of fuel converted into soot and entrained into the oil required the knowledge of the fuel consumption. This was necessary to estimate the amount of fuel consumed during the distance travelled by the vehicles between oil changes. As the data was not available, this was assumed to be equal to that calculated over the NEDC cycle. Values of fuel consumption for the fifteen samples tested were taken from government data and are listed in Table 3.1 [81]. Those from L/100km were converted to mg/km to match the TGA format results. The diesel fuel density used for the calculation was 837 kg/m^3 [90]. The percentage of fuel converted into soot and transferred to the oil sump is also shown in Figure 3.12. Values vary from 5.3 x 10^{-3}% to 1.6 x 10^{-2}%, with an average of 7.9 x 10^{-3}% and standard deviation of 2.6 x 10^{-3}%.

Results presented in Figure 3.12 are based on the assumptions that the data on fuel consumption from the NEDC test are representative of real world conditions. Mock et al. [87] reported that real world fuel consumption can be between 7% and 30% higher than that reported from the NEDC test. A higher value of fuel consumption will reduce the soot-fuel ratio by the same factor reported by Mock et al. [87], with the consequence that the calculated value could overestimate the fraction of fuel in oil as soot by up to 30%.

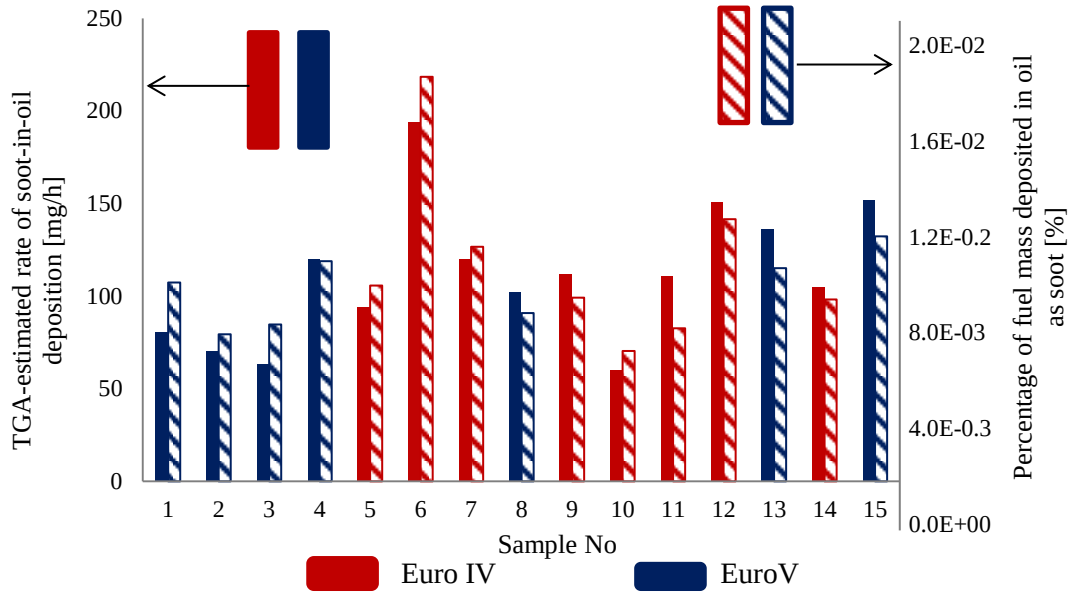

Figure 3.12: Rate of soot-in-oil deposition estimated from TGA results (Filled columns). Percentage of fuel mass transferred to oil as soot mass (pattern fill).

Finally, typical outcomes from an NEDC test are also the PM, NO_x, CO and HC values. Some of these are reported in Table 3.1. However, the values of PM, NOx, CO and HC are tailpipe measurements, and as previously discussed in Chapter 1, these are not representative of in-cylinder conditions due to the influence of the after-treatment system. Consequently, the amount of soot estimated from the TGA investigation, could not be compared with pollutant emissions calculated over the NEDC.

3.3 NTA Investigation

As discussed in Section 2.6.2, TEM and DLS are the most commonly used techniques for determining the size distribution of nanoparticles in liquid suspensions. However, due to the large number of samples investigated and due to the polydispersed nature of the samples, both techniques were considered to be inappropriate for this study. Instead, the NTA method was used throughout the investigation to estimate the soot particle size distribution of the fifteen oil samples.

3.3.1 NTA Methodology

NTA, similar to DLS measures the soot particle size as hydrodynamic diameter from the particle Brownian motion using the Stokes-Einstein equation. A focused laser beam illuminates the particles in suspension, and light scattered from each particle is visible through magnified optics fitted to a Charge-Coupled Device (CCD) camera that records the Brownian motion of each particle. The dedicated NTA software identifies and tracks the motion of every particle recorded by the camera. Results are, therefore, particle by particle number-based, unlike DLS that produces an intensity distribution which is then converted to a volume distribution. This eliminates the problem of measuring particle size distribution on polydispersed samples. Furthermore, compared to TEM, this technique has the advantage that data acquisition can be as fast as one minute, allowing high data acquisition at relatively low cost.

The instrument used for the NTA investigation is the Nanosight LM14. The instrument shown in Figure 3.13 consists of a temperature-controlled viewing unit mounted on a modified microscope stage.

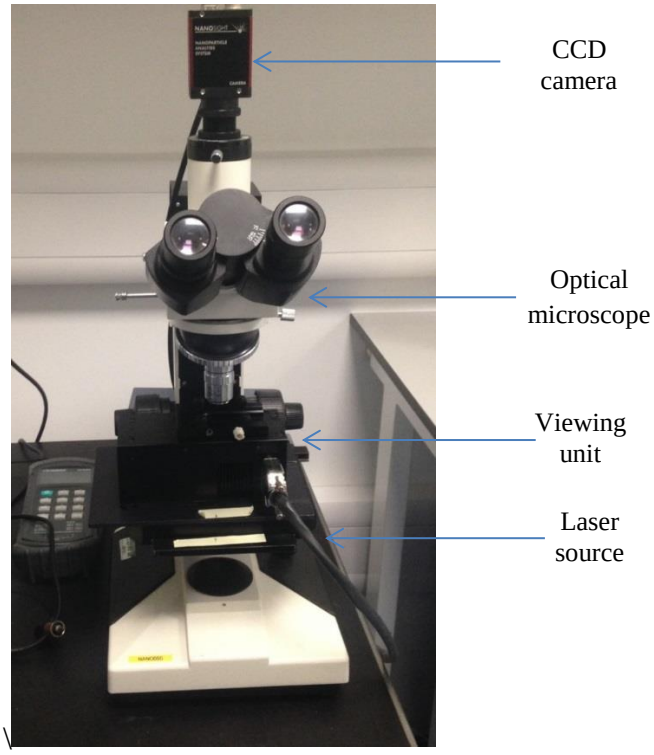

Figure 3.13: Nanosight LM14 instrument used throughout the NTA investigation.

The unit includes a sample chamber of 0.25 ml volume and a laser source that illuminates the scatter of the moving particles moving under Brownian motion. These scattered particles are then seen as small dots by the optical microscope via an X20 objective. Mounted on the microscope is a CCD camera that captures the video of the moving particles at a frequency of 30 frames per second. The image is transmitted to a PC running the NTA V3.0 software, from where the video then is analysed and the main parameters set.

The method followed to obtain the soot-in-oil size distribution is schematised in Figure 3.14. The main sequences are: sample preparation, the video capture, the video pre-process and the video analysis.

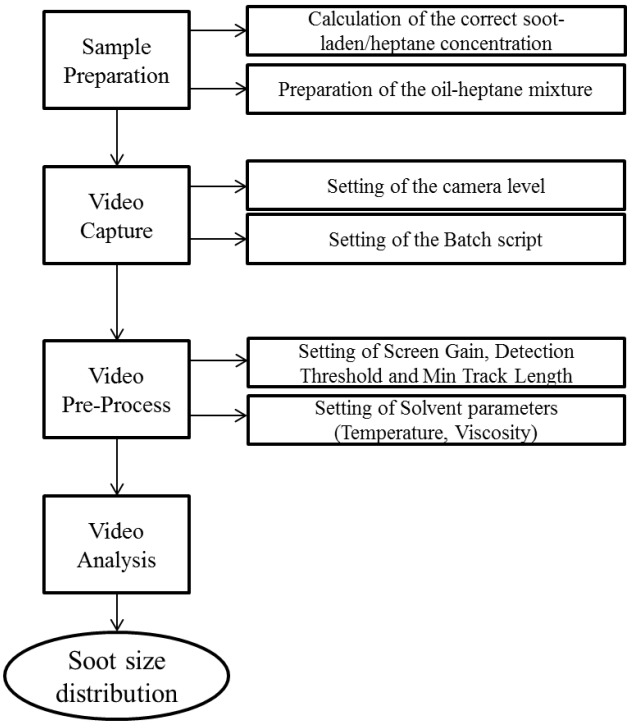

Figure 3.14: Schematic of the NTA experiment methodology.

The sample preparation required the dilution of the soot-laden oil into heptane. This was necessary as the high viscosity of the oil reduces the Brownian motion of the particles, preventing thus, the hydrodynamic diameter from being determined. The oil dilution ratio is an important parameter for ensuring reliable and repeatable results. As suggested by Malloy et al. [91], a particle concentration

of 10^5 to 10^{10} particle/ml is needed in order to balance the requirement between minimum number of particles tracked and particle track lengths. The effect of the number of valid tracks on the mean particle size measured is shown in Figure 3.15, where the same oil sample has been analysed at different concentration ratios. It was found that in order to obtain results independent from number of tracks, a minimum of 4,000 valid tracks was required. Samples too low concentrated did not allow to track enough particles while, on the contrary, samples too concentrated contained too many particles crossing each other preventing thus the software from tracking them correctly. As the concentration of soot in the oil for the fifteen samples changed from sample to sample, the oil-heptane dilution ratio had to be varied accordingly. An empirical correlation able to determine the ideal dilution ratio as a function of the TGA-calculated concentration was developed and used throughout the work:

$$\frac{4.7}{wt\%} = \frac{1\ [\mu l_{oil}]}{25\ [ml_{heptane}]} \qquad 3.3$$

Dilution concentrations were in the range of 10^{-5} to 10^{-4}, which resulted in between 3.5 and 13 μL of oil diluted in 25 ml of heptane. The small amount of oil needed for obtaining a minimum of 4,000 valid tracks permitted to consider the oil-heptane mixture as solely constituted by the solvent.

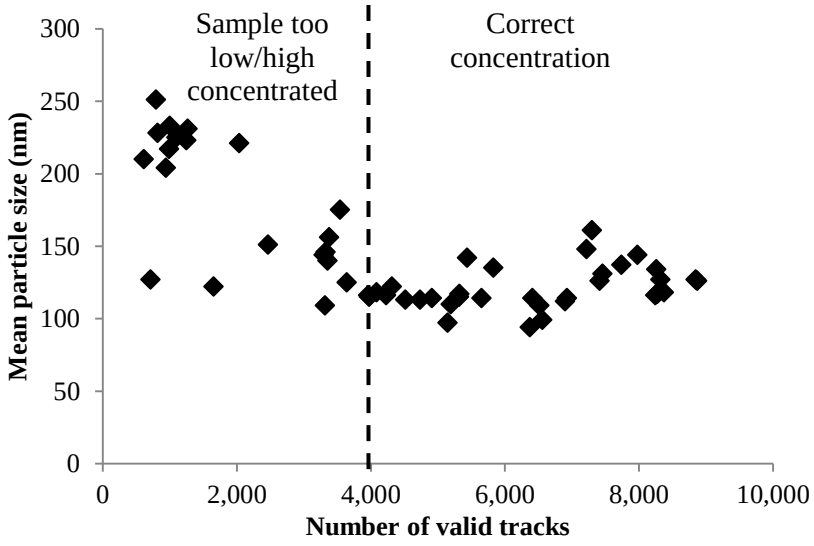

Figure 3.15: Number of valid tracks for the same oil sample diluted at different oil-heptane concentrations ratio.

Once the sample preparation was completed, approximately 1 ml of the mixture was loaded into the sample chamber. The laser was then turned on in order to illuminate the moving particles. During this step it is fundamental to avoid the presence of any air bubbles within the sample chamber as these may cause some degree of specular reflection on the laser beam of the bubble surface. It was observed that due to dilution in heptane, the loaded sample was becoming unstable after approximately 20 minutes due to solvent evaporation, producing thus low quality recording. Each batch was then used for no more than 10 minutes. The focus of the instrument was set on a location where the soot particles are present and well illuminated by the laser beam. Before capturing the video it was necessary to set the camera level to adjust the brightness of the image and set the recording time (60 seconds, for a total of 1,800 frames). The software allows recording multiple videos (batch) in order to increase repeatability and reduce statistical errors. Typically five videos per batch were recorded. This procedure was repeated for three batches of the same sample in order to obtain a total of fifteen records. Between each batch the sample chamber was cleaned with water and heptane in order to remove any traces of oil and soot left from the previous experiment.

The data obtained was then analysed using the NTA V3.0 software. Parameters such as screen gain, detection threshold, minimum tracking length and heptane dynamic viscosity, were set up prior to analyse the videos. A dynamic viscosity of 0.4 mPa·s (n-heptane at 20°C) was used throughout the investigation [92]. Once having selected the appropriate image settings, each particle is identified and its path followed on a frame by frame basis throughout the recorded video. The mean squared displacement is resolved for all the period for which the particle is visible. The tracked paths are considered valid and taken into account for the calculation only if the trajectories are successfully followed for at least 10 frames. If the particle is not visible, or cross the path of another particle before the threshold frame limit, the trajectory is discounted. It is important to mention that the white dots shown in top-right hand side of Figure 3.16 are not the soot particles, but are the scattered light of the particles from the laser beam magnified by the X20 optical microscope and tracked by the NTA software. As a consequence, higher

resolutions are not required for the calculation, and a standard resolution of 1680x1024 pixels is used for the acquiring particle distribution. Finally, the NTA software measures the diffusion coefficient of the particles (D from Equation 2.1 representing the mean squared displacement), and from the Stokes-Einstein equation calculates the hydrodynamic diameter of the particle [93]. The assumption of considering the particle to be spherical is valid if the particle asymmetry does not exceed an aspect ratio greater than three. As reported in [25], soot particles are well below this value and the assumption can be considered valid.

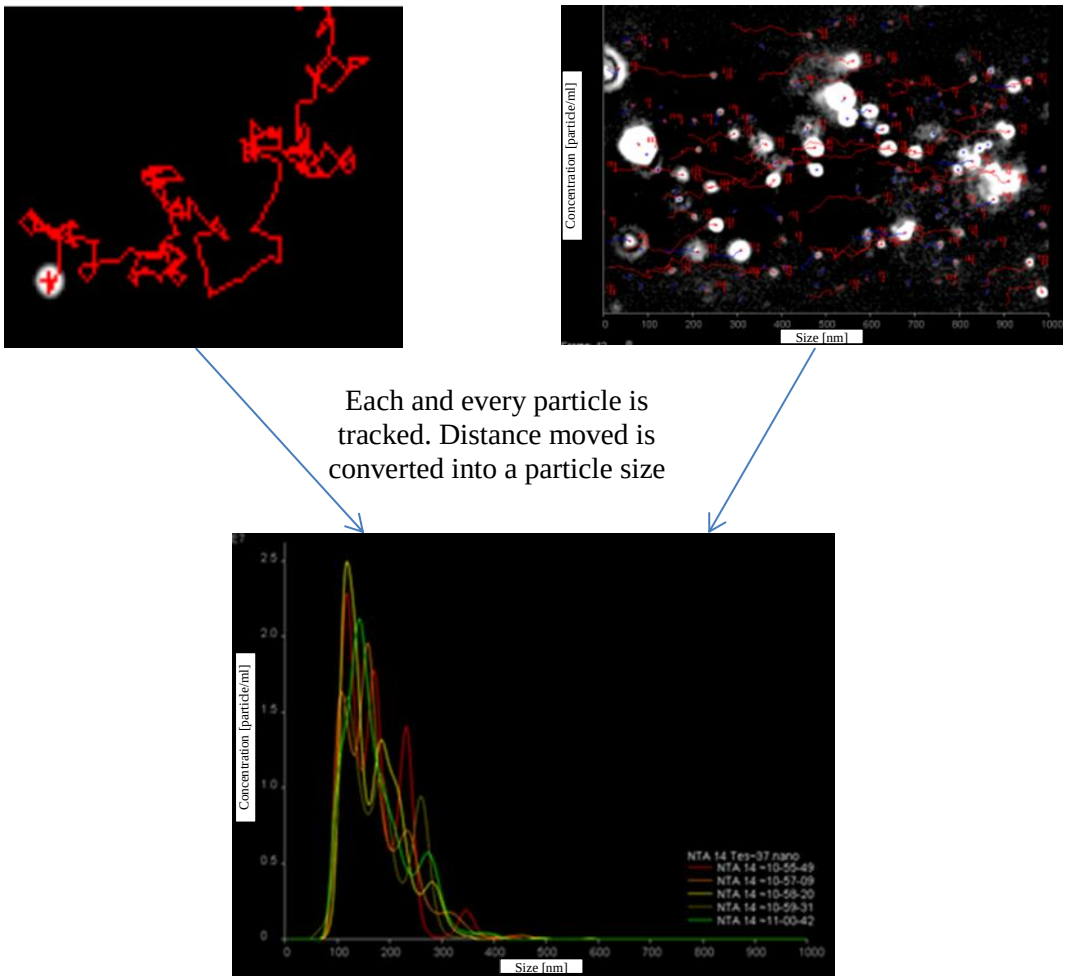

Figure 3.16: NTA video capturing steps. White dots on the top-right hand side represent light scattered from the particle by the laser beam, magnified by a optical microscope with X20 magnification level.

3.3.2 Validation of NTA Results against TEM and DLS Results

The NTA technique, developed in 2006, has become an accepted tool for evaluating particle size in liquid samples from 10 to 1,000 nm, especially in the medical and pharmaceutical fields. However, when this work was initiated, the technique was not yet used for determining size distribution of soot particles dispersed into oil; the author applied NTA to oil samples drained from diesel engines for the first time [1, 2]. Due to the novelty of the investigation, results were verified against common techniques, such as TEM and DLS.

This section is intended to only provide main results of the comparison between NTA, TEM and DLS. Details on the oil samples and sample preparation for each of the techniques can be found in the two articles published from this work [1, 2].

The NTA validation against TEM and DLS was performed prior conducting the investigation on the fifteen oil samples collected at the end of service interval and used throughout the thesis. The fifteen oil samples were collected and analysed only after having established the NTA capability both in terms of quality, cost effective and time.

The oil sample used to verify NTA results was instead drawn from a single cylinder variant of a multi-cylinder HPCR DI diesel engines meeting Euro 4 emissions requirements. The engine was installed on a test bed and filled with clean SAE 5W/30 lubricating oil at the start of a 10 day period during which the engine was run daily for typically three hours. The results from the three techniques investigated are shown in Figure 3.17 and Figure 3.18. For simplicity, the NTA results have been presented in the same figure as an average of the 10 batches. Results from the three methods are also summarised in Table 3.3.

Unlike NTA and DLS which measure the hydrodynamic diameter of the particle, TEM allows measuring the particle size as a two-dimensional projection of the agglomerate. La Rocca et al. [25] suggested that measuring the skeleton length of the agglomerate, provides a more appropriate characterisation of soot-in-oil. TEM results are therefore expressed in terms of skeleton length. The particle skeleton length was measured using an open architecture image processing program, ImageJ.

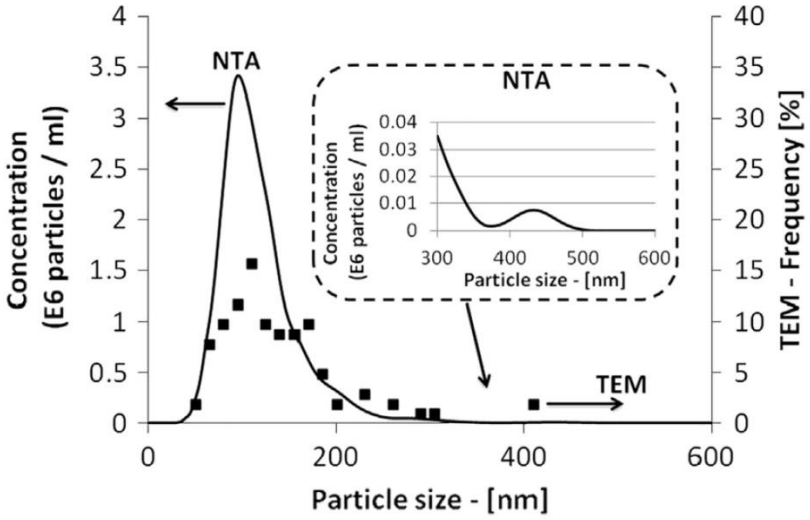

Figure 3.17: Particle size distribution results from NTA (continuous line) and TEM (square marker) techniques. Oil sample collected from HPCR single cylinder diesel engine [1, 2].

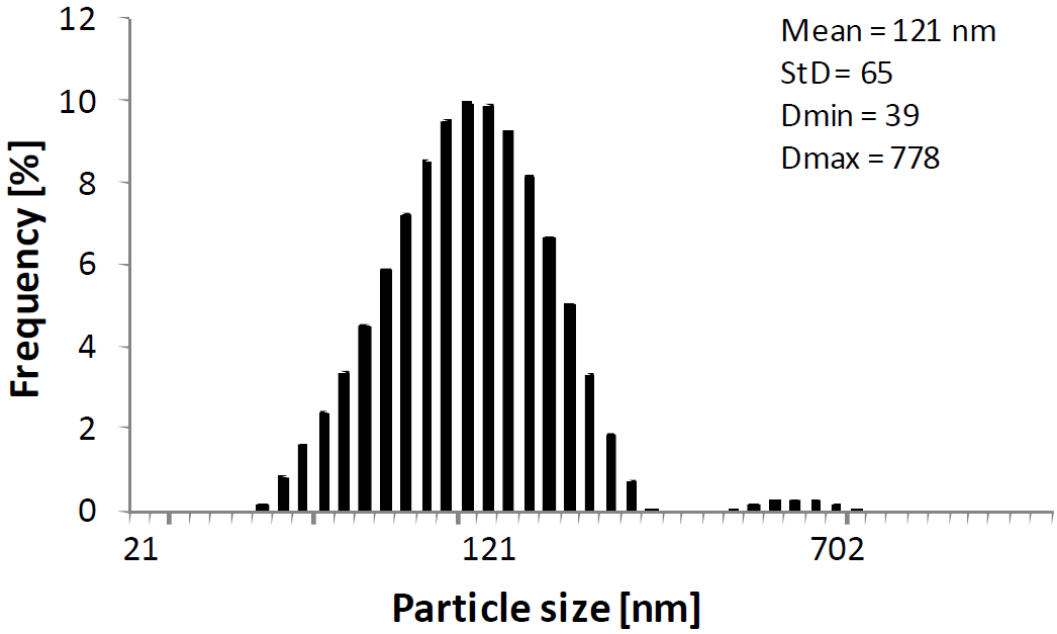

Figure 3.18: Particle size distribution results from DLS technique. Oil sample collected from HPCR single cylinder diesel engine [1, 2].

Oil sample	Measurement technique	Mean [nm]	Mode [nm]	Standard Deviation [nm]
HPCR Single Cylinder	NTA	118	98	41.5
	TEM	132	110	57.8
	DLS	115	109	35

Table 3.3: Comparison of measured particle size and statistical data from NTA, TEM and DLS techniques [1, 2].

The three techniques showed similar results. Both NTA and TEM reported soot particles in the 35-45 nm range, accounting approximately for 2% of the total present in the sample analysed. The smallest particles detected by DLS were instead 39 nm in diameter and accounted for 0.5% of the total percentage available in the sample analysed. The lack of particles below 40 nm may be due to the fact that the intensity of the scattered light is proportional to the sixth power of the particle size, and therefore the presence of large particles can lead to an underestimation or missing of small particles.

The three techniques showed a remarkable similarity, with most of the particles being between 100 and 200 nm. Also, statistical parameters such as mean, mode and standard deviation, were very similar for the three methods used for the investigation. The comparison confirms NTA as a suitable method to estimate the particle size distribution of soot agglomerates from soot-laden oil samples.

3.3.3 Soot-in-Oil Size Distribution from NTA

In Table 3.4 the mean, mode, standard deviation and 10^{th} and 90^{th} percentiles for the fifteen samples via the NTA technique are listed. The mean particle size distribution varies from 100 nm to 205 nm, with an average value of 155 nm and standard deviation of 60 nm. Similar results were obtained by La Rocca et al. [1, 25] who reported a mean particle size distribution of approximately 130 nm with an HPCR single cylinder.

The mean particle size of each sample is shown in Figure 3.19 as a function of their oil drain interval. The particle size results did not correlate with the oil drain interval period. Oil samples that ran for approximately 20,000 km showed a

similar particle size to those that ran 5,000 km. Also the samples collected after 10,000 to 15,000 km showed scattered results. Similarly, particle size did not appear to be correlated to the amount of soot in oil standardised at 15,000 km either. Results are shown in Figure 3.20 and clearly illustrate the scattering in particle size across the entire range of soot-in-oil quantity.

According to [13] particle agglomeration can occurs in two stages: firstly, during the soot production in the combustion chamber (primary agglomeration), and secondly in the crankcase oil by virtue of van der Waals forces (secondary agglomeration) . Results presented in this work suggest that the size of soot-in-oil particle is representative of the primary agglomeration, with oil mileage weakly or not affecting particle size distribution. The fact that secondary agglomeration was not measured can be due to two reasons: first the bonds for the secondary agglomeration are weak and are repeatedly made and broken. Second, anti-dispersant oil additives may still perform well even at high mileages, avoiding formation of micro-particles.

Due to the nature of the samples, it has not been possible to assess the influence of parameters such as engine load and speed, EGR level or other factors that may have an impact on the particle size and therefore justify the scattered results.

The percentiles values shown in Table 3.4 indicate that on average 80% of the particles are within 100 nm and 235 nm. Soot particles of 20 nm were detected in all the samples although in relatively small numbers. Finally, the maximum particle size measured was between 475 nm and 840 nm; however, for all the samples tested, particles larger than 400 nm represented only 1% of the entire population.

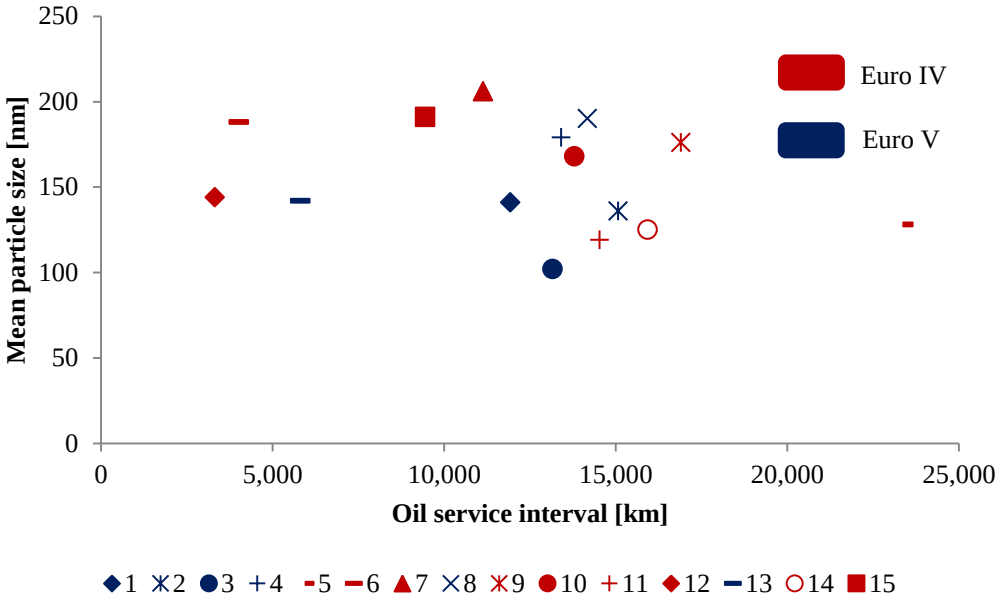

Figure 3.19: Soot particles size distribution for the fifteen samples of Table 3.1 as a function of the oil drain interval.

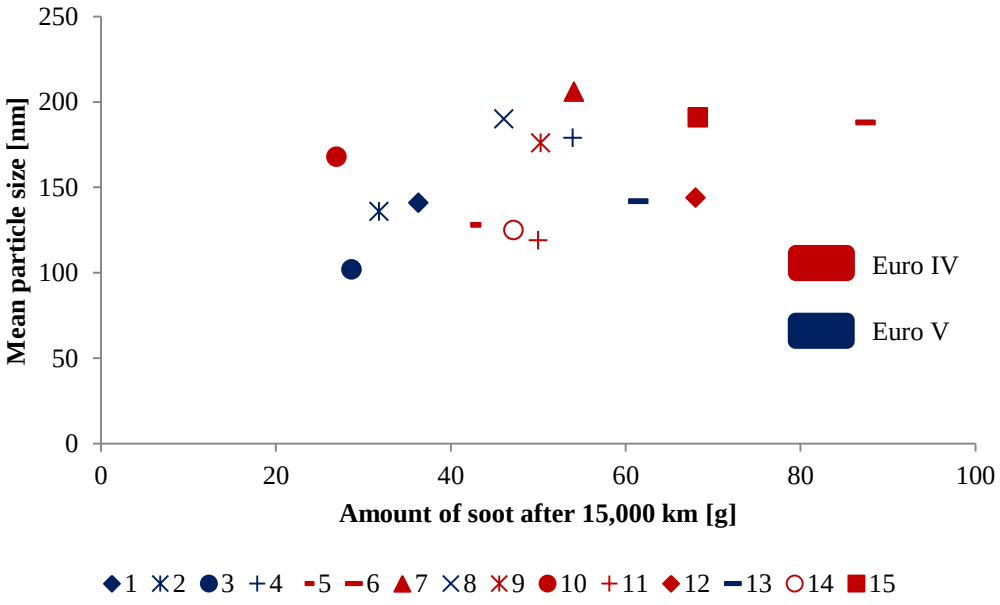

Figure 3.20: Soot particles size distribution for the fifteen samples of Table 3.1 as a function of the amount of soot-in-oil standardised at 15,000 km.

Sample [n]	Oil mileage [km]	Mean [nm]	Mode [nm]	StD [nm]	D10 [nm]	D90 [nm]	Min [nm]	Max [nm]
1	11,925	141	111	50	95	194	7	710
2	15,075	136	104	47	92	194	31	570
3	13,155	102	79	33	72	143	16	475
4	13,406	179	178	57	132	321	10	770
5	23,386	128	93	52	91	187	34	680
6	4,013	188	149	88	112	291	5	740
7	11,136	205	151	72	123	309	33	783
8	14,174	190	133	62	119	276	46	658
9	16,896	176	119	62	106	264	29	712
10	13,797	168	117	53	92	231	14	689
11	14,526	119	98	39	81	164	24	827
12	3,320	144	112	49	96	203	41	770
13	5,805	142	110	50	93	207	24	646
14	15,933	125	96	44	91	185	24	605
15	15,120	191.0	128	64	118	279	22	705
Average	**14,417**	**155**	**115**	**60**	**99**	**236**	**24**	**708**

Table 3.4: Particle size results from NTA investigation. D10 and D90 represent the 10^{th} and 90^{th} percentiles, respectively.

3.4 Discussion and Conclusions

Experimental results obtained with TGA showed that on average, 3.9 mg of soot are deposited into oil per kilometre. This results in approximately 1 wt% or 50 g of soot after 15,000 km. Results could not be directly compared with other researchers' results as to the author's best knowledge this is the first time that the concentration of soot from light-duty diesel engine vehicles driven under real-world conditions is investigated.

Results allowed estimating the amount of time and fuel that would be required to produce an oil sample of similar concentration to those collected from the fifteen vehicles at the time of oil service with a laboratory test engine. Sample 3, which had the lowest soot mass is considered for the exercise. Its amount of soot-in-oil, 29 g, is multiplied by its estimated percentage of fuel mass converted into soot and deposited in oil, $6 \cdot 10^{-3}$%. This gives the amount of fuel required, estimated to be 483 kg for Sample 3. By assuming a value of fuel consumption of 3 kg/h for a typical mid-load engine test condition [94], an engine test time of approximately 160 h is calculated. Both the amounts of fuel and time required to produce a single oil sample with the amount of soot similar to Sample 3, were beyond the capability of the present work. This confirms, that although analysing oil samples collected during regular oil services put limitations on determining the correlation between rate of soot deposition and engine conditions, this approach allows analysing a large amount of samples in a cost-effective way.

NTA analysis, used for the first time to analyse soot-laden oil samples, was proven to be a reliable, repeatable and fast technique. This permitted the analysis of a large number of samples while maintaining the accuracy of more traditional techniques such as TEM, without the drawback of the costs associated to the TEM technique. For example, the analysis of a single oil sample with TEM, requires to obtain approximately 200 soot particles sampled, up to three days of work between sample preparation, microscope analysis and data analysis, raising the costs to approximately £1,000. With NTA, the entire process can be performed in approximately 3 hours at significantly reduced costs compared to TEM. The

major limitation of the NTA technique is that it does not allow the characterisation of particle morphology. However, this was not a concern as the morphology of the soot particles did not fall within the scope of this work.

Despite the wide variety of samples collected during the investigation (ranging from different engine capacities, powers, car manufacturers, as well as different driving conditions), all the samples analysed showed a particle size between 100 nm and 200 nm. Furthermore, for all the samples investigated, the number of particles larger than 400 nm in diameter, was below 1%. These results allowed the author to use an average value from the fifteen oil samples for the thermophoretic velocity investigation discussed in Chapter 5, as representative of the typical particles found into oil.

4 Soot Availability in Regions of Interest for Deposition in Oil

4.1 Introduction

The focus in this chapter is on the influence of operating conditions and level of EGR on the concentration of soot in regions of the combustion chamber likely to contribute to deposition in oil. These regions, depicted in Figure 4.1, are the near-liner for deposition via thermophoresis, and the piston crown-liner corner for deposition in the piston ring pack during blow-by. A range of operating conditions at different engine speed and load, and EGR levels between 0 and 35% have been considered by using a computational and analytical approach. Unlike other studies on soot in oil deposition [3-5], EGR has not only been considered for its effects on the soot formed during the combustion process (In-cycle source), but also taking into account the fraction of soot exhausted from the previous cycle that re-entered the combustion chamber with the EGR gas (Re-cycled source).

The chapter is divided into two parts. In the first sections focus is given to the spatial-averaged in-cylinder soot amount. This is of particular interest for the Re-cycled source, which directly depends on the amount of engine-out soot. The Kiva-3V CFD model and the range of parametric engine conditions used for the investigation are also described. A novelty of the work has been the extension of the period of deposition to the entire engine cycle. Assumptions used to evaluate the loss of soot after EVO are discussed and results presented.

The pre-existing Kiva-3V model developed by [26] and used throughout this investigation, considers EGR only by adjusting the typical intake gas composition without EGR, i.e. 21% of O_2 and 79% of N_2 [95], by performing a mass air flow balance for a closed system. The Re-cycled source was not included in the code, and it has been instead estimated by post-processing output data from a simulation

run, including in-cylinder combustion and emission quantities, inferred from values at EVO.

In the second part of the chapter, results on the distribution and availability of soot in the near-wall and piston crown-liner corner regions are presented and discussed. For each of the two pathways, the contribution from the Re-cycled and In-cycle sources of soot is investigated and compared.

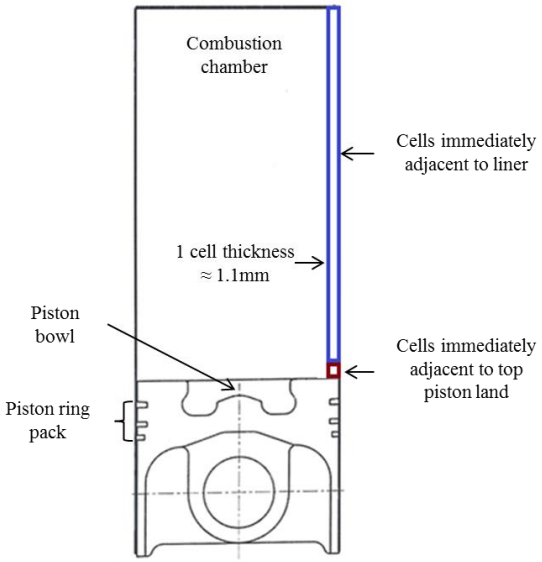

Figure 4.1: Diagram of the regions modelled with Kiva-3V to estimate the amount of soot near to the cylinder wall and above the piston land-liner corner.

4.2 "In-Cycle" and "Re-Cycled" Sources of Soot

The term Exhaust Gas Recirculation refers to the practice of recycling part of the exhaust gas flow by mixing this with the fresh intake air. Due to the higher fraction of carbon dioxide and water vapour of the exhaust gas compared to air, less oxygen is available for the combustion, resulting in a lower effective O_2-fuel ratio which affects the fuel oxidation rate decreasing the flame temperature. In addition, exhaust gas has a higher specific heat compared to air. This increases the gas mixture specific heat by about 1.5% [20], leading to a lower flame temperature. Due to the high sensitivity of NOx formation to temperature, both the lower amount of oxygen and the higher heat capacity of the charge reduce the

NOx formation reaction [96], with the former reported as the dominant reducing mechanism [20]. These conditions, however, promote the formation of soot and reduce the rate of soot oxidation, increasing thus the net amount of soot produced [19]. In particular, this is mainly given to the effects of the lower concentration of O_2 on the rate of soot oxidation [97].

Light-duty diesel engines are commonly equipped with one of the two following types of EGR systems: High Pressure Exhaust Gas Recirculation (HP-EGR), or Low Pressure Exhaust Gas Recirculation (LP-EGR) systems. As shown in the left-hand side of Figure 4.2, the HP-EGR system works at boost pressures. The exhaust gas are extracted upstream to where the turbocharger turbine and the aftertreatment systems are. Before the exhaust gas is mixed with the fresh charge at the intercooler outlet, the gas is cooled down by an EGR cooler. Cooling the hot recirculated gas allows reducing the intake gas temperature, increasing the volumetric efficiency and reducing the peak gas temperature [19]. In a LP-EGR, right-hand side of Figure 4.2, the exhaust gas is extracted downstream to where the turbine and aftertreatment systems are, and it is re-introduced in the intake system before the compressor inlet.

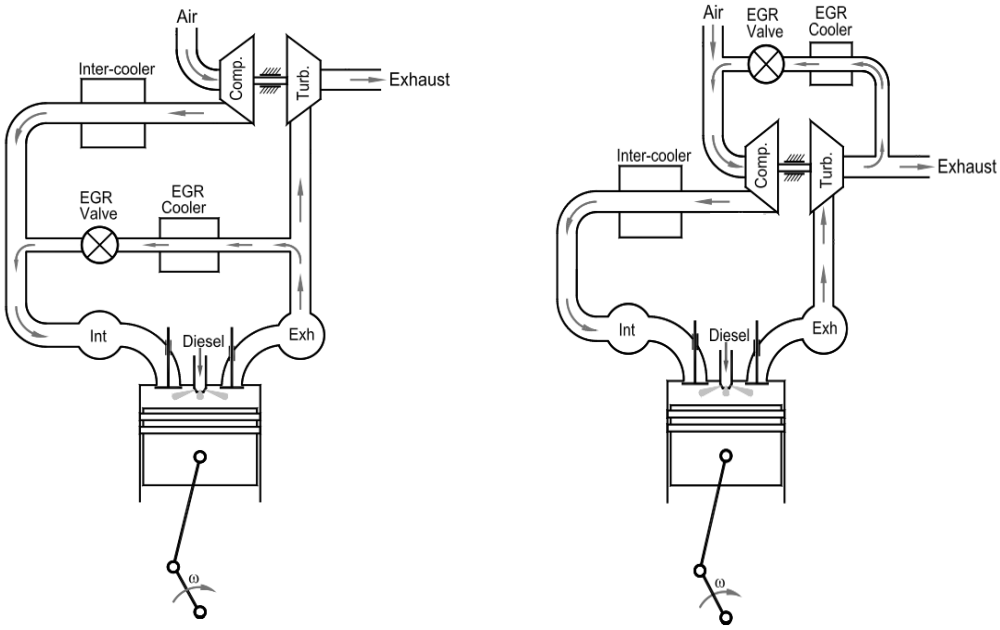

Figure 4.2: Schematics of HP-EGR (left-hand side) and LP-EGR (right-hand side) systems [98].

Nowadays, almost all light-duty diesel vehicles are equipped with HP-EGR systems. This is due to the poor response to load variation, high temperatures at the compressor inlet and insufficient delta pressure across the EGR loop of the LP- EGR line compared to the HP-EGR [99]. Another downside of the low pressure loop is that the compressor is highly sensitive to possible condensation or presence of particulate matter carried within the exhaust gases [100].

A downside of the HP-EGR is that the exhaust gases are extracted upstream the aftertreatment system, including the DPF which is commonly placed downstream the turbocharger turbine. With the return of the "untreated" exhaust gas to the combustion chamber, EGR not only increases the in-cylinder soot concentration by promoting soot formation, but also by reintroducing a portion of the engine-out soot back into the combustion chamber. This is shown diagrammatically in Figure 4.3. As the diesel engine used as a model throughout this thesis was equipped with a HP-EGR system, the contribution on soot-in-oil from both the In-cycle and Re-cycled sources of soot is investigated. The increase of in-cylinder soot concentration from both the In-cycle and Re-cycled sources of soot has been quantified in the next sections of this chapter. The availability of the In-cycle source has been estimated by using CFD results, while the concentration of Re-cycled particles has been calculated by post-processing the results of the CFD investigation.

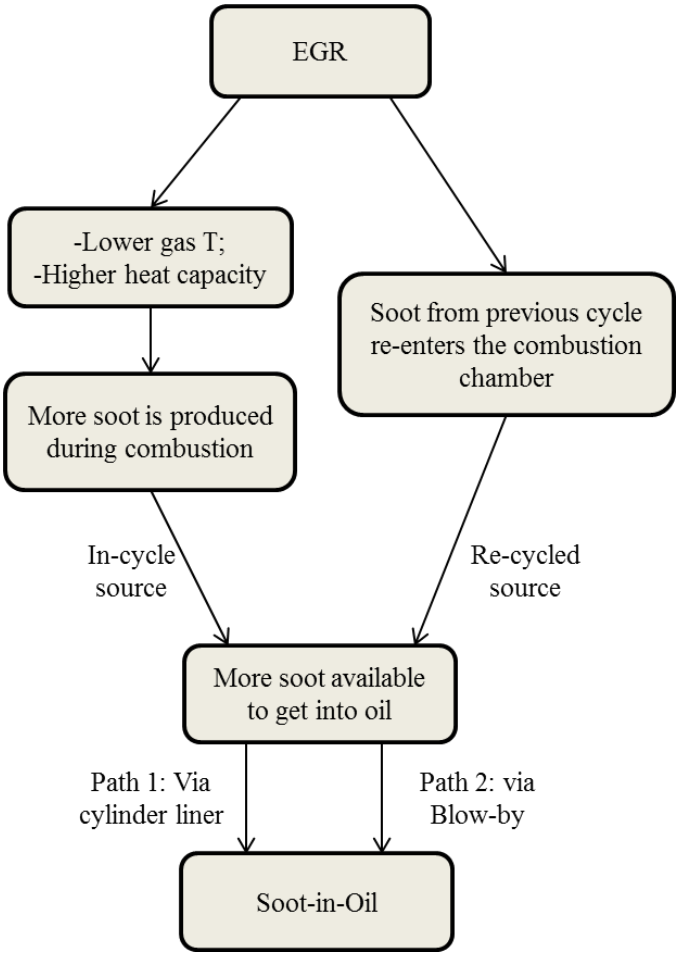

Figure 4.3: Schematic of the effect of EGR on the sources of soot available for deposition into oil.

4.3 Amount of In-Cylinder Soot via Kiva-3V

In the absence of a diesel engine with optical access, CFD was the natural choice for investigating the soot mass and distribution within the combustion chamber and in particular in the regions of interest for deposition into oil. The soot produced during the combustion process and its distribution was modelled using a CFD code. Kiva-3V release 2 was used with the modifications described in [26], which enabled the code to run on PCs using a Linux operating system. Simulations were carried out for the combustion system and injector arrangement of a Ford Puma HPCR light-duty 2.0 L diesel engine. The same model and code have been also used in previous studies [26, 39, 101] carried out at the University of Nottingham. Specifications of the modelled engine are provided in Table 4.1.

Specification	Value
Displacement [cm^3]	2,000
Number of Cylinders	4
Valves per Cylinder	4 (2 Inlet / 2 Exhaust)
Bore [mm]	86
Stroke [mm]	86
Compression Ratio	18.2:1
Swirl Ratio	1.6
Injection System	Denso 7 holes centrally mounted

Table 4.1: Specification of the engine used for the validation of CFD results.

4.3.1 Kiva-3V Sub-models

As shown in Figure 4.4, the combustion system used for the computational study is defined by a mesh describing a 51.4° sector. The assumed symmetry is consistent with the use of the 7-hole (diameter 0.15 mm) injector installed centrally and vertically. A semi-fine mesh with 28,389 cells (typical grid size of 1.11 mm by 1.44 mm by 2.0°) gave grid independent solutions – where further reduction in cell size gave negligible change in results [26] [102]. Ng [26] calculated that a finer mesh with a grid system with 60% more cells in the axial and radial directions, resulted in an improvement in accuracy of below 2% for in-cylinder peak pressure and temperature, and for emission concentrations, such as NO, CO_2 and O_2. These values were computed with a percentage error relative to experimental results of within 6%. Furthermore, increasing mesh accuracy would result in an increase in computational time of approximately 3.5 times. Accordingly, the semi-fine mesh was selected and used throughout the study. The trilinear interpolation technique was used to evaluate velocity vectors, soot, fuel, temperature and pressure, and other parameters within Kiva-3V [102]. The method approximates the value within the hexahedral cell linearly, using data taken from the adjacent cells. As the cell within the computational domain varied in quantity and size with time and location, the identification of the eight corners

of the cells surrounding the interpolated point was performed by a Matlab subroutine. This allowed determining the variables of interest for this study such as in-cylinder gas pressure and temperature, heat flux through the wall, soot mass distribution, at any location and time of interest.

No modifications were made to the fundamentals of either the fuel spray or combustion sub-models in the code, and $C_{12}H_{26}$ was selected as the fuel model to represent light diesel fuel [103-105]. The dynamics of the evaporating fuel spray are described using the Monte Carlo-based discrete particle technique [106, 107]. The model considers the fuel spray as being represented by individual particles each having the same initial temperature, velocity and size. Initial fuel droplet size, calculated in terms of Sauter mean radius, was set equal to the injector hole dimension of 0.75mm. The model used takes into account interaction between fuel droplets including collisions, coalescences and breakup, as well as evaporation. Collisions are accounted for by considering droplet coalescence, when particle velocity is low, and particle grazing, when relative velocity is high. The second type of collisions leads to either the temporary coalescence with also small satellite droplets formed, or separation of droplets, having the same temperature and velocity. Droplet collisions and coalescence are calculated using the discrete element analysis method [26]. Due to the typical high Weber number of diesel fuel spray, droplet oscillation, distortion and break up must be considered. These are described using the Taylor-Analogy Breakup (TAB) model, based on the discrete element analysis [107, 108].

Spray evaporation is considered by calculating the rate of change of droplet size and temperature [26]. The former is determined from the mass transfer from liquid to fuel vapour at the droplet surface. The latter is determined via an energy balance between heat provided to the droplet to heat it up or to vaporise it.

Soot particles, as described in the next section of this chapter, are produced from the competition between the soot formation and oxidation processes. The soot particles produced are assumed to be spherical in shape, and all the soot formed contributes to the growth of the particle being distributed uniformly on the surface of the particle. Coagulation and agglomeration of single soot particles is not taken

into account by the model. This has an effect on the particle size of the computed soot particles as these are treated as primary particles, but not on their spatial distribution or on the mass of soot produced. Particle size did not affect in-cylinder soot distribution as soot particles were treated as massless. Results from NTA in Chapter 3 showed that soot-in-oil particles are mostly on the range between 100nm and 200nm in size, which is similar to size of engine-out soot particles [12]. On the other hand, primary particles have a diameter of approximately 20 nm [25]. Mahmood [102] calculated that soot particles smaller than 400nm can be considered as massless and therefore will closely follow the fluid flow. As both the size range of primary particles and agglomerates can be considered as massless, neglecting coagulation and agglomeration has no influence on the soot distribution in the bulk region of the combustion chamber, which governs the amount of soot available for deposition into oil. In addition it was assumed that particle concentration is lower enough for particulate-particulate interaction to be not considered. Furthermore, as discussed in Chapter 5, soot-in-oil deposition is dominated by particle mass concentration, rather than from particle size distribution, which is in agreement with the mass-based soot formation and oxidation models described in the section of this chapter.

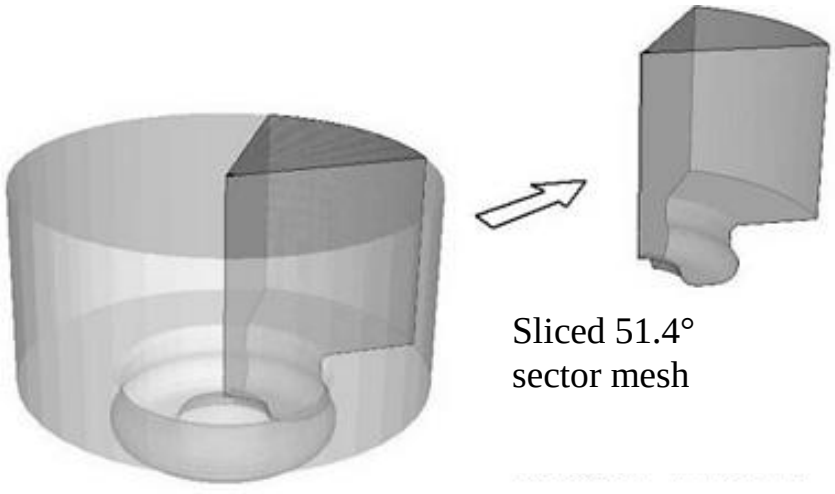

Figure 4.4: Computational mesh of 51.4° representing the sector where modelling takes place.

4.3.2 Kiva-3V Soot Formation and Oxidation models

In diesel engines, the net amount of soot (m_s) is considered as the difference between two processes: the formation, with soot directly linked to the fuel vapour molecules, and the oxidation:

$$\frac{dm_s}{dt} = \frac{dm_{sf}}{dt} - \frac{dm_{so}}{dt} \quad 4.1$$

Soot formation and oxidation processes are evaluated using semi-empirical models consistent with recent literature on diesel engines [109, 110]. For the soot formation model, the standard Kiva-3V release 2 code has been replaced with the Hiroyasu model [111], given by Equation 4.2. The Hiroyasu model is computationally simpler and stated as more robust to uncertainties in user-specified parameters than the standard Kiva-3V model [112]:

$$\frac{dm_{sf}}{dt} = A_f \, M_{fv} \, p^{0.5} \, exp\left(-\frac{E_{sf}}{R \, T_g}\right) \quad 4.2$$

Where p, A_f, M_{fv} and E_{sf} are the gas pressure [bar], a calibration parameter, the mass of fuel vapour [g] and the reaction activation energy, respectively. A value of $A_f = 65$ was used according to measured data [26]. The activation energy $E_{sf} = 5.2 \times 10^4$ [J/mol] was used according to [109, 111].

Soot oxidation is evaluated via the semi-empirical formula for pyrolytic graphite oxidation proposed by Nagle and Strickland-Constable (NSC) [113]. This model is widely used by researchers in diesel engine simulations [109, 110]:

$$\frac{dm_{so}}{dt} = A_{O_2} \frac{M_C}{\rho_s \, D_p} \cdot m_s \cdot \dot{R}_{NSC} \quad 4.3$$

Where M_C is the carbon molar weight (12.011 [g/mol]), D_p the soot diameter and A_{O_2} a calibration factor of value 20 [26]. The net soot oxidation rate, $\dot{R}_{NSC}$, is expressed in [g-atom/(s·cm^2)] and is given by:

$$\dot{R}_{NSC} = \left(\frac{K_A \, p_{O_2}}{1 + K_Z \, p_{O_2}}\right) x + K_B \, p_{O_2} (1 - x) \quad 4.4$$

K_A, K_B and K_Z are rate constants listed in Table 4.2, which are dependent on the gas temperature. p_{O_2} is the partial pressure of oxygen expressed in [atm].

The NSC model is based on the approach that there are two types of sites susceptible to O_2 oxidation attack on the particle surface: the more reactive type A, controlled by the fraction of sites not covered by oxides, and the less reactive type B. Reaction of A sites with oxygen gives a further A site +2CO (Equation 4.5). Type B sites reacting with oxygen are converted into type A sites +2CO (Equation 4.6). Finally, type A sites are converted into type B due to thermal rearrangement (Equation 4.7):

$$A + O_2 \rightarrow A + 2CO \quad 4.5$$

$$B + O_2 \rightarrow A + 2CO \quad 4.6$$

$$A \rightarrow B \quad 4.7$$

x and (*1-x*) from Equation 4.4 represent the proportion of sites covered by A and B respectively, with *x* defined as:

$$x = \frac{p_{O_2}}{p_{O_2} + \left({}^{K_T}/_{K_B} \right)} \quad 4.8$$

With the rate constant Kt also listed in Table 4.2.

Rate Constants	Units
$K_A = 20 \times e^{-({}^{15,000}/_{T})}$	[g/(cm^2 ·s· atm)]
$K_B = 4.46 \times 10^{-3} \times e^{-({}^{7,640}/_{T})}$	[g/(cm^2 ·s· atm)]
$K_T = 1.51 \times 10^{5} \times e^{-({}^{48,800}/_{T})}$	[g/(cm^2 ·s)]
$K_Z = 21.3 \times e^{({}^{2,060}/_{T})}$	[atm^{-1}]

Table 4.2: Rate constants used for the Nagle and Strickland-Constable oxidation model [113].

A limitation of the NSC oxidation model is that it does not take into account the role of OH as oxidiser of soot precursors and incipient particles. Although other authors have shown that oxidation via OH attack plays only a minor role (5-10% of total oxidation [32, 44, 114]), its contribution was also calculated in addition to the NSC model, as given by Equation 4.9:

$$\frac{dm_{so}}{dt} = \frac{M_C}{\rho_s D_p} m_s \dot{R}_{OH} \quad 4.9$$

Where $\dot{R}_{OH}$ is the net rate of OH oxidation given by:

$$\dot{R}_{OH} = A_{OH} W_C \rho_{OH} \frac{N_A}{M_{OH}} \sqrt{\frac{R T_g}{2\pi M_{OH}}} \quad 4.10$$

Where A_{OH}, $\rho_{OH,}$ M_{OH}, Wc and N_A are a calibration factor, the concentration and the molecular weight of OH, the weight of one carbon atom and the Avogadro's number, respectively. The calibration factor A_{OH} used for this study was 2.5 x 10^{-3} [44]. The role of the calibration factors A_f, A_{O_2} and A_{OH} is to partially compensate for the value chosen as mean particle diameter.

4.3.3 Engine Conditions for Parametric Study

The effects of EGR, engine load and engine speed on soot-in-oil has been explored by modelling conditions at the sixteen engine operating points defined in Table 4.3. Four of the sixteen engine conditions, one for each engine load, were calibrated with experimental data (highlighted in Table 4.3) [39, 101]. These four test points were previously used in an early work to study the influence of the swirl ratio on soot emissions [39, 101]. Detail of their agreement with experimental points is shown in Figure 4.5, with predictions accurate to within ±10% [101].

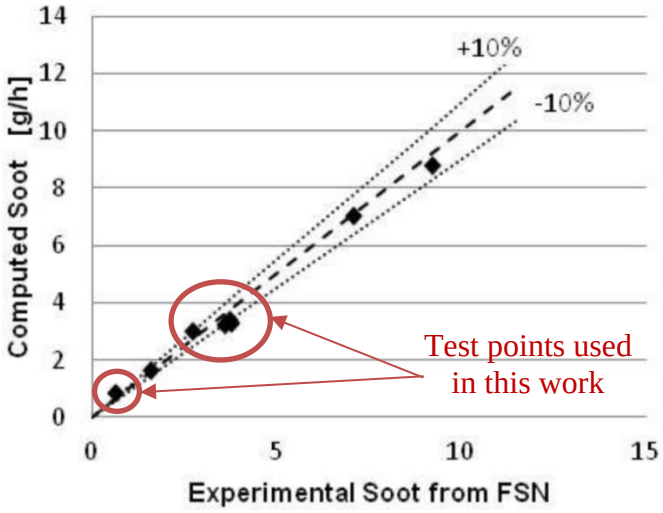

Figure 4.5: Computed values of soot at EVO validated against experimental results obtained from the diesel engine used as a model for the simulations [101].

With the aim of conducting an investigation analogues to realistic engine conditions, the remaining twelve points at different EGR levels from the calibrated points were obtained by changing the intake gas composition according to both the exhaust gas composition from the preceding cycle and the EGR level.

For a given intake charge pressure and temperature, the application of EGR displaces some of the air, diluting the intake charge which remains constant. Consequently, if the percentage of exhaust gas recycled is defined as the percentage of the total charge which is recycled exhaust, (Equation 4.11), as the percentage of EGR is increased, the amount of air available for the combustion is reduced [96]. This results in an increase of the fuel-air equivalent ratio, ϕ. Heywood [11] reported a ϕ threshold value of 0.8 for diesel engines. According to the ϕ values given in Table 4.3, only Case 3d exceeded this value.

$$EGR = \frac{\dot{m}_{EGR}}{\dot{m}_i} \cdot 100 = \frac{m_{EGR}}{m_a + m_{EGR}} \cdot 100 \qquad 4.11$$

In this analysis the influence of EGR on the turbocharge system was neglected, and it was assumed that the temperature of the exhaust gas was cooled by the EGR cooler to the same temperature and pressure of the calibrated test point. This allowed the mass of charge inducted to be considered independent from EGR and changing only with engine speed and load. A further assumption was to consider the amount of fuel changing only with engine speed and engine load, remaining constant with EGR. As the test points from Table 4.3 operate at lean equivalence ratio, their combustion efficiency can be considered to be constant, approximately 98% [11]. This, together with the previous assumptions, allowed considering the Brake Mean Effective Pressure (BMEP) independent from the EGR level. A similar approach was followed by Wagner et al. [115] who studied the influence of EGR on emissions and on engine combustion parameters. They reported that the EGR had a greater effect on PM and NO_x emissions, compared to the slight effects on net heat release and Indicated Mean Effective Pressure (IMEP), which were varied by only 3% and 14%, respectively as EGR was increased from 0 to 35%.

Case	Engine Speed	Engine Load (BMEP)	EGR	$\dot{m}_{fuel}$	ϕ	In-cylinder Soot @ EVO
n	[rpm]	[bar]	[%]	[kg/h]	[-]	[g/h]
1a	2,000	2	0	2.189	0.31	0.06
1b	2,000	2	15	2.189	0.36	0.09
1c	2,000	2	25	2.189	0.41	0.18
1d	2,000	2	35	2.189	0.47	0.78
2a	2,000	6	0	4.74	0.49	0.85
2b	2,000	6	15	4.74	0.58	3.32
2c	2,000	6	25	4.74	0.66	5.5
2d	2,000	6	35	4.74	0.76	9.62
3a	2,000	8	0	6.116	0.56	1.14
3b	2,000	8	15	6.116	0.66	3.51
3c	2,000	8	25	6.116	0.75	7.03
3d	2,000	8	35	6.116	0.86	11.4
4a	2,500	6	0	6.081	0.48	0.94
4b	2,500	6	15	6.081	0.56	3.19
4c	2,500	6	25	6.081	0.63	4.87
4d	2,500	6	35	6.081	0.73	8.26

Table 4.3: Engine conditions used for the CFD model. Cases 1d, 2b, 3b and 4b were validated against experimental results (light blue fill)[39, 101].

4.4 Amount of Soot in the Combustion Chamber

There are two contributions to in-cylinder soot concentration. The majority is produced during the cycle during the combustion process. A minority contribution is when EGR is used as this returns some of the soot exhausted on the earlier cycle.

As mentioned in Section 4.3, the pre-existing CFD code used throughout this thesis only considers EGR by adjusting the inducted gas composition according to the level and composition of the exhaust gas recirculated, as shown in Figure 4.6. The particles re-entering the combustion chamber with the EGR gas, named Re-cycled soot, were not taken into account by the CFD model. The Re-cycled particles were instead calculated by post-processing output data from the simulation runs such as in-cylinder combustion and emission quantities. Due to the different approach followed for the calculation of the In-cycle and Re-cycled particles, the two sources could be studied separately, allowing the evaluation of their relative contribution to soot-in-oil contamination.

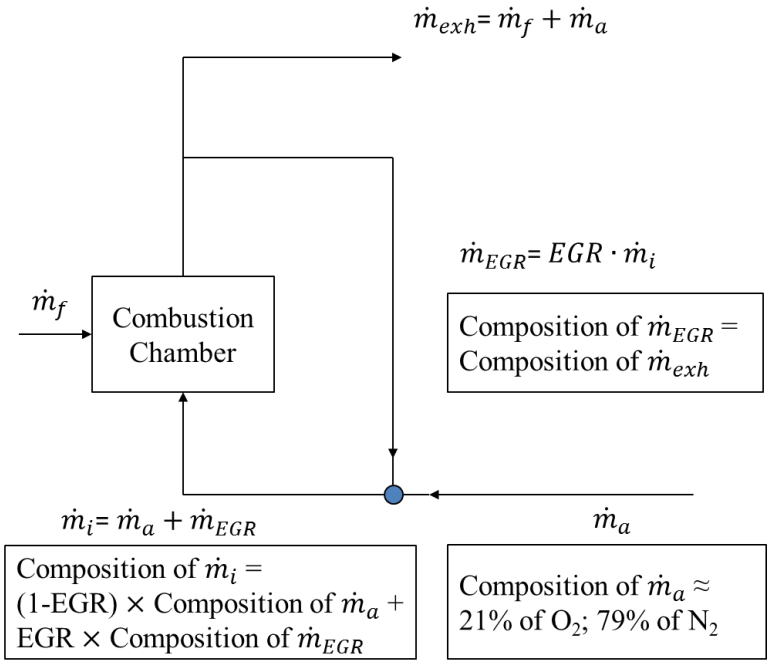

Figure 4.6: Gas composition and mass balance of the EGR system.

4.4.1 In-cycle Source

Values of In-cycle soot at EVO are shown in Figure 4.7 as a function of EGR and engine load. The reported values refer only to the soot produced during the combustion process, i.e. In-cycle source. The soot that re-entered the combustion chamber with EGR gases is not taken into account here as this is not calculated via simulations.

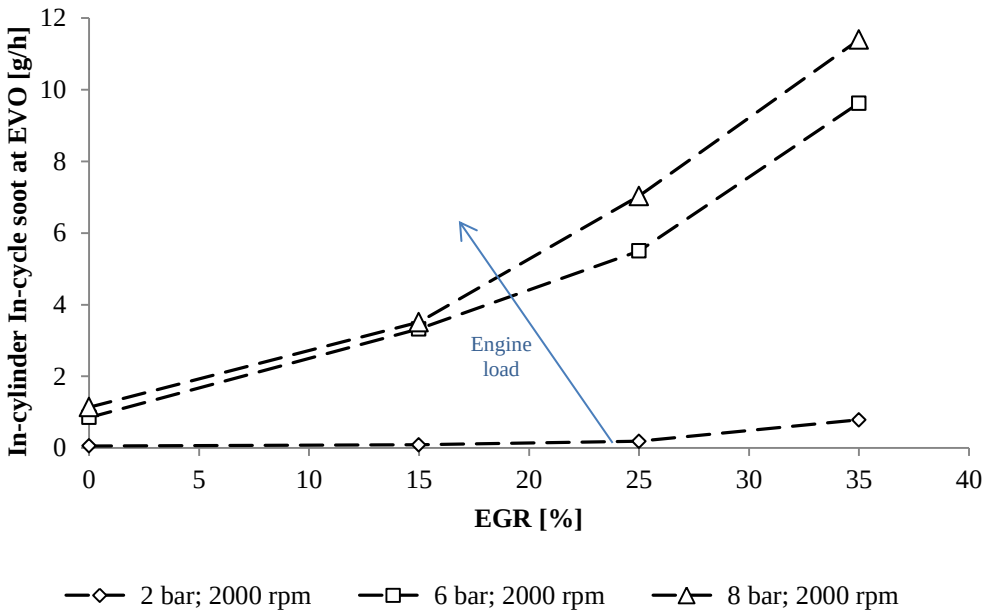

Figure 4.7: CFD-predicted In-cycle soot emissions at EVO as a function of EGR level and engine load for fixed engine speed of 2,000 rpm (Cases 1-3 from Table 4.3). In-cycle source of soot only.

Overall, the in-cylinder soot produced at EVO increases with both engine load and EGR level. The increase in soot with engine load is attributed to the higher amount of fuel injected, to the higher fuel-air equivalence ratio and to the increased gas pressure and temperature which promotes the formation of soot. On the other hand, as more EGR is applied, the amount of air available in the combustion chamber is reduced, increasing thus the fuel-air equivalence ratio (richer mixture) and lowering the in-cylinder gas temperature. These two effects have consequences on both the amount of soot formed and oxidised. These are shown in Figure 4.8 where the soot formation and oxidation curves for Cases 2a and 2d from Table 4.3 are shown. The two cases have been chosen to represent

two engine conditions at fixed engine speed and load, at two different levels of EGR, respectively 0% and 35%. Results indicated that the main EGR effects are on soot oxidation: the lower oxygen content and gas temperature at high level of EGR decrease the rate of soot oxidation, increasing the net amount of soot produced. Similar effect was also observed by Kim et al. [97]

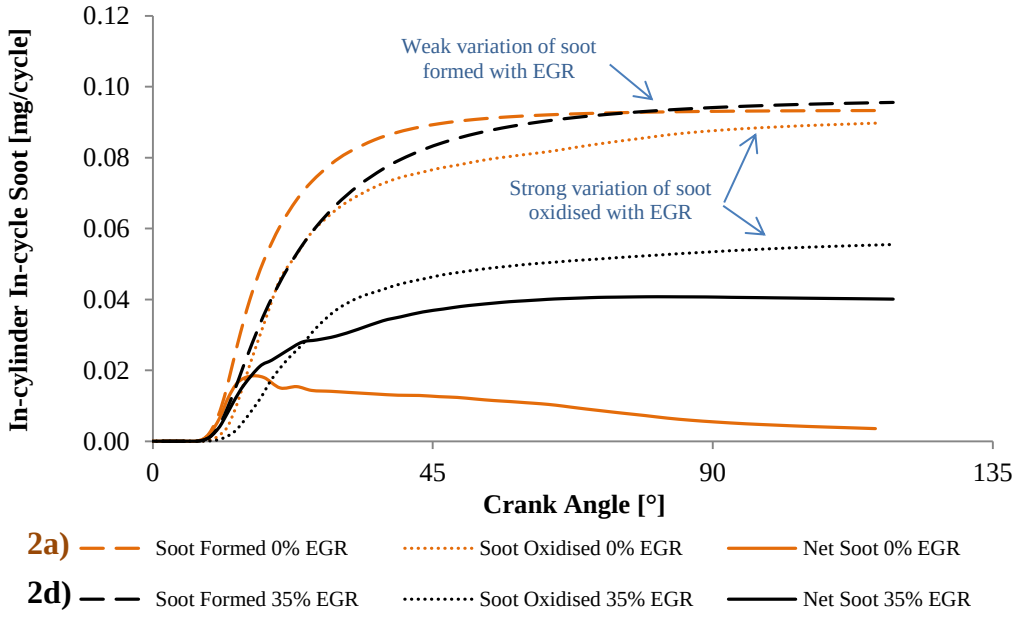

Figure 4.8: Computed in-cylinder In-cycle soot formed (dash lines), oxidised (dotted lines) and net (solid lines) profiles. Engine conditions of 6 bar BMEP, 2,000 rpm and two different levels of EGR: 0% (orange) and 35% (black). In-cycle source of soot only.

The effect of engine speed on engine-out soot is shown in Figure 4.9, representing Cases 2a-d and 4a-d from Table 4.3. Engine speed, compared to engine load and EGR level plays only a minor role in the net amount of soot produced. Especially at low EGR levels, soot values at EVO for engine speeds of 2,000 rpm and 2,500 rpm are almost identical. The largest difference is observed at 35% EGR (Cases 2d and 4d). The profiles of the soot formed, oxidised and net for these two cases are shown in Figure 4.10. The soot formed at 2,000 rpm is higher than at 2,500 rpm. This can be attributed to the fact that at lower engine speed the air-fuel mixing is reduced, increasing the local fuel-air equivalence ratio. The effects of the mixing can also be observed from the soot oxidised curve: the two values at 2,000 and 2,500 rpm are very similar, indicating that a larger proportion of soot is oxidised at higher engine speeds.

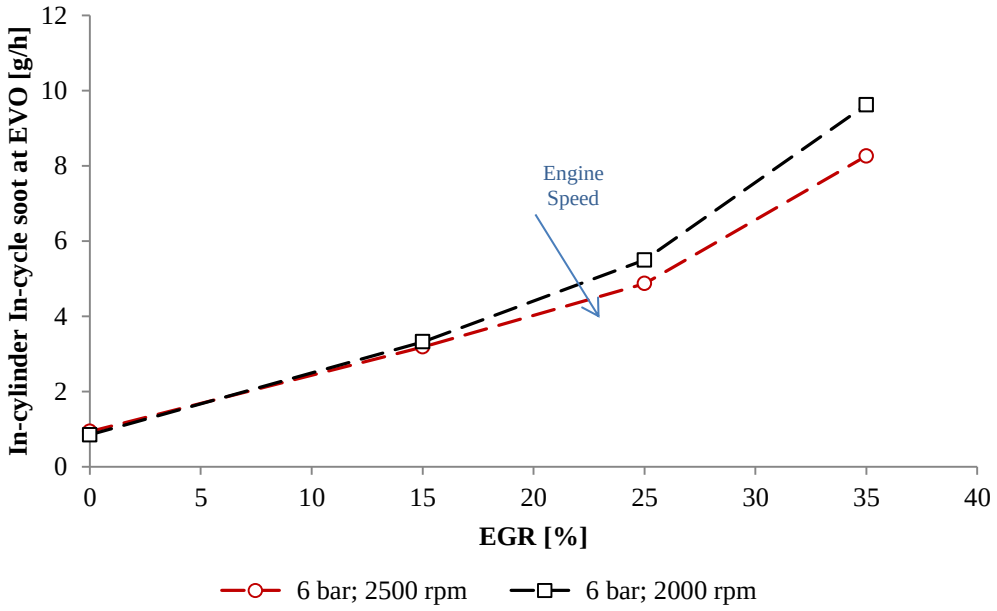

Figure 4.9: CFD-predicted In-cycle soot emissions as a function of EGR level and engine speed, for fixed engine load of 6 bar BMEP. In-cycle source of soot only.

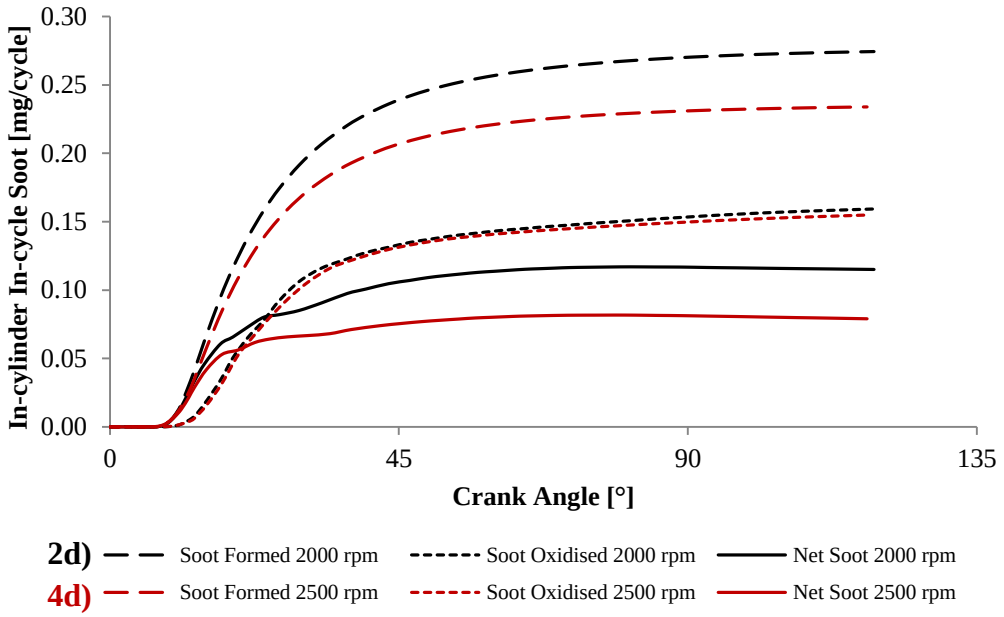

Figure 4.10: Computed in-cylinder In-cycle soot formed (dash lines), oxidised (dotted lines) and net (solid lines) profiles. Engine conditions of 6 bar BMEP, 35% EGR and two different engine speed: 2,000 rpm (black) and 2,500 rpm (red). In-cycle source of soot only.

In Figure 4.11 and Figure 4.12 the values of in-cylinder soot at EVO from Table 4.3 are presented as a proportion of soot at 0% EGR. For the engine conditions modelled, increasing the level of EGR from 0% to 35% increases the amount of soot produced at EVO between 8 and 14 times. Similar values were observed by Wagner et al. [115]. The smallest proportion increase was observed for the higher engine speed condition. The highest proportion increase was instead computed for Case 1, representing the lowest engine load condition. This is considered to be due to the extremely low amount of soot produced without EGR, as a consequence of the low value of fuel-air equivalence ratio.

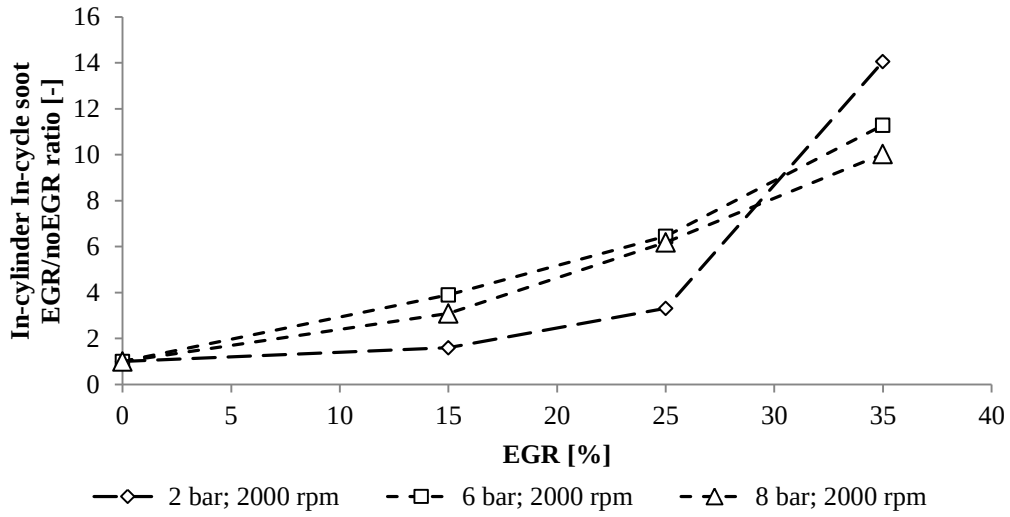

Figure 4.11: In-cylinder In-cycle soot at EVO for Cases 1, 2 and 3 from Table 4.3 shown as a proportion of soot at 0% EGR. In-cycle source of soot only.

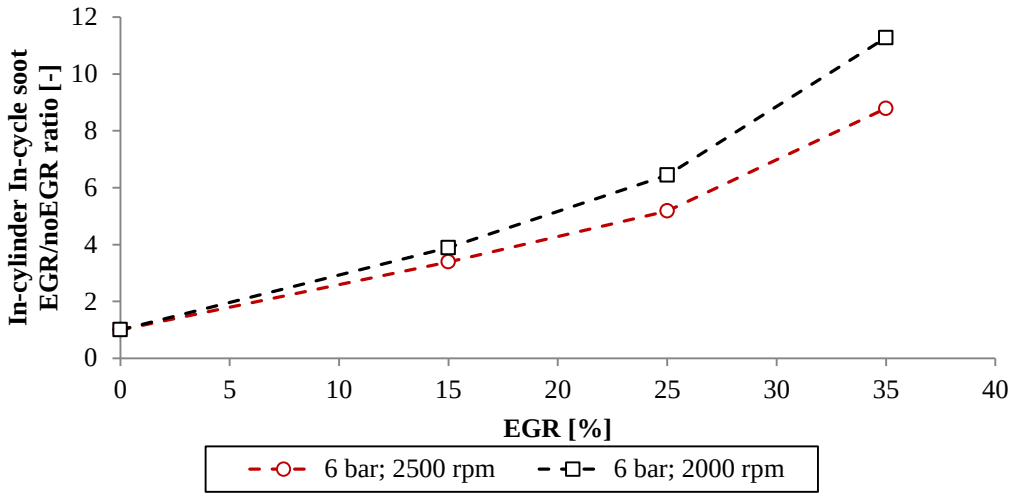

Figure 4.12: In-cylinder In-cycle soot at EVO for Cases 2 and 4 from Table 4.3 shown as a proportion of soot at 0% EGR. In-cycle source of soot only.

4.4.2 Re-cycled Source

The amount of soot extracted from the exhaust system and recirculated through the EGR loop is calculated from the values of soot at EVO and from the EGR rates. By assuming the soot particles in the exhaust ($m_{s@EVO}$) to be uniformly distributed within the carrying gas [51], the amount of soot in the EGR gas, ($m_{s,EGR}$) is given by:

$$m_{s,EGR} = m_{s@EVO} \cdot EGR \qquad 4.12$$

As shown on the left-hand side of Figure 4.2, the soot-laden exhaust gases pass through the EGR cooler prior to mixing with the air at the intercooler output. The EGR cooler reduces the exhaust gas temperature while maintaining the desired fuel-air equivalence ratio. Several authors have investigated the deposition of soot and hydrocarbons at the EGR cooler surface. This problem, named fouling, is mainly caused by the difference in temperature between the hot recirculated gas and the cold EGR cooler surface. This is of concern as fouling can reduce the heat capacity and efficiency of the heat exchanger by up to 25-30% of the nominal value [99, 116, 117]. In this work, the effect of fouling is neglected and it is assumed that the mass of soot re-entering the combustion chamber is equal to that extracted from the exhausts, calculated as in Equation 4.12.

This assumption is justified by the results found in literature relative to fouling. Epstein [118] described particle fouling as a mechanism commonly characterised by a first rapidly increase of the mass deposited, followed by a falling rate, with a rate of mass deposited approaching an asymptotic value. Epstein [118] assumed that the plateau was due to the reentrainment of these particles, mainly associated with the shear forces of gas flow over the layer. This mechanism was also observed by Lepperhoff et al. [119]. Lepperhoff et al. [119] found that mass deposition occurred only during the first hours of operation, approximately within the first 10 hours, with 4 to 10% of the particles being trapped in the EGR cooler. The steady state condition approach followed in this study, together with the typical small trapping percentages, allowed the author to neglect soot deposition across the EGR cooler.

The inducted mass is assumed to be a uniform homogeneous charge, as the exhaust gas and the fresh air streams had sufficient time to mix completely [26, 51]. As a result, also the Re-cycled particles were assumed to be uniformly distributed within the combustion chamber. This is of particular interest for soot-in-oil as this will directly affect the concentration of soot in the regions of interest for deposition, such as close to the cylinder liner and close to piston ring pack.

As the onset soot oxidation temperature, i.e. between 550 and 570 K [74] [120] is exceeded for most of the engine cycle, the oxidation of the Re-cycled soot has been analytically evaluated for all the engine conditions listed in Table 4.3. Soot oxidation has been calculated by using the same oxidation model used previously in Section 4.3.1 for evaluating the oxidation of the In-cycle soot, i.e. the NSC model [113] and Neoh's OH oxidation mechanisms [44]. Gas temperature was obtained from Kiva-3V.

In Figure 4.13, the percentage of soot oxidised and the in-cylinder bulk gas temperature used for the calculation are shown for Case 3c from Table 4.3 (engine conditions of 8 bar BMEP, 2,000 rpm and 25% EGR). Although the soot oxidation onset temperature is exceeded at approximately 60° BTDC, the amount of soot oxidised during the compression stroke is negligible. This is due to the relatively low in-cylinder gas pressure, and of the resulting low partial pressure of

the oxidising agents. This, according to Equations 4.3 to 4.10 has a strong influence on the rate of oxidation. Most of the oxidation occurs instead between 7° After Top Dead Centre (ATDC) and 55° ATDC in the range of temperature 900-1,200 K and pressure 20-70 bar. After 55° ATDC soot oxidation is again negligible. This, as for during the compression stroke it is due to the relatively low partial pressure of the oxidising agents. Overall, for Case 3c shown in Figure 4.13 the percentage of re-cycled soot oxidised is over 85%. Results for all the engine conditions modelled are summarised in Table 4.4.

The amount of soot oxidised for all the cases listed in Table 4.3 was found to be mainly dependent on engine load, as this has a strong effect on in-cylinder gas temperature and pressure. Furthermore, as the EGR level increases the amount of soot oxidised decreases due to both the lower amount of oxidants and the in-cylinder gas temperature decrease, with the latter being the main factor. Finally, the rate of soot oxidation decreased as the engine speed was increased. This is due to the less time available for the particle to be oxidised.

Previously, it was found that the amount of In-cycle soot oxidised increased with engine speed. This was due to the higher particle-oxidiser mixing. This does not occur on the Re-cycled oxidation due to the fact that these particles are considered to be homogeneously distributed within the combustion chamber and therefore engine speed did not influence the fuel-charge mixing.

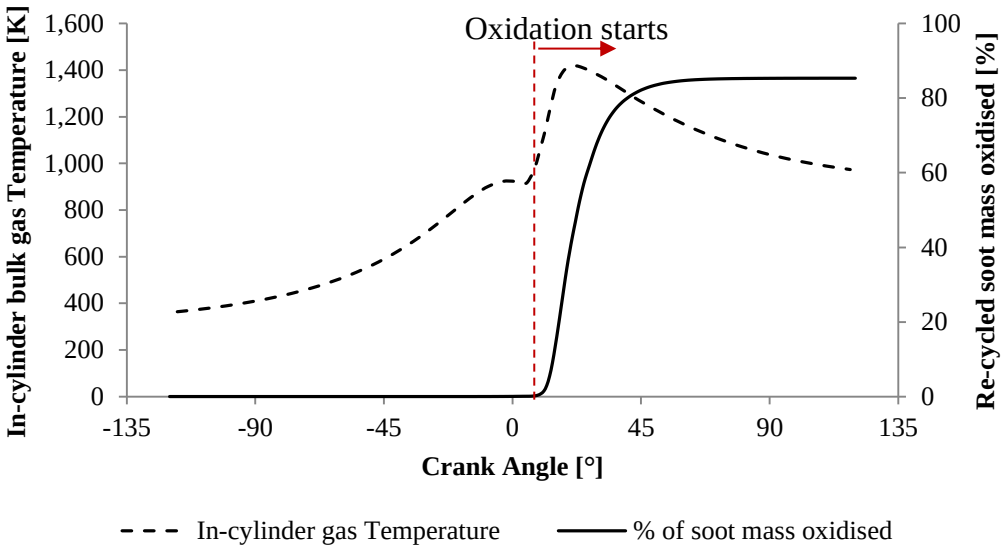

Figure 4.13: Percentage of soot re-cycled with EGR oxidised and in-cylinder gas temperature. Engine conditions of 2,000 rpm, and 8 bar BMEP and 25% EGR (Case 3c from Table 4.3).

In Section 4.3.2 soot formation was modelled by linking the formation directly to the fuel vapour molecules. As their amount in the exhaust gas is in the order of magnitude of 10^{-6} as a mass fraction, the soot formation process from the fuel contained in the exhaust gases re-entering the combustion chamber with EGR gases was neglected.

Case (from Table 4.3)	Engine Speed [rpm]	Engine Load [bar]	Level of EGR gas [%]	Re-cycled soot oxidised [%]
1a	2,000	2	0	-
1b	2,000	2	15	35.4
1c	2,000	2	25	33.3
1d	2,000	2	35	30.2
2a	2,000	6	0	-
2b	2,000	6	15	62.1
2c	2,000	6	25	50.0
2d	2,000	6	35	44.4
3a	2,000	8	0	-
3b	2,000	8	15	86.9
3c	2,000	8	25	85.3
3d	2,000	8	35	80.5
4a	2,500	6	0	-
4b	2,500	6	15	51.6
4c	2,500	6	25	50.6
4d	2,500	6	35	45.8

Table 4.4: Amount of soot re-entering the combustion chamber with EGR gases, and their rate of oxidation during the engine cycle.

4.5 Availability of Soot during post-EVO Period

Soot availability in the combustion chamber after EVO is estimated by post-processing output data obtained from Kiva-3V. It was assumed that the fraction of mass soot loss after EVO was the same as the fraction of in-cylinder gas charge loss after EVO. The estimation of the gas charge mass loss after EVO required the study of the exhaust flow.

The real exhaust flow is pulsating, and can be described by two different phases: the blowdown and the displacement [11]. Blowdown takes place during the power stroke between EVO and BDC. During this phase, gases are discharged due to the pressure difference between cylinder and exhaust system environments. In-cylinder gas and temperature vary continuously until the cylinder pressure approaches the exhaust pressure. Displacement occurs from BDC to until exhaust valves are closed. The gases during this stage are displaced due to the fact that the cylinder gas is scavenged by the piston moving upwards.

In this work the two mass loss phases were studied with an ideal model. This model proved to be able of providing good agreement with real data [11]. In the ideal model, blowdown occurs instantaneously at constant volume, with the gas remaining inside the cylinder that expands isentropically [11]. Therefore, the mass loss during blowdown, $m_{exh\_blowdown}$, can be estimated from the ideal gas law as [121]:

$$m_{exh\_blowdown} = \left[1 - \left(\frac{p_{exh}}{p_{@EVO}}\right)^{\frac{1}{\gamma}}\right] \cdot \left(m_i + m_f\right) \qquad 4.13$$

With the exhaust manifold pressure (p_{exh}) assumed to be at the atmospheric pressure.

The in-cylinder mass loss during blowdown for the sixteen cases of Table 4.3, equivalent to soot mass loss, was found to be weakly affected by engine speed and EGR levels (variation limited to within 2%), as these have a limited influence on in-cylinder gas pressure. However, as shown in Figure 4.14 mass loss increased as engine load increased.

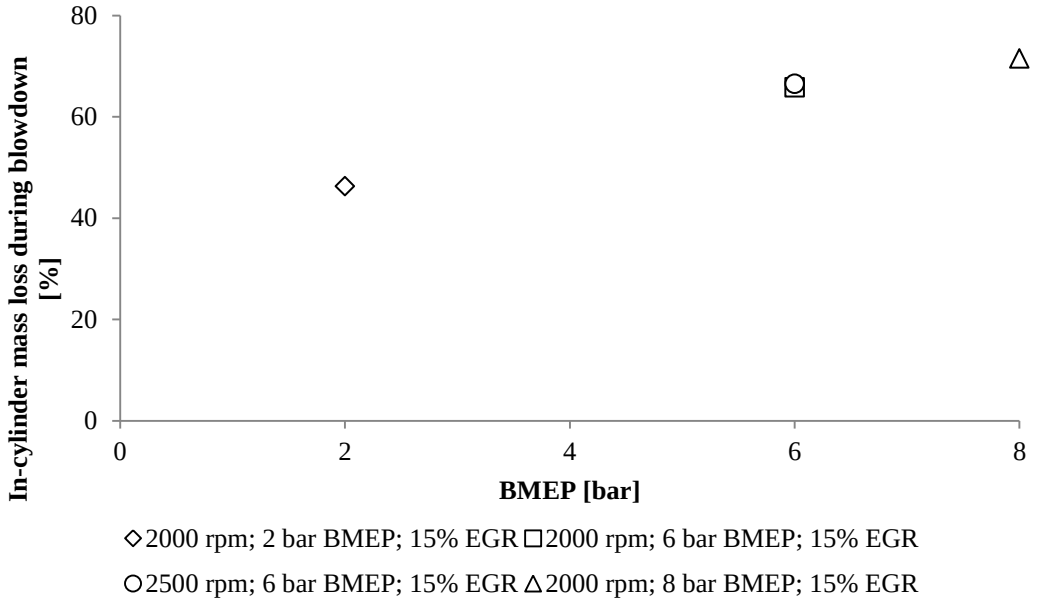

Figure 4.14: Percentage of mass loss during ideal exhaust blowdown process for engine conditions from Table 4.3.

The mass loss during displacement is instead estimated to be proportional to the volume variation during the exhaust stroke. At the end of the exhaust stroke, the in-cylinder mass was further reduced by the ratio of the volume at TDC and BDC [11]:

$$m_{i,TDC} = \frac{V_{TDC}}{V_{BDC}} \cdot m_{i,BDC} \qquad 4.14$$

4.6 Amount of Soot near the Cylinder Liner

In this section, the spatial and temporal soot distribution in the near-wall region is investigated for the sixteen cases of Table 4.3. The amount of soot in this region of interest is estimated for both the In-cycle and Re-cycled sources of soot. The main differences between the two sources are that the latter is available during the entire engine cycle and is uniformly distributed within the combustion chamber, having mixed with the air prior to the induction stroke.

4.6.1 "In-Cycle" Source near Cylinder liner

Most of the soot produced during the combustion process is concentrated in the piston bowl region, where it is originally formed. Therefore, to estimate the spatial average amount of soot available at the liner for deposition, rather than monitoring the in-cylinder soot distribution, it is important to evaluate the amount of soot in the proximity of the cylinder walls. This was achieved by modifying the code in order to extract crank angle resolved net soot mass in the cells at the entire exposed area adjacent to the liner (region with blue borders from Figure 4.1) [26]. The amount of soot in this region was monitored at every 1°CA as given in Equation 4.15:

$$\begin{aligned} &I\mathit{nstantaneous\ net\ soot\ mass\ at\ liner} = \\ &\mathit{Instantaneous\ net\ soot\ mass\ retained\ from\ last\ timestep} + \\ &\mathit{Soot\ mass\ transported\ in} + \\ &\mathit{soot\ mass\ formed\ inside\ region} - \\ &\mathit{Soot\ mass\ transported\ out} - \\ &\mathit{Soot\ mass\ oxidised\ inside\ region} \end{aligned} \qquad 4.15$$

The cells adjacent to the cylinder liner have a thickness of 1.1 mm, bordering the wall of the computed 51.4° sector mesh. The one-seventh of the combustion chamber, by taking advantage of the symmetry imposed by the 7-hole injector, allowed evaluating crank angle-resolved value which took into account the azimuthal distribution variation generated by the rotational motion of the hot gases. A block-structured mesh of Kiva-3V was used for the calculations, with boundary planes located at a distance of 51.4°. Swirl motion was simulated by specifying an initial swirl velocity, with the azimuthal velocity increasing moving away from the axis. A limitation of this approach is that because only one spray is taken into account, spray interactions are not considered. The thickness of the cells was able to represent the typical hydrodynamic boundary layer at the cylinder wall, i.e. 1-2 mm [122]. In Figure 4.15 the amount of soot at the liner at EVO is shown as a function of engine load and EGR for Cases 1, 2 and 3 from Table 4.3. Similar to what was observed with the amount of in-cylinder soot, the soot at the cylinder liner region increases with both engine load and EGR level.

The influence of engine speed on the soot at the liner is shown in Figure 4.16. In this case, the amount of soot at the liner, unlike the net in-cylinder soot, increases with engine speed. This is due to the fact that by increasing the engine speed the level of turbulence and hence of transport towards the outer region of the combustion chamber increases accordingly.

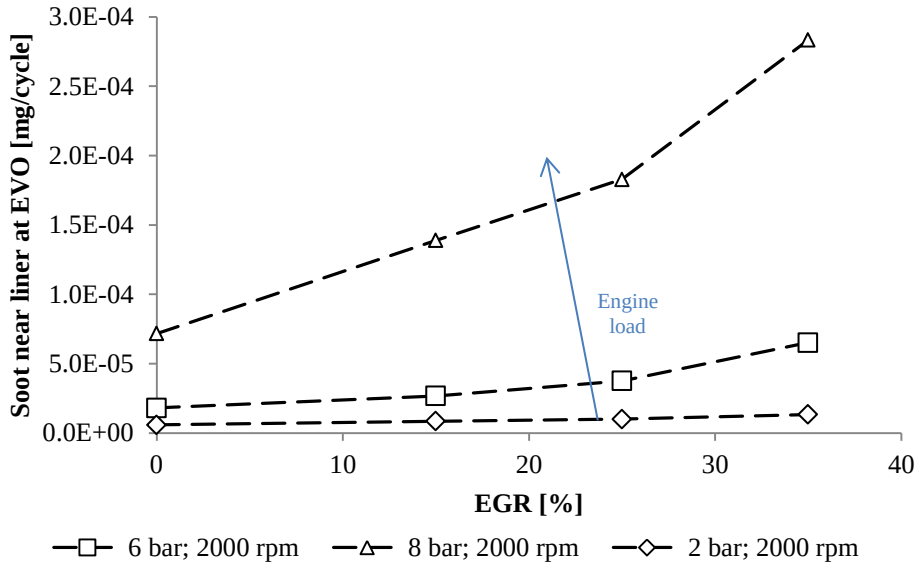

Figure 4.15: Amount of In-cycle soot near liner at EVO as a function of engine load and EGR level for Cases 1, 2 and 3 from Table 4.3.

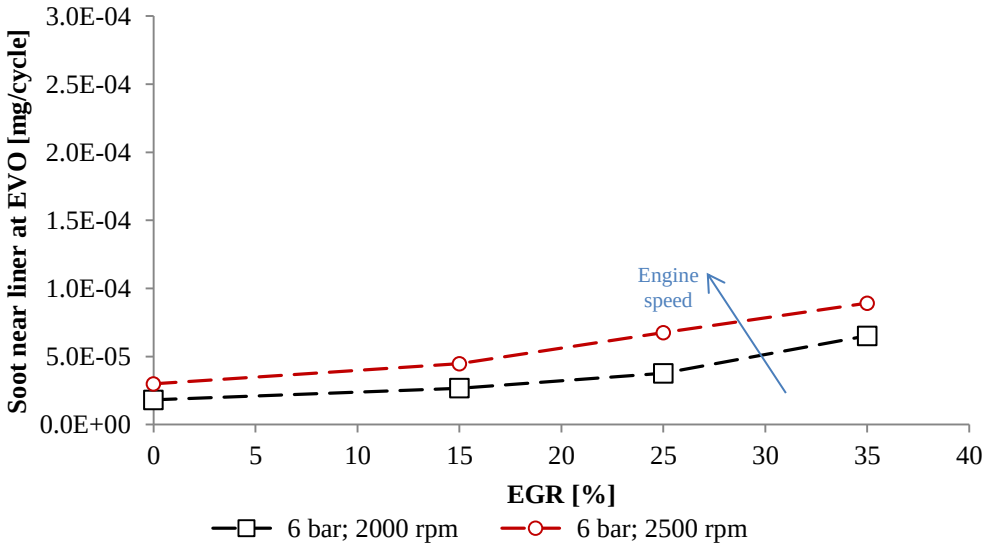

Figure 4.16: Amount of In-cycle soot at EVO as a function of engine speed and EGR level for Cases 2 and 4 from Table 4.3.

The particle concentration at the liner (ϱ_{liner}) has been compared with the in-cylinder soot concentration (ϱ_{cyl}). The ratio between the two is here named "distribution coefficient", and given by:

$$Distribution\ coefficient = \left.\frac{\varrho_{liner}}{\varrho_{cyl}}\right|_{@EVO} \qquad 4.16$$

A uniform particle distribution within the combustion chamber would be represented by a unitary value of the distribution coefficient, while a value smaller or higher than one would be associated with a smaller or higher concentration of soot at the cylinder liner. Results for the cases modelled in this work showed that the distribution coefficient at the liner varied between 0.1 and 0.5. This indicates that most of the soot is confined in the core region of the combustion chamber. The distribution coefficient was observed to decrease with engine load and EGR level. These two conditions increase the fuel/air equivalence ratio, increasing the soot formation, which mainly occurs in the core region of the combustion chamber.

Similarly to Figure 4.11 and Figure 4.12, results at the liner are shown in Figure 4.17 and Figure 4.18 as a proportion of liner soot at 0% EGR. Increasing the EGR level from 0% to 35% approximately, increases the amount of soot produced during the combustion process at the liner between 2 and 4 times. This shows that the increase of soot at the liner with EGR is weaker compared to that on the in-cylinder, which was found to be 8-14 times.

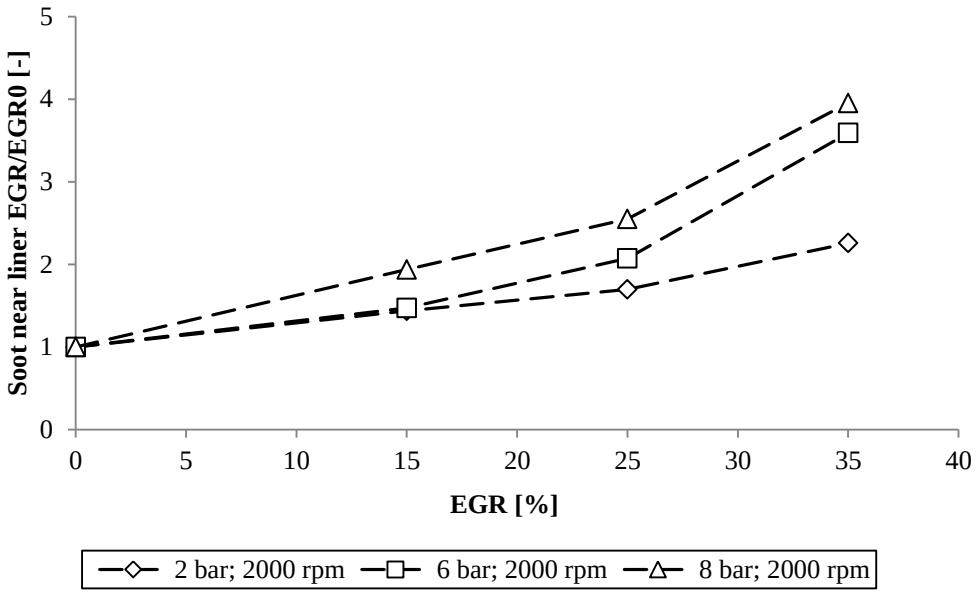

Figure 4.17: In-cycle soot at the near liner at EVO for Cases 1, 2 and 3 from Table 4.3 shown as a proportion of soot at 0% EGR.

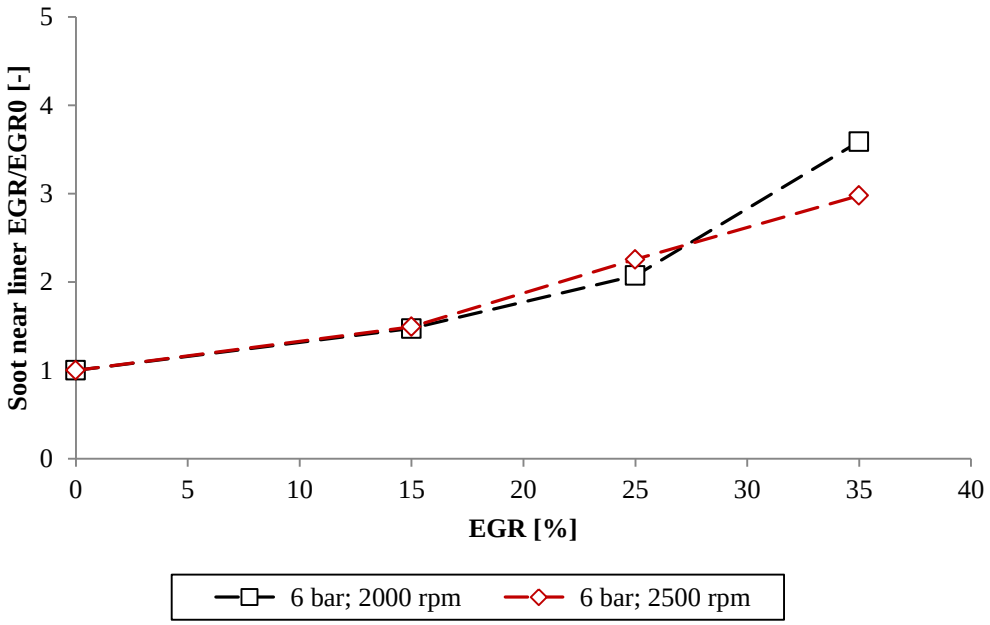

Figure 4.18: In-cycle soot at the near liner at EVO for Cases 2 and 4 from Table 4.3 shown as a proportion of soot at 0% EGR.

4.6.2 "Re-Cycled" Source near Cylinder Liner

Due to the assumption of considering the Re-cycled particles uniformly distributed, the distribution coefficient at the cylinder liner for this source of soot, calculated from Equation 4.16 is equal to one.

To allow comparison with the CFD-calculated In-cycle source, Re-cycled particles at the near-liner region, $m_{s,EGR@liner}$, were calculated considering the same volume used by the CFD, V_{liner}, having a thickness of 1.1 mm.

$$m_{s_{,EGR@liner}} = m_{s_{EGR}} \cdot \frac{V_{liner}}{V_{cyl}} \qquad 4.17$$

The amount of Re-cycled soot available at the liner changes with time, as both V_{liner}/V_{cyl} and m_{sEGR} change with crank angle. As shown in Figure 4.1, V_{cyl} is composed by the clearance volume $V_{clearance}$ and the piston bowl volume V_{bowl}. V_{liner} and $V_{clearance}$ vary with the stroke, while V_{bowl} remains constant. As a result, as shown in Figure 4.19, the liner volume fraction has a typical V-shape, with smaller values close to TDC. m_{sEGR} changes because of the oxidation process occurring during the cycle. Values of m_{sEGR} at EVO are listed in Table 4.4.

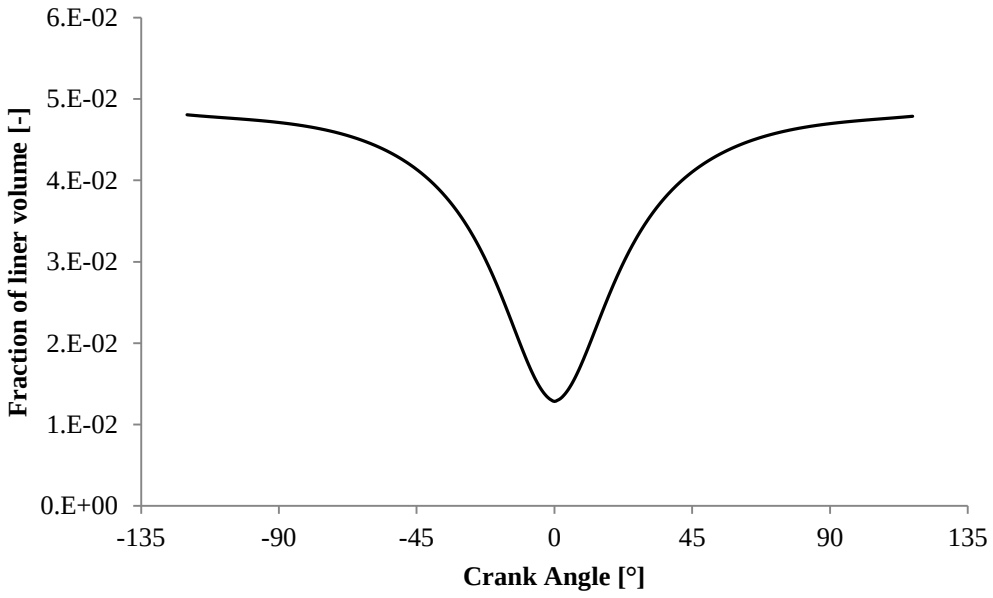

Figure 4.19: Fraction of near liner volume considered by the CFD model as a fraction of In-cylinder volume.

4.6.3 Overall Amount of Soot Available near Cylinder Liner

For all the cases listed in Table 4.3 the Re-cycled source of soot is available at the liner during the entire engine cycle. The In-cycle source, which is directly formed from the combustion process, is instead available at the liner only after the Start Of Ignition (SOI). Another difference between the two sources is that the availability of the Re-cycled is directly linked to the net in-cylinder soot at EVO. This, as shown in Figure 4.11 and Figure 4.12, increased up to fourteen times as the EGR level is increased from 0% to 35%. The availability of In-cycle soot at the liner instead, was found to be weakly correlated to the net in-cylinder amount of soot, and its increase with EGR is limited to up to three times as the EGR is increased from 0% to 35%. As a result, EGR has a stronger effect on the Re-cycled source of soot, rather than on the In-cycle source.

In Figure 4.20 the availability of particles at the liner at EVO from both sources is shown as a function of engine load and EGR level for Cases 1-3 of Table 4.3. In-cycle soot values are directly obtained from CFD results. The particles re-introduced in the combustion chamber with EGR gas are not taken into account directly by the computational model as EGR is only considered by adjusting the intake gas composition. Instead, the re-cycled particles have been estimated by post-processing CFD results at EVO from the previous cycle, as discussed in Section 4.4.

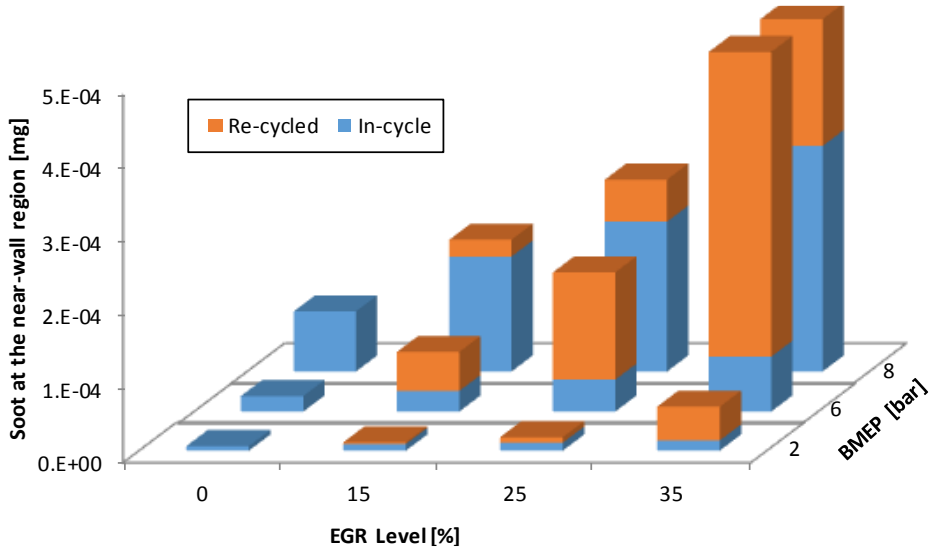

Figure 4.20: Amount of soot at the cylinder liner from Re-cycled and In-cycle sources at EVO as function of engine load and EGR level. Cases 1-3 of Table 4.3.

For all the three engine load cases investigated, the availability from both Re-cycled and In-cycle sources strongly increases with EGR, with the former increasing approximately four times faster than the In-cycle source. However, as engine load increases, the In-cycle and Re-cycled sources behave differently. The first source monotonically increases with engine load for all the EGR levels investigated. The Re-cycled source instead, increased as BMEP increased from 2 to 6 bar, while it decreased as the engine load is further increased to 8 bar BMEP. This can be explained by the fact that the amount of in-cylinder soot at EVO between the two cases at 6 and 8 bar BMEP (which governs the amount of soot recirculated in the combustion chamber with the EGR gases) are similar (Figure 4.7). However, at high engine load, due to the higher gas temperature and pressure, a higher fraction of Re-cycled soot is oxidised after it is re-introduced in the combustion chamber (Table 4.4), reducing thus the availability during the engine cycle.

Similarly to Figure 4.20, in Figure 4.21 the availability of soot at the liner is shown as a function of engine speed and EGR level (Cases 2a-d and 4a-d from Table 4.3).

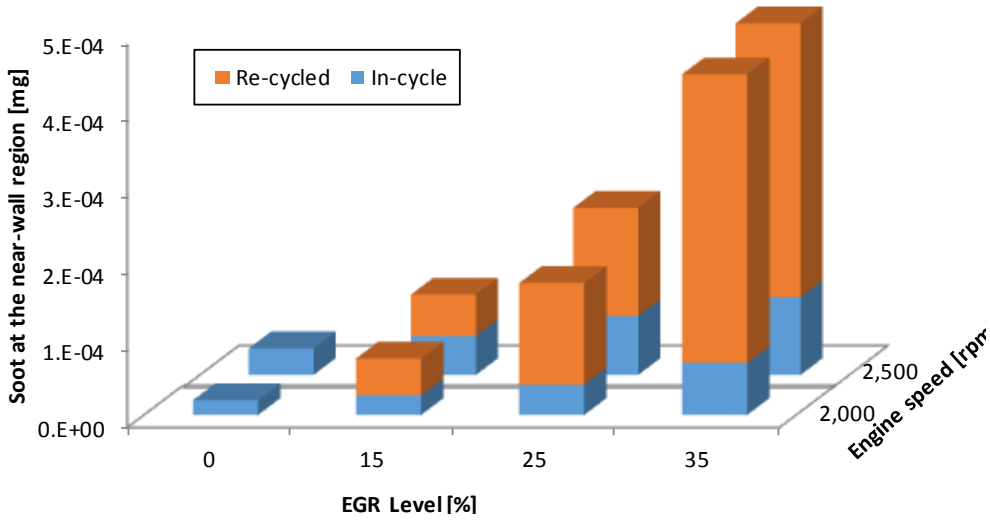

Figure 4.21: Availability of soot at the cylinder liner from the Re-cycled and In-cycle sources at EVO as a function of engine speed and EGR level. Cases 2 and 4 from Table 4.3.

The influence of engine speed between 2,000 rpm and 2,500 rpm on the overall availability at the liner is weaker when compared to that of engine load and EGR level. However, the relative contribution of the In-cycle and Re-cycled sources varies with engine speed. The In-cycle increases with engine speed due to the higher convection of particles towards the near-wall region. The Re-cycled instead, decreases due to the fact that the amount of soot at EVO from the previous cycle, which governs the amount of Re-cycled soot, is smaller.

Although the values of soot at the liner at EVO presented in Figure 4.20 and Figure 4.21 allow the comparison between the In-cycle and Re-cycled sources, they do not provide information about the actual availability during the engine cycle, which governs the soot-in-oil deposition. The availability of the In-cycle and Re-cycles sources of soot as a function of crank angle at the near liner region is shown in Figure 4.22 for Case 3c of Table 4.3. During the compression stroke, as the combustion process did not take place, only the soot recirculated with the EGR gases is available in the combustion chamber, with only a small fraction of it subjected to oxidation. The amount at the liner decreases with the piston moving towards TDC as the fraction of liner available decreases (Equation 4.17). During the expansion stroke, a large proportion of the Re-cycled soot is subjected to oxidation. This occurs simultaneously with the combustion process which raises the gas temperature and pressure. Meanwhile, the combustion event causes the formation of In-cycle soot. The first soot particles are formed in the piston bowl where the fuel spray is injected at 4° ATDC. As the piston moves downwards during the power stroke, the expanding squish volume is partially replaced by the piston bowl charge which contains the soot particles formed during the combustion process. The first particles to approach the near-wall region were detected at 8° ATDC, while a sensible increase is observed only at 20° ATDC. Continuing with the expansion stroke, the amount of soot at the liner increases monotonically until the exhaust valve opens, exceeding the Re-cycled particles at approximately 45° ATDC.

As discussed in Section 4.5, the CFD model is restricted to the closed part of the cycle. The amount of soot after EVO (illustrated by the dotted lines) has been estimated by assuming the fraction of soot loss to be the same as the fraction of

charge loss, calculated as in Equations 4.13 and 4.14. As a result, the soot distribution is characterised by a loss at constant volume at EVO during the blowdown phase, followed by the displacement phase, where the loss of particles is a function of the volume scavenged.

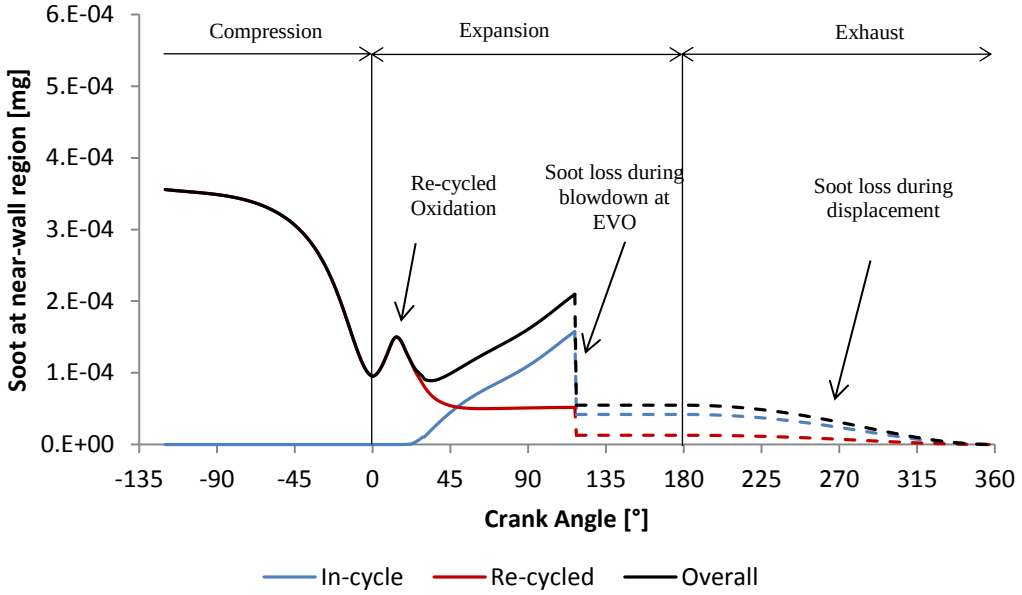

Figure 4.22: Amount of soot available near the wall region throughout the engine cycle for both In-cycle and Re-cycled sources. Engine conditions of 2,000 rpm, 8 bar BMEP, 25% EGR (Case 3c).

4.7 Soot Available for Deposition in the Piston Ring Pack during Blow-by

The amount of soot entering the piston ring pack is mainly governed by the rate of blow-by gas and by the availability of soot within it. The former is calculated in Chapter 6, while the latter, as shown by the red region of Figure 4.1, is studied by monitoring all the cells (1.1 mm thickness) adjacent to the corner between the piston head and the liner, region here referred to as top piston corner [26]. The instantaneous net soot mass in this region was extrapolated at every 1° CA as given by Equation 4.18. The volume at the top piston corner is shown in Figure

4.23 as a fraction of the in-cylinder volume. The fraction increases as the piston approaches TDC due to the dynamic mesh used in this work [26].

$$\begin{aligned} &Instantaneous\ net\ soot\ mass\ at\ top\ piston\ corner \\ &= Instantaneous\ net\ soot\ mass\ retained\ from\ \ last\ timestep \\ &+ Soot\ mass\ transported\ in \\ &+ soot\ mass\ formed\ inside\ region \\ &- Soot\ mass\ transported\ out \\ &- Soot\ mass\ oxidised\ inside\ region \end{aligned} \qquad 4.18$$

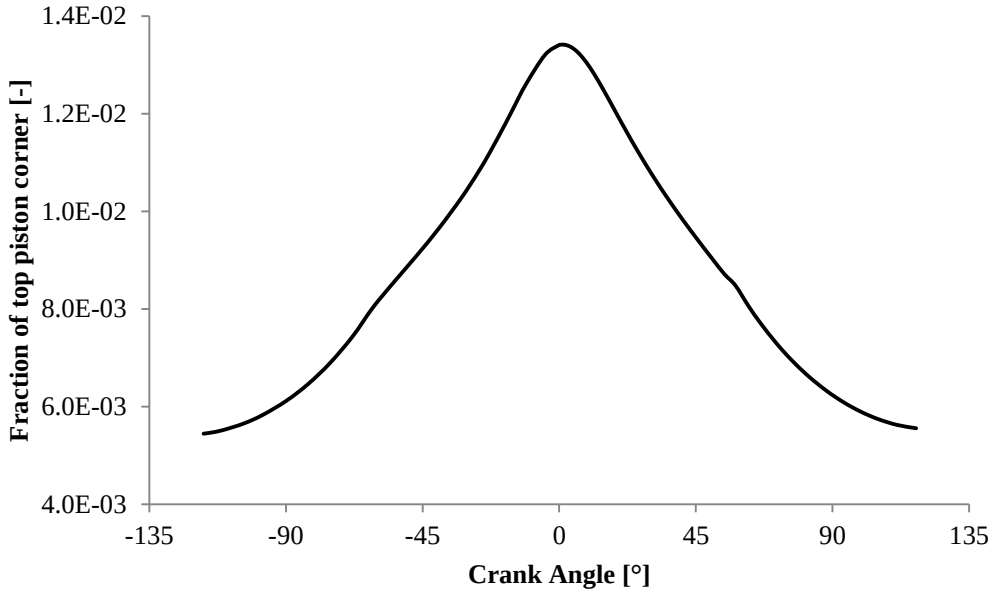

Figure 4.23: Piston head-liner corner volume considered by the CFD model as a fraction of In-cylinder volume.

In Figure 4.24 the amount of In-cycle and Re-cycled soot available at the piston head-liner corner at EVO is shown as a function of engine load and EGR level for Cases 1-3 from Table 4.3. It is worth mentioning that the y-axis scale for the soot available at the piston top corner of Figure 4.24, is one order of magnitude smaller than that at near liner region, previously shown in Figure 4.20 and Figure 4.21.

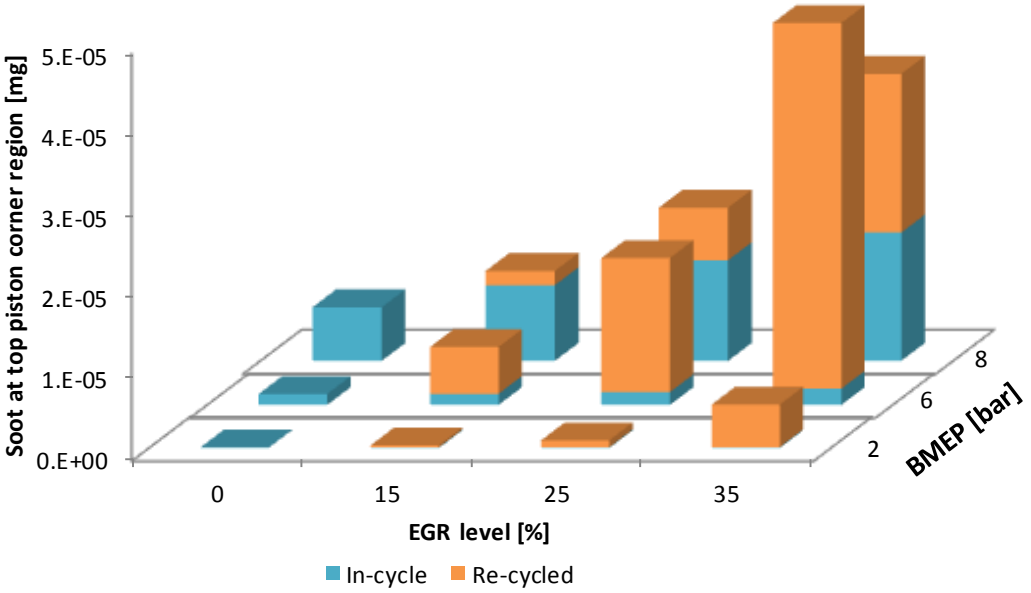

Figure 4.24: Instantaneous amount of soot at EVO in the region of interest for deposition during Blow-by as a function of engine load and EGR, for both In-cycle and Re-cycled sources of soot. Cases 1-3 from Table 4.3.

Results show that the amount of soot strongly increases with EGR. In particular, the Re-cycled particles increase faster than the In-cycle particles due to their direct correlation with the exhausted soot levels from the previous cycle. This is similar to the effect observed at the near-liner region. Regarding the influence of load, it is observed that the amount of In-cycle soot drastically increases with engine load, while the Re-cycled increases from 2 to 6 bar BMEP and decreases as the load is further increased at 8 bar BMEP. For example, it can be observed that at 8 bar BMEP, 15% EGR, the availability of In-cycle soot is larger than the Re-cycled. However, as shown in Figure 4.25 from the temporal availability during the cycle, this occurs after 60° ATDC during the expansion stroke. As it is discussed in Chapter 6, most of the blow-by occurs during the compression stroke and early stages of the expansion stroke, i.e. when the Re-cycled particles are the dominant source of soot at the piston head-liner corner.

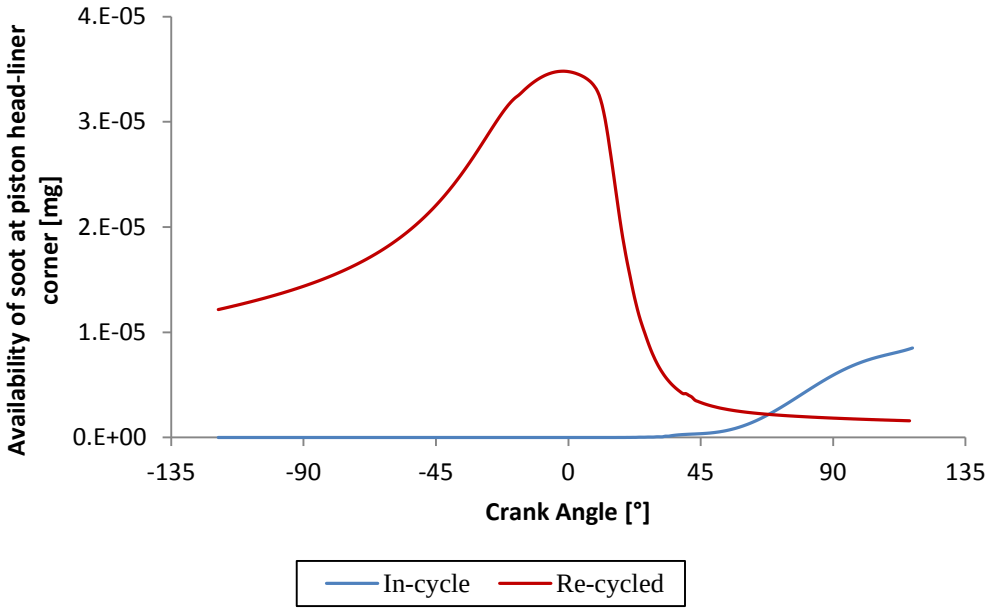

Figure 4.25: Amount of soot available at the piston head-liner corner during the cycle for both In-cycle and Re-cycled sources of soot. Case 3-b from Table 4.3 (8 bar BMEP, 2,000 rpm and 15% EGR).

The influence of engine speed on the availability at the top piston corner is shown in Figure 4.26. Also for the cases at 2,500 rpm, the dominant source of soot is the Re-cycled, with the overall amount of soot at EVO weakly affected by engine speed.

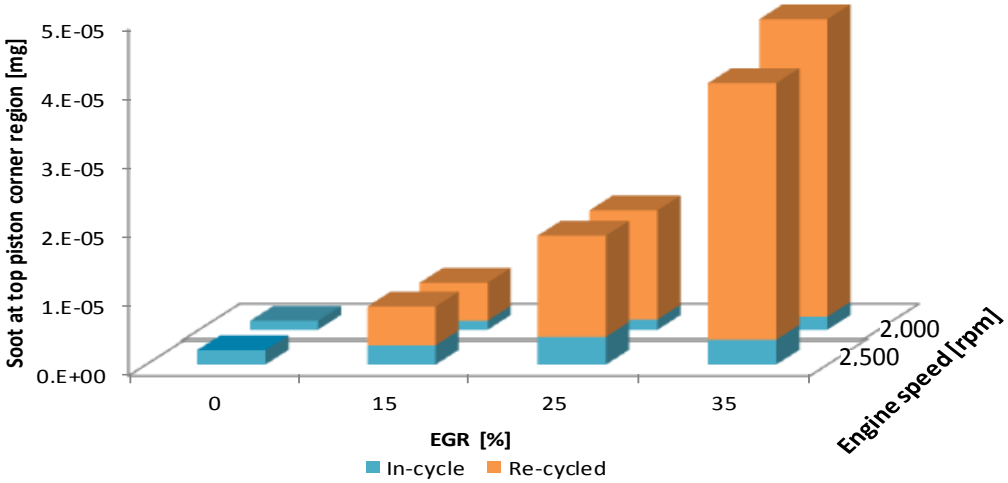

Figure 4.26: Instantaneous amount of soot at EVO in the region of interest for deposition during Blow-by as a function of engine speed and EGR, for both In-cycle and Re-cycled sources of soot. Cases 1-3 from Table 4.3.

4.8 Discussion and Conclusions

While studying the influence of soot deposited in the cylinder head on particle emission, Kittelson et al. [48] assumed the combustion chamber as a well-stirred reactor, i.e. uniform particle distribution. Results from the current work show that by considering the In-cycle source as a well-stirred mixture, the availability of soot in the key regions for deposition will be overestimated by up to an order of magnitude. The concentration of In-cycle soot at the near-wall and piston crown-liner corner regions, defined by the Distribution Coefficient in Equation 4.16, is 10-50% and 1% of the spatial-averaged in-cylinder soot concentration, respectively.

At the near-liner region for an EGR level of approximately >15%, the Re-cycled source becomes a more significant contributor of soot particles. This is due to the fact that these particles re-enter the combustion chamber uniformly mixed with the in-cylinder charge. Furthermore, results indicate that when EGR is applied, the amount of soot increases more in the exhaust compared to that at the near-wall region. Therefore, the Re-cycled source which is directly correlated to engine-out values, increases approximately three times more the In-cycle source.

Unlike the In-cycle particles that are only produced after SOI, the Re-cycled particles are available during the entire engine cycle. Therefore, when EGR is applied, particles become available for deposition also outside the SOI-EVO period. For instance, the compression stroke may play an important role on soot deposition. This is due to the fact that the amount of Re-cycled soot during this stroke is not subjected to oxidation.

Results showed that the concentration of In-cycle soot at the piston crown liner corner is negligible and that the Re-cycled source is the dominant source of soot for deposition in the piston ring pack during blow-by. The very small amount of In-cycle soot available at the piston head-liner corner for deposition, agrees with results from [3-5] who, considering only this source of soot, neglected deposition during blow-by. However, deposition during blow-by in the piston corner may play an important role when the Re-cycled particles are also taken into account.

The comparison between the two regions of interest indicated that the majority of the soot available for deposition is at the liner. This is due to the larger liner exposed-surface of deposition, compared to that at the piston crown-liner corner. The rate of deposition however, depends on the transfer mechanism to oil, which will be discussed in the next chapters of the thesis.

5 Transfer of Soot to the Oil Film on the Cylinder Liner via Thermophoresis

5.1 Introduction

Having calculated the factors affecting the concentration of soot particles in the near-wall regions of the combustion chamber in the previous chapter, the focus in this chapter will be on the mechanisms by which soot transfers from these regions to the oil film on the liner.

Potential transfer mechanisms are Brownian motion, turbulent diffusion, inertial impingement and thermophoresis. Previous investigations on deposition towards cold surfaces of diesel engine combustion chambers concluded that thermophoresis is the dominant soot transfer mechanism onto combustion chamber walls [48, 49]. Accordingly, thermophoresis was the only transfer mechanism considered in this work for studying the soot-in-oil entrainment at the cylinder liner.

In the first part of the chapter, the other potential transfer mechanisms are introduced for completeness. After, a more complete description of the theoretical thermophoretic model used for calculating the thermophoretic deposition velocity is given. The analytical model used is that developed by Talbot et al. [9] and no credit is taken by the author for its development. The author's contribution in this chapter is towards evaluating the influence of parameters such as particle size, engine load and speed, and EGR level on the thermophoretic deposition velocity. This is done by evaluating the influences of these parameters on the variables that govern deposition via thermophoresis: particle size, temperature gradient at the gas-liner interface and kinematic viscosity of the gas. This was necessary as

information on these variables throughout the entire engine cycle is not available from the literature.

Previous experimental works [48, 49, 123] validating Talbot et al. [9] model showed that it can be successfully applied to predict the deposition velocity of soot particles within diesel engines combustion chamber walls. They compared the rate of deposition predicted from Talbot's model with that directly measured over several cycles in regions continuously exposed to the hot combusted gases, such as cylinder head and piston bowl walls. This approach could not be followed in this work because the soot-laden oil film at the liner is continuously washed by the scraping action of the piston rings. Accordingly, a more effective way to measure the rate of deposition would have been to measure the amount of soot accumulated in the oil sump. However, this approach could not be followed as at the time of the investigation a diesel engine able to replicate the engine conditions simulated in Chapter 4 with Kiva-3V was not available. Consequently, the study of deposition via thermophoresis was limited to the theoretical application of the Talbot et al. [9] model.

Regarding soot deposition in the piston ring pack during blow-by, it has been assumed that all the soot escaping the combustion chamber with the blow-by gas are entrained into oil. A similar approach has been followed also by other authors [3-5], while Tokura et al. [51] proved that the rate of entrainment was very high, approximately 80%.

5.2 Theoretical Background

This section addresses some fundamental aspects of the particle transport mechanisms at the near-wall region of the combustion chamber. It is intended as a brief introduction as it is not within the scope of this thesis to cover extensively this topic.

In the core region of the combustion chamber, outside the hydrodynamic boundary layer, particles, due to their small size, are considered massless and therefore closely follow the hot combustion gases. Soot particles are transported to within the hydrodynamic boundary layer by convection, which for turbulent flow is defined as eddy diffusion. Mahmood [102] calculated that this assumption is valid for soot particles smaller than 400 nm. As measured in Section 3.3.3, particles larger than 400 nm represent only 1% of the particles found in oil, and therefore, this assumption can be considered valid. Within the hydrodynamic boundary layer very close to the wall, assuming a no-slip condition, the fluid velocity decreases and the direction of the velocity vector is orientated only tangentially to the cylinder liner. Therefore, very close to the wall, another transport mechanism has to be responsible for the deposition of soot particles to the cylinder liner oil film. Potential transfer mechanisms within this region are Brownian diffusion, turbulent diffusion, inertial impingement and thermophoresis, with the latter reported as the dominant mechanism [48, 49]. The importance of these mechanisms has been thoroughly discussed by Suhre et al. [49] and a summary description of each is provided below. Deposition via thermophoresis will be analysed in the next section.

5.2.1 Brownian Diffusion

Brownian diffusion can be the dominant mechanism for small particles when a particle concentration gradient in the gas exists. The mechanism follows Flick's law which states that particles will move towards low concentration regions with a magnitude proportional to the concentration gradient. This is the typical scenario present in the combustion chamber of diesel engines: as discussed in Chapter 4 most of the soot is concentrated in the bulk region of the combustion chamber

near the piston bowl where it is firstly formed and less concentrated in the squish region close to the liner. However, with increasing particle size and gas velocity this mechanism becomes negligible [124]; Suhre et al. [49] concluded that soot particles would require approximately 9 seconds in order to be deposited solely via Brownian motion. Therefore, this mechanism can be considered negligible.

5.2.2 Turbulent Diffusion

Turbulent diffusion, similarly to Brownian diffusion, also follows Flick's law, with the difference that the diffusive flux of particles is instead due to turbulent fluctuations. This is the dominant particle transport mechanism in the core region of the combustion chamber, where soot is produced at the turbulent flame front and a particle concentration gradient exists with the rest of the chamber, convecting particles from the core to the near-wall region. However, as the intensity of the turbulences at near-wall regions decays, this mechanism cannot cause soot particles deposition into oil [49].

5.2.3 Inertial Impingement

Deposition due to inertial impingement may occur if the particle has enough mass to aerodynamic drag ratio; hence particles may be thrown out of a turbulent eddy and travel towards the wall. On the other spectrum, if soot particles are small they will follow closely the flow without leaving the eddies. A simple approach to evaluate the possibility of deposition due to inertial impingement is through a stop distance model [125]. The model evaluates the theoretical distance that a particle travels due to inertia to decelerate to rest from a given initial velocity, u_{p0}. This is then compared with the distance that the particle should travel in order to be deposited. The stopping distance, $L_{p\infty}$, (Equation 5.1) is calculated from the instantaneous particle velocity, $u_p(t)$:

$$L_{p\infty} = \int_0^{\infty} u_p(t) \exp\left(-\frac{t}{\tau_p}\right) dt \qquad 5.1$$

$$u_p(t) = u_p(0) \exp\left(-\frac{t}{\tau_p}\right) \qquad 5.2$$

The instantaneous particle velocity requires knowledge of both the initial particle velocity, $u_p(0)$, and of the particle relaxation time, τ_p, defined as the characteristic time that a particle spends to respond to a change in the surrounding gas. As first approximation, the initial particle velocity can be assumed to be equal to the gas velocity (estimated as the average piston velocity, $\bar{S}_p$).

$$u_p(0) = \bar{S}_p = 2LN \tag{5.3}$$

With L the engine stroke and N the engine speed. The particle relaxation time is given by:

$$\tau_p = \frac{Cc\ \rho_s\ D_p^2}{18\ \mu} \tag{5.4}$$

With ρ_s the soot particle density, 2,000 kg/m^3 [11], D_p the soot particle diameter, μ the dynamic gas density and Cc the Cunningham slip correction factor, estimated by:

$$C_c = 1 + Kn\left(1.257 + 0.4\ e^{-\left(\frac{1.1}{Kn}\right)}\right) \tag{5.5}$$

Where the Knudsen number, Kn, is defined as the free mean gas path, λ, and particle diameter ratio:

$$Kn = \frac{2\lambda}{D_p} \tag{5.6}$$

And the Gas Mean Free Path, λ, defined as:

$$\lambda = 2\frac{\mu}{\rho_g}\sqrt{\frac{\pi}{8R_gT}} \tag{5.7}$$

Where T is the temperature of the gas, μ the dynamic viscosity, ρ the density and R_g the specific gas constant of the gas, assumed to be air.

Considering a maximum particle diameter of 400 nm, calculated in Section 3.3.3, and assuming the typical diesel engine gas conditions, τ_p is calculated to be approximately 3 x 10^{-7} s. This, together with an initial particle velocity of 7.1 m/s (at engine speed of 2,500 rpm and engine stroke of 0.086 m), resulted in a stopping distance of 5 x 10^{-6} m. This is approximately an order of magnitude

smaller than the distance that the particle should travel to reach the wall (Suhre et al. [49] reported a laminar sub-layer thickness of 6.6 x 10^{-5} m). Consequently, inertial impingement cannot be the soot-in-oil transfer mechanism. Even more so if considered that both the values of D_p and $u_p(0)$ chosen for this estimation overestimate the stopping distance $L_{p\infty}$.

5.3 Thermophoretic Model

Results obtained in Chapter 3 from the NTA investigation of the 15 engine oil samples indicated that 80% of the particles deposited into the lubricant are between 100 and 235 nm in size. These particles, according to the review discussed in the previous section, are too large to be deposited via Brownian diffusion and too small in order to be deposited via inertia. As a consequence of their size distribution and of the high temperature gradient present at the near-wall of the combustion chamber, thermophoresis is the most likely significant mechanism for soot-in-oil deposition.

Thermophoresis is the phenomenon by which a particle suspended in a gas where a temperature gradient exists, experiences a force, named thermophoretic force (F_{th}), in the direction opposite to the temperature gradient. This is the scenario occurring to soot particles as they enter the thermal boundary layer formed between the cold cylinder liner and the hot soot-laden in-cylinder gases. The velocity resulting from the thermophoretic force is called thermophoretic velocity, U_{th}, and represents the quantity of major interest for determining the rate of soot-in-oil deposition. Several attempts to model the thermophoretic deposition velocity have been made since it was first observed by Tyndall [126] in 1870. These are categorised depending on the flow regime, which is characterised by the Knudsen number. Kn was previously defined in Equation 5.6 as the ratio between the free mean gas path, λ, and the particle diameter, D_p. In the *free molecular* regime, for values of $Kn>>1$, the thermophoretic velocity does not depend on particle size. On the other limit, when $Kn<<1$, i.e. particles larger than λ, the regime is defined as *near continuum* and the thermophoretic velocity arises from

the thermal slip along the particle surface due to the temperature gradient existing at the gas-particle interface. The thermophoretic velocity in the *free molecular* regime can be successfully estimated from the expression derived by Waldmann et al. [127]. The first expression for the thermophoretic velocity in the *near continuum* regime was developed by Epstein [128]. Although this expression agreed reasonably well with experimental results, it overestimated the thermophoretic velocity when the thermal conductivity of the particle, k_p is much higher than the thermal conductivity of the gas, k_g. This is the condition occurring in an internal combustion engine, where the thermal conductivity of the soot particle is reported to be 0.26 W/(m·K) [129], over an order of magnitude higher than the thermal conductivity of air. Epstein's analysis [128] was successively improved by Brock [130], who followed a hydrodynamic analysis based on the Navier-Stokes-Fourier theory, with slip corrected boundary conditions, Equation 5.8. This led to an expression that allowed the calculation of the thermophoretic velocity also for $k_g/k_p<<1$. Its application is however limited to $Kn<0.1$ as the Brock's formula is based on the continuum equation with slip-corrected boundary conditions.

As calculated in Section 5.4.4, Kn during the cycle changes so that the flow regime varies between the *free molecular* and the *near continuum.* Therefore, the only application of either the Waldmann et al. [127] or Brock [130] models would not be satisfactory to evaluate the thermophoretic deposition velocity. Talbot et al. [9] constructed an interpolation formula able to estimate the thermophoretic velocity on both the *near continuum* and *free molecular* regimes. As stated by the authors in their article, "although there is no mathematical justification for doing so", they observed that the limit as $Kn\rightarrow\infty$ of the thermophoretic force expression proposed by Brock [130] (Equation 5.8), valid in the near continuum regime, is identical to the expression suggested by Waldmann [127] (not shown here), valid in the free molecular regime, apart from a factor C_s/C_m. C_s and C_m are the Thermal slip and Momentum exchange coefficients respectively, obtained from kinetic theory. As the ratio proposed by Talbot et al. [9] is $C_s/C_m=1.17/1.14/=1.03$, the difference from Waldmann et al. [127] expression is only 3%. Consequently, Brock's expression valid for the near continuum regime can be extended to the

free molecular regime. Its applicability on soot deposition within DI diesel combustion chambers has been proved experimentally by Kittelson et al. [48], Suhre et al. [49] and Tree et al. [123].

$$F_{th} = -\frac{6\pi\ \mu\ \nu\ D_p C_s \left(\frac{k_g}{k_p} + C_t\ Kn\right)}{(1 + 3C_m\ Kn)\left(1 + 2\frac{k_g}{k_p} + 2C_t\ Kn\right)} \cdot \frac{1}{T_0} \cdot \frac{dT}{dy} \qquad 5.8$$

With *dT/dy* the temperature gradient normal to the surface and T_0 the mean gas temperature in the vicinity of the particle. The value of the third constant also obtained from the kinetic theory, the Temperature Jump coefficient C_t, is 2.18 [9].

The thermophoretic velocity, given in Equation 5.10, is then obtained by equating the thermophoretic force of Equation 5.8 to the Stokes-Cunningham drag force formula, F_d, [9] given in Equation 5.9. As this expression of the drag force is accurate for Kn values smaller than one, it is able to cover the range of Knudsen number present in this study [48]. The condition $F_{th} = F_d$ implies that these are the only two forces acting on the particle and that the particle is instantaneously accelerated to the thermophoretic velocity. These assumptions lead to an error of less than 0.01% compared to the exact solution [49].

$$F_d = \frac{3\pi\ \mu\ U\ D_p}{C_c} \qquad 5.9$$

$$U_{th} = -\nu \cdot \left[\frac{2C_s C_c \nu \left(\frac{k_g}{k_p} + C_t Kn\right)}{(1 + 3C_m)\left(1 + 2\frac{k_g}{k_p} + 2C_t Kn\right)}\right] \cdot \frac{1}{T_0} \cdot \frac{dT}{dy} \qquad 5.10$$

The expression assumes the particles to be spherical, despite their typical chain-like, cluster shapes. Rosner et al. [131] calculated that this approximation leads to an error on the thermophoretic velocity of within 8%. This was explained by the fact that due to Brownian rotation, all the possible particle orientation fluctuations cancel out the dependency of the thermophoretic velocity on particle morphology.

The k_g/k_p ratio depends on the temperature as thermal conductivity is a function of temperature. However, no data for the thermal conductivity of soot particles as a function of the temperature were found in the literature. The best available value

for the thermal conductivity ratio is that reported by Kittelson et al. [48] who used a constant value of 0.02; this is used throughout the calculations.

5.4 Influence of Engine Conditions and EGR on the Thermophoretic Deposition Velocity

The kinematic viscosity, the mean gas temperature in the vicinity of the particle and the temperature gradient, as shown in Equation 5.10, all have a linear effect on the thermophoretic deposition velocity. In order to investigate the dependence of the other variables, the term in square brackets, named thermophoretic constant, K_{th} is considered as a single variable. Accordingly, Equation 5.10 is rewritten as:

$$U_{th} = -\nu \cdot K_{th} \cdot \frac{1}{T_0} \cdot \frac{dT}{dy} \qquad 5.11$$

All the terms within K_{th} are constant apart from Kn and Cc, with the latter being also a function of Kn. Consequently, K_{th} is a sole function of the Knudsen number. The objective of the following sections is to investigate how engine conditions and EGR level influence the thermophoretic velocity. This is done by investigating their effects on the variables that govern the magnitude of the deposition velocity: temperature gradient, kinematic viscosity of the gas and thermophoretic constant. These variables have been calculated using proprieties taken from simulation results.

5.4.1 Temperature Gradient Normal to the Wall

Temperature gradient was estimated from the instantaneous heat flux, the in-cylinder bulk temperature and the cylinder wall temperature. The former two were obtained from Kiva-3V results, while the wall temperature was assumed to be constant and equals to 410K. The instantaneous heat flux for the sixteen engine conditions investigated is computed via Kiva-3V by using a modified law of the wall heat transfer model. The model, fully described in [107], assumes that: the flow is quasi-steady, the fluid velocity is parallel to the cylinder wall and it only varies in the direction normal to the wall, the pressure is constant, and that Mach numbers are small so that the internal energy is independent from dissipation of

turbulent kinetic energy. Heat flux as a function of the crank angle is therefore calculated as:

$$\dot{Q}_w = h_c\, A\, (T_g - T_w) \qquad 5.12$$

In which A is the heat transfer surface, T_g is the gas temperature, T_w is the wall temperature, constant at 410 K, and h_c is the heat transfer coefficient which depends on local gas properties and velocities. The calculation of the heat flux as in Equation 5.12 does not account for the heat loss through the walls via radiation. This may contribute for 20-30% of the total heat flux [132]. However, as thermophoresis is only associated with the convective component of the heat flux, radiation can be neglected [48]. Ng [26] using the same heat flux model applied in this work estimated a percentage error relative to experimental data of below ten percent.

Temperature gradients, necessary to determine the thermophoretic deposition velocity of the particles, are calculated from the computed heat flux values using the Fourier's law of heat conduction [11, 48, 133], as given in Equation 5.13.

$$\dot{q}_w = k_g \frac{dT}{dy} \qquad 5.13$$

Where k_g is the thermal conductivity of the gas and $\dot{q}_w$ is the local heat flux determined in the CFD model by Equation 5.12:

This leads to:

$$\frac{dT}{dy} = \frac{\dot{q}_w}{k_g} \qquad 5.14$$

The thermal conductivity is calculated assuming the gas to be air, at the average bulk gas temperature and wall temperature [48]. The bulk gas temperature as a function of crank angle was taken from CFD results, while the wall temperature was kept constant at a value of 410 K. The model assumes a linear thermal boundary layer between cylinder wall and bulk gases. Borgnakke et al. [133] compared results from the one-dimensional heat flow model against experimental results and other heat transfer correlations such as those of Annand [134] and Woschni [135]. The simplified model was able to successfully predict

instantaneous heat transfer during the engine cycle, apart from a sharp front predicted by the model which was not observed in the experimental results. As discussed in Chapter 6, deposition via thermophoresis does not take place during the peak of the heat transfer as the cylinder liner is not yet exposed to the cylinder liner oil film, and therefore this does not influence the deposition model via thermophoresis.

In Figure 5.1, the cumulative heat loss through the cylinder walls of the combustion chamber is shown as a function of engine load. Cases are representative of engine conditions 1b, 2b and 3b from Table 4.3, representing engine loads of 2, 6 and 8 bar BMEP at constant engine speed (2,000 rpm) and EGR level (15%). The heat loss for these cases represents approximately 15-20% of the heat released from the combustion. Similar results are reported by Heywood [11]. For all the engine conditions investigated, until approximately 60° BTDC during the compression stroke the heat flux is negative, i.e. towards the combustion chamber, and the thermophoretic force in the direction away from the wall. Consequently, soot particles during this period cannot be deposited via thermophoresis, which, due to the fact that thermophoresis is the only possible transfer mechanism, implies that particles until 60° BTDC cannot be transferred to oil. This is of particular importance for the EGR Re-cycled soot particles that at this stage of the engine cycle are the only source available for deposition.

Continuing in the compression stroke the gas temperature becomes higher than the liner temperature and the heat loss is directed towards the cylinder liner. Therefore, Re-cycled particles are subjected to deposition at the liner via thermophoresis. During this period, the difference in heat loss between the low and high engine load cases is limited to 20%. The heat loss gradient, and therefore the instantaneous heat flux reach their maximum values short after the combustion event as a consequence of the sharp increase in gas temperature and pressure, and gas velocity. As a result during this period the gradient significantly increases as engine load is increased. As calculated in Section 6.2, near TDC the portion of liner subjected to the scraping action of the piston rings is completely covered by the piston. The only fraction of liner exposed to the soot-laden hot gases is that

close to the cylinder head, which is never involved in the recirculation of soot-laden oil from the combustion chamber to the oil sump. Consequently, deposition during this interval around TDC (32°BTDC to 32°ATDC) does not contribute to soot-in-oil.

Continuing with the expansion stroke, the gas temperature decreases reducing the rate of heat transfer. For all the engine conditions investigated, heat loss after approximately 60°ATDC was only 10% of the total heat transfer. This resulted in a temperature gradient during the late period of the expansion stroke over an order of magnitude smaller compared to the peak values achieved near TDC. Due to the different gas temperature and pressure involved, the heat loss during this period for the low engine case condition investigated (2 bar BMEP) was approximately 70% smaller than for the high engine load condition (8 bar BMEP). This is considerably higher than the difference observed during the compression stroke, and it is due to the different magnitude of the combustion processes.

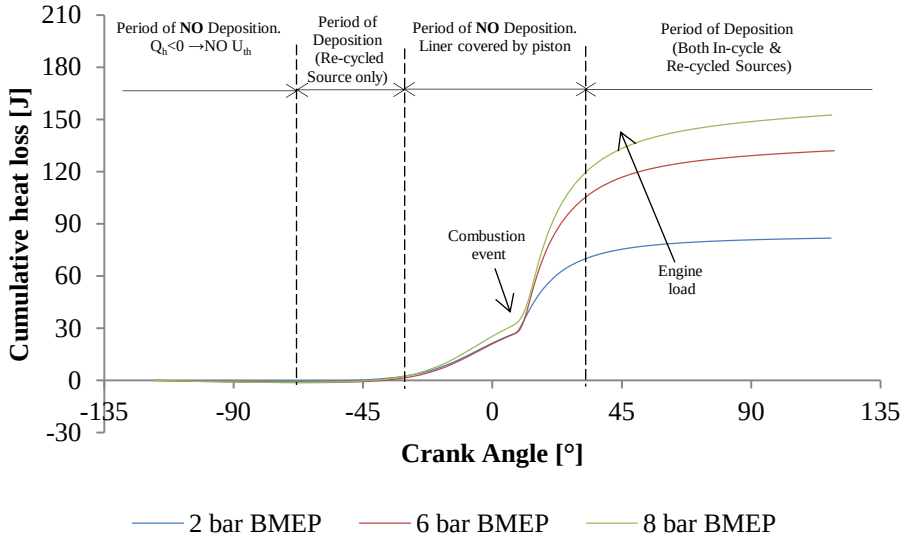

Figure 5.1: Cumulative convective heat loss through cylinder walls calculated with Kiva-3V as a function of engine load. Engine conditions at 2, 6 and 8 bar BMEP, at a constant engine speed of 2,000 rpm and constant EGR rate of 15%.

The influence of engine speed on the temperature gradient was studied by comparing results for Cases 2b and 4b from Table 4.3, representing condition at a constant engine load and EGR level of 6 bar BMEP and 15%, respectively, at

2,000 and 2,500 rpm. Results indicated that the difference is negligible and limited to within 5%. Consequently, the boundary layer temperature gradient is only slightly dependent on engine speed.

Finally, the effect of EGR on the heat loss is shown in Figure 5.2 for the four cases at 6 bar BMEP and 2,000 rpm, with EGR levels varying from 0 to 35%. The profiles are similar to those described in Figure 5.1. Consequences of EGR on the heat loss, and hence temperature gradient, are clearly showed in the expansion stroke period of the cycle. The heat loss is reduced as the EGR level is increased. This is a consequence of the lower amount of oxygen available for the combustion, which results in a lower bulk gas temperature. Overall, as EGR is increased from 0 to 35% the heat flux and the temperature gradient are lower by approximately 15%.

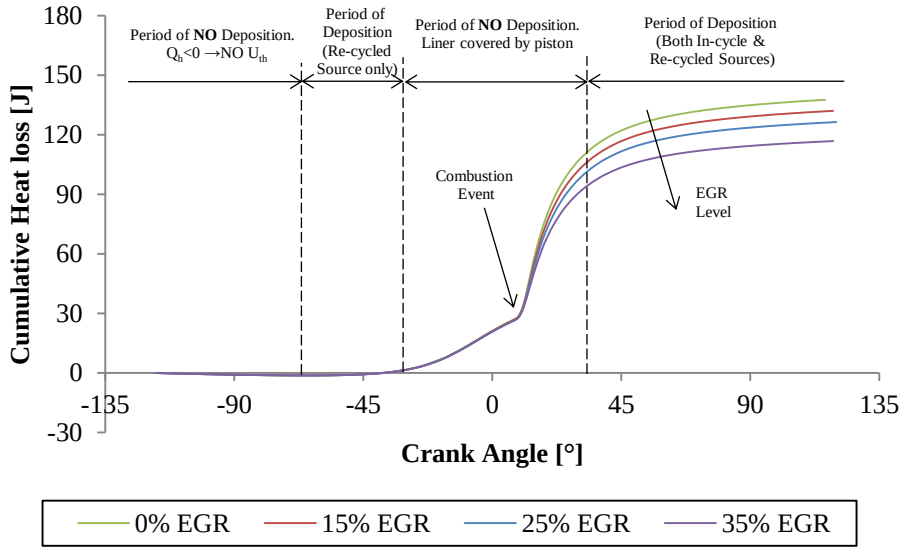

Figure 5.2: Cumulative convective heat loss through cylinder walls calculated with Kiva-3V as a function of EGR level. Engine conditions at four levels of EGR, at a constant engine speed of 2,000 rpm and constant engine load of 6 bar BMEP.

5.4.2 Kinematic Viscosity of the Gas

The kinematic viscosity of the gas, ν, as given in Equation 5.15 is defined as the dynamic viscosity to density ratio. As dynamic viscosity and density depend on in-cylinder gas pressure and temperature, which drastically vary during an engine cycle, the kinematic viscosity of the gas is also expected to drastically vary during the cycle, affecting the thermophoretic velocity.

$$\nu = \frac{\mu}{\rho} \tag{5.15}$$

To help the discussion on the kinematic viscosity, the typical profiles of the gas density and dynamic viscosity are shown in Figure 5.3 for an engine condition (Case 2b, 2,000 rpm, 6 bar BMEP, 15% EGR). The two gas properties are calculated at the bulk gas temperature from simulation output results. This because it is assumed that when the soot particles leave the bulk gas and enter the thermal boundary layer are still governed by the conditions present in the bulk region of the combustion chamber [48].

The gas is assumed to be air throughout the engine cycle despite EGR gas are reintroduced in the combustion chamber during the induction stroke. The difference in gas properties introduced of considering combustion gases as air is typically less than 2% [136]. Assuming the gas to be air and incompressible, the dynamic viscosity of the gas can be considered to be independent from gas pressure. Therefore, its profile closely follows that of the gas temperature, increasing during the compression stroke, followed by a sharp increase after the combustion process and then a decrease during the expansion process. The gas density increases as gas pressure increases, and decreases as gas temperature increases. As shown in Figure 5.3, the effect of the gas pressure on the density dominates over the temperature. This can be explained from the relations that describe a polytropic process which characterise the compression and expansion strokes. Pressure and temperature are related to the change in the combustion chamber volume by the expressions in Equations 5.16 and 5.17. As the piston moves during the compression and expansion stroke, the pressure will vary faster than the temperature, governing the gas density profile during the engine cycle.

$$p\,V^{n} = constant \tag{5.16}$$

$$T\,V^{n-1} = constant \tag{5.17}$$

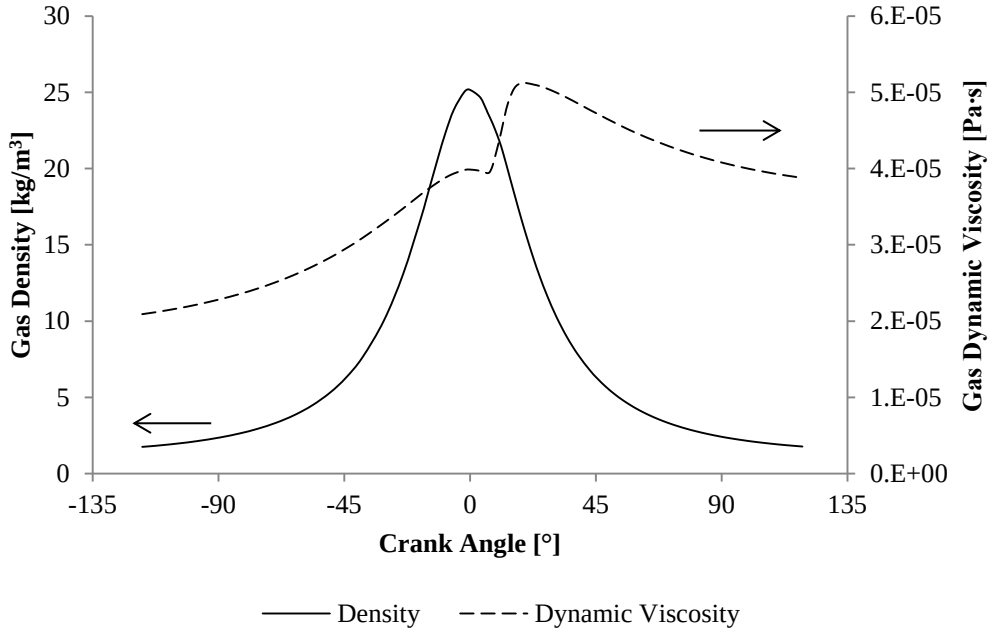

Figure 5.3: Density and dynamic viscosity of the gas for Case 2b from Table 4.2.

Finally, the variation of the kinematic viscosity during the engine cycle at different engine loads is shown in Figure 5.4. Kinematic viscosity showed an opposite trend to that of density, decreasing during the compression stroke and increasing during the expansion stroke. This is due to the fact that the density is at the denominator in Equation 5.15 and that its effect is dominant over that of the dynamic viscosity. This implies that the kinematic viscosity is mainly dependent on gas pressure. The profile of the kinematic viscosity is opposite to that of the temperature gradient discussed in the previous section: when ν is maximum dT/dy is minimum and vice versa. Furthermore, as gas pressure is higher at high engine load, the kinematic viscosity is decreased by approximately 15% as the engine load is increased from 2 to 8 bar BMEP. Again, this is the opposite effect of what was observed for the temperature gradient. The variation in kinematic viscosity with engine speed and EGR level is for the engine conditions investigated within 5%.

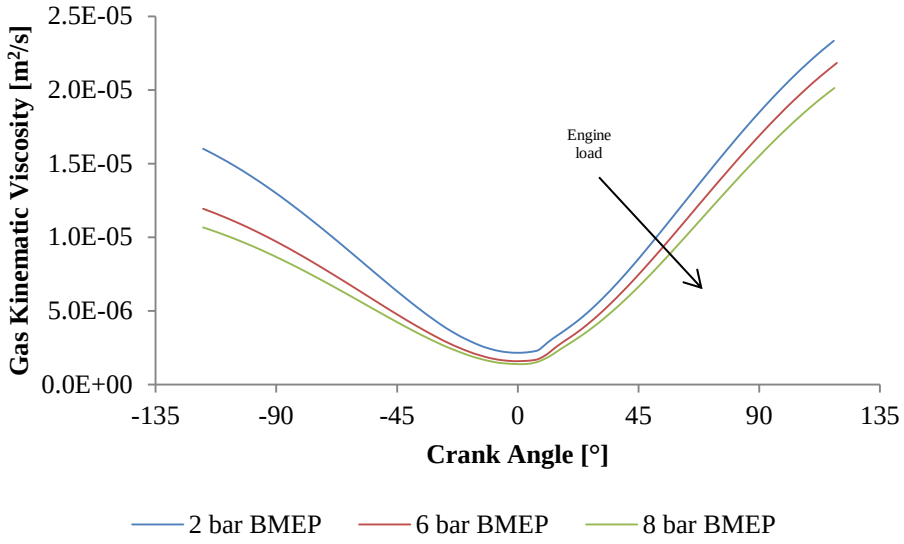

Figure 5.4: Kinematic viscosity of the gas at different engine loads during the engine cycle for Cases 1b, 2b and 3b from Table 4.3.

5.4.3 Thermophoretic Constant

According to Equations 5.6 and 5.7, the Knudsen number varies with particle size and with in-cylinder gas conditions. The objective of this section is to evaluate the influence of these variables on the thermophoretic constant and thus on the thermophoretic velocity.

The variation of Knudsen number with particle size is investigated by using the results obtained during the NTA investigation discussed in Chapter 3. Five different particle sizes are considered: *I)* Average (155 nm), *II)* 10^{th} percentile (100 nm), *III)* 90^{th} percentile (236 nm), *IV)* Minimum (24 nm) and *V)* Maximum (700 nm). Values are taken from the last row of Table 4.3, and represent the average of the 15 samples analysed.

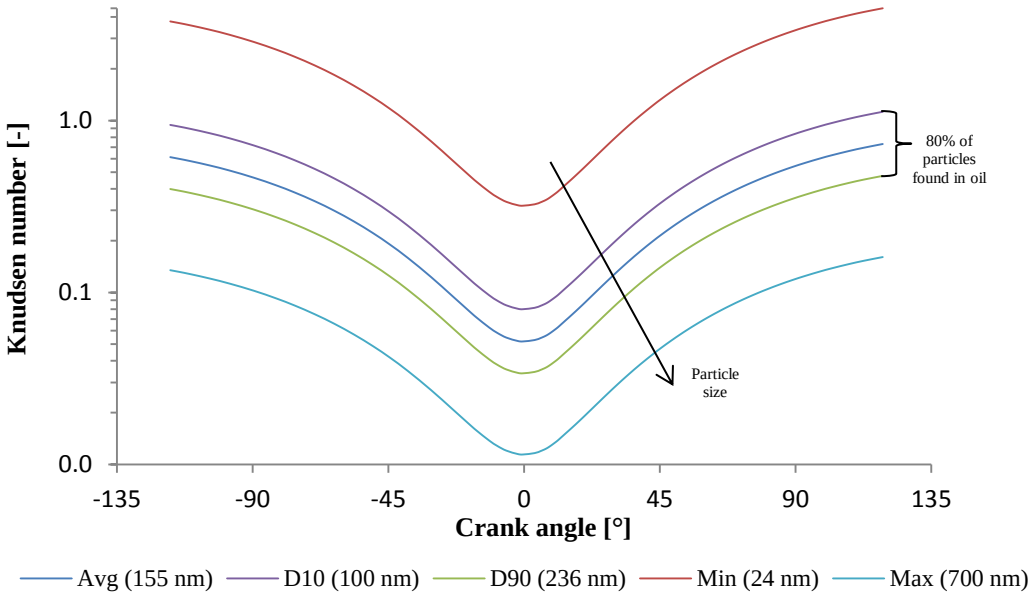

Figure 5.5: Knudsen number as a function of particle size for Case 2b of Table 4.3 (6 bar BMEP, 2,000 rpm and 15% EGR).

For all the particle sizes investigated, Knudsen number decreases during the compression stroke and re-increases during the expansion stroke, reaching its minimum value around TDC. The profile of Kn during the cycle follows that of the kinematic viscosity, which is at the numerator of the free mean gas path term.

According to Equations 5.6, the Knudsen number linearly decreases as particle size increases. This is shown in Figure 5.5, where Kn varies significantly as particle size varies from 25 nm to 700nm. The variation of Kn due to in-cylinder gas conditions and particle size is such that both the *continuum* (Kn<0.1) and *free molecular* (Kn>>1) flow regimes are encountered during the engine cycle. This confirms that the interpolation equation proposed by Talbot et al. [9] is necessary in order to evaluate the thermophoretic velocity across the wide range of Kn present within the combustion chamber.

The profile of the Knudsen number during the cycle agrees well with that reported by Kittelson et al. [48]. However, their Kn used for the calculations was smaller as based on a larger particle diameter (1 μm). According to the NTA results, this particle size is not representative of soot-in-oil particles.

Of even more interest for the thermophoretic velocity, is how the variation of Kn with particle size affects the thermophoretic constant. Results for the five different particle sizes are shown in Figure 5.6.

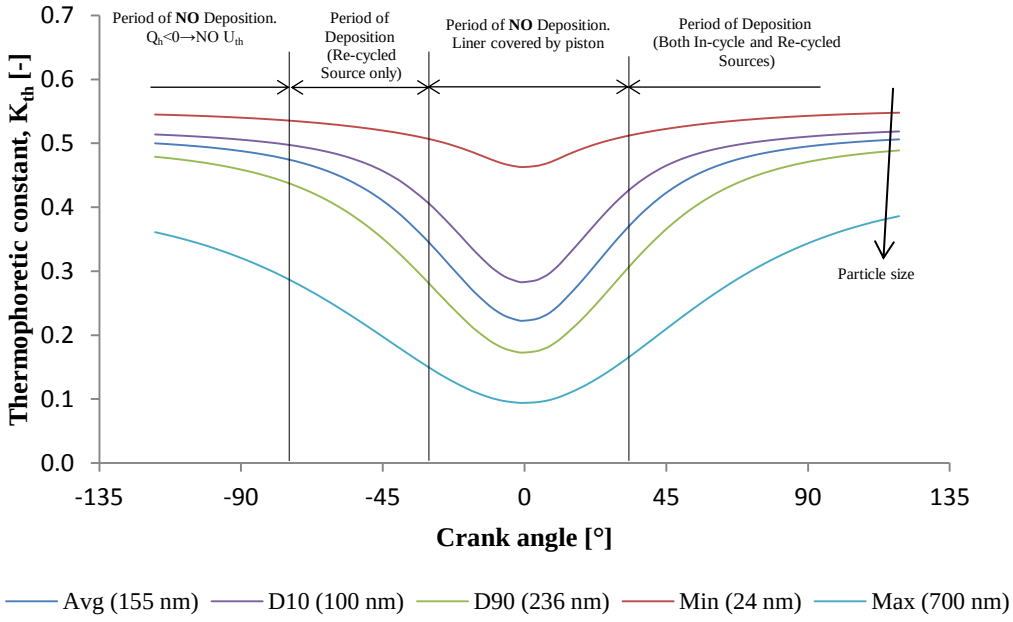

Figure 5.6: Variation of the Thermophoretic constant, K_{th}, during the cycle for different particle sizes.

According to what was discussed and calculated in Sections 5.3.1 and 6.2, during the cycle there are two periods of no deposition. The first occurs between the induction stroke and first part of the compression stroke as the heat flux is directed from the wall to the in-cylinder gas. The second occurs close to TDC when the portion of oil film on the liner subjected to the scraping action of the piston rings is still completely covered by the piston. As shown in Figure 5.6, the second period is of particular interest as it is close to TDC that K_{th} significantly decreases due to the Kn trend described in Figure 5.5.

Considering only the period where soot transfer to oil contributes to soot-in-oil accumulation, the thermophoretic constant for particle size of 24 nm can be considered as constant and equal to approximately 0.55, which is the limit of K_{th} for $Kn \rightarrow \infty$. This agrees with the conditions within the *free molecular* regime, in which the thermophoretic velocity is considered to be independent from particle

size and only dependent on gas conditions. As the particle size increases (Kn decreases), the variation of K_{th} during the engine cycle also increases. For particles between 100 nm and 236 nm (80% of the particles found in oil), the K_{th} variation during the cycle is between 18% and 53%, respectively. In particular, for the average particle size value, 155 nm (used to evaluate the thermophoretic velocity throughout this work), K_{th} moderately varies from approximately 0.51 to 0.38. This indicates that using a constant value for K_{th} of 0.55 would overestimate the thermophoretic deposition of up to 34%. Finally, the thermophoretic constant, and hence the thermophoretic velocity for particles of 700 nm is up to two times smaller compared to the other particle size investigated.

The engine conditions investigated in this work considered different engine load, speed and EGR level. These may all affect the thermophoretic constant through the Knudsen number via the mean free gas path. According to Equation 5.7 engine conditions may vary the mean free path via two variables: kinematic viscosity and temperature of the gas. In Figure 5.7 the effects of engine load on K_{th} are studied by comparing the engine conditions at 2,000 rpm and 15% EGR at 2, 6 and 8 bar BMEP, representing respectively Cases 1b, 2b and 3b from Table 4.3. All the calculations are relative to a particle size of 155 nm.

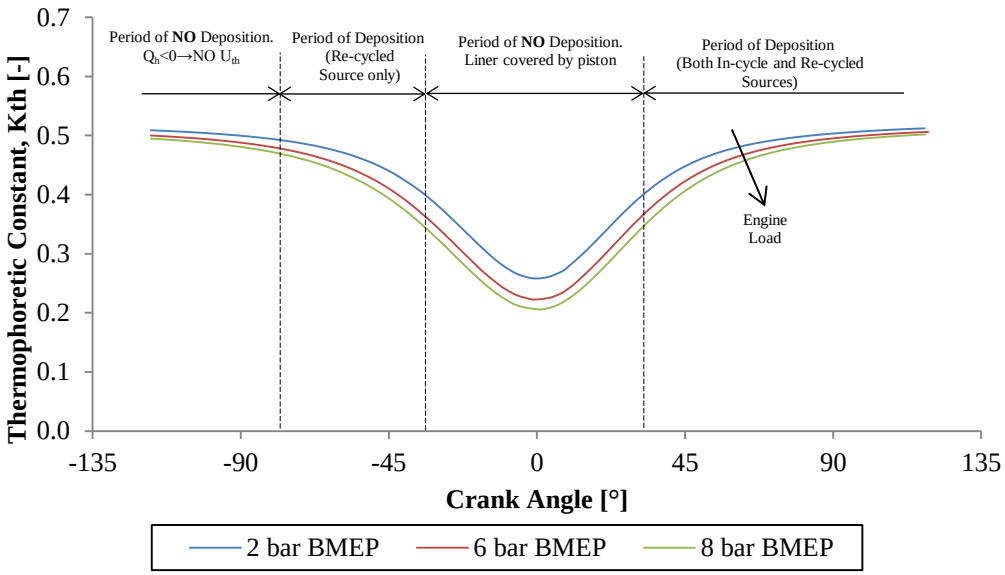

Figure 5.7: Influence of engine load on the thermophoretic constant, K_{th}.

As engine load increases, the thermophoretic constant decreases. This is explained by the associated decrease of the kinematic viscosity with engine load. Furthermore, because the in-cylinder gas temperature is at the denominator within the square root term, as the temperature increases with engine load, the mean free gas path is further decreased. The effect engine load on K_{th} is however weaker compared to that of particle size.

The thermophoretic constant is found to be almost independent from engine speed. This is due to the fact that the variation of the in-cylinder gas temperature and pressure (and therefore Kn) with engine speed is minimal. K_{th} can be therefore considered independent from engine speed.

The effect of EGR on K_{th} is investigated by considering the engine conditions at 6 bar BMEP and 2,000 rpm, at four EGR levels from 0 to 35%, representing Cases 2a-d from Table 4.3, respectively. Also the level of EGR is found to have a weak effect on the thermophoretic constant. This can be explained as follows. The main effect of EGR is to lower the in-cylinder gas temperature. This decreases the dynamic viscosity and increases the gas density, lowering the μ/ρ ratio (kinematic viscosity). On the other hand, as T decreases, the square root term within λ increases. It is found that the two effects counteract each other with the result that the influence of EGR on Kn and therefore on K_{th} can be neglected.

5.5 Discussion and Conclusions

In-cylinder gas conditions vary drastically during a diesel engine cycle with the consequence that also the conditions at which soot deposition via thermophoresis takes place change. Deposition via thermophoresis starts after the gas temperature rises above the liner temperature. This, for all the engine conditions investigated, occurs at approximately 60° BTDC. Discussion before this period is therefore not included in this work as not of interest for soot-in-oil accumulation. During the compression stroke only the Re-cycled source is available in the combustion chamber. The temperature gradient increases by over an order of magnitude. This is, however, not followed by a proportional increase in thermophoretic deposition

velocity as the kinematic viscosity, thermophoretic constant and $1/T_0$ terms decrease during the compression stroke. The former two decrease as a direct consequence of the increase in gas pressure during the compression stroke which affects the kinematic viscosity and the Knudsen number.

The maximum value of the thermophoretic velocity is reached together with the combustion process (approximately between TDC and 20° ATDC). This is because the combustion causes a peak in the heat flux and, consequently, in the temperature gradient at the boundary layer. The peak in thermophoretic velocity however, is not of interest for soot-in-oil deposition as the oil film subjected to recirculation to oil sump is not exposed to the hot gases. This last aspect is discussed in Section 6.2 of this thesis.

Continuing with the expansion stroke, the piston moves downwards exposing the portion of liner subjected to the washing of the piston rings; at this point both In-cycle and Re-cycled sources are available for deposition. The magnitude of the thermophoretic velocity decreases by over an order of magnitude compared to the peak values at around TDC. This is due to the fall in heat flux and therefore, in the temperature gradient at the cylinder liner. However, the drastic decrease in temperature gradient is partially balanced by the increase in the other three terms governing U_{th}: kinematic viscosity of the gas, $1/T_0$ and thermophoretic constant. As a consequence, deposition during the expansion stroke occurs at rates of the same order of magnitude as for the compression stroke.

The influence of EGR level, engine conditions and particle size on the thermophoretic velocity is summarised in Table 5.1. The deposition velocity is found to mainly vary with particle size and engine load. Particle size affects the thermophoretic velocity only via the thermophoretic constant. As the soot particle size increases, the Knudsen number and therefore the thermophoretic velocity decrease, reducing thus the deposition velocity. For example, the deposition velocity of a particle 700 nm in size is between 2 and 4 times smaller than that of a 100 nm particle. Furthermore, the thermophoretic constant, K_{th}, for small particles can be considered as constant and equal to 0.55, while K_{th} for large particles varies considerably during the engine cycle. This may explain why the

number of large particles detected in oil is very small, with particles larger than 1 µm not being detected in any of the 15 engine oil samples tested with NTA. As the mesh grid size of a typical engine oil filter is able to only trap particle larger than approximately 5-10 µm, this may result in an almost complete ineffectively of these filters against soot particles deposited into oil.

The thermophoretic velocity is found to increase as engine load is increased. This can be explained as follows. As engine load increases, the gas temperature and pressure sensibly increase as a consequence of the higher boost pressure and energy released during the combustion process. This led to an increase of approximately 70% in the temperature gradient at the wall between a low load and a high engine load conditions. This drastic increase is however partially counteracted by the decrease in the kinematic viscosity of the gas, and consequently in the thermophoretic constant. Furthermore, the increase in the temperature gradient on the overall deposition velocity is further attenuated by the mean gas temperature in the vicinity of the particle, T_0, term. Results discussed in Chapter 4, showed that as the engine load is increased from two to 8 bar, the availability of soot at the liner increases by approximately two orders of magnitude. Consequently, although engine load affects the thermophoretic deposition velocity, its dominant effect is on the availability of soot particles at the near-wall region.

This is even more enhanced when comparing the effect that EGR level has on the thermophoretic velocity and on the availability of soot particles at the near-wall region. In Chapter 4 was discussed that EGR strongly increases the concentration of soot particles at the liner of the combustion chamber, from both the particles produced during the combustion chamber and that recycled back with the EGR gas. On the other side, the effect on the thermophoretic velocity when EGR is increased from 0 to 35% is limited to within 5%. Therefore, it can be concluded that EGR affects the amount of soot-in-oil by increasing the concentration of particles in the region of interest for deposition, rather than by influencing the particle deposition velocity.

Similarly to EGR, also engine speed has a weak effect on the thermophoretic deposition velocity. Its main effect is to increase the heat transfer to the wall as engine speed is increased. This is due to the higher gas velocity, which increases the convective heat transfer. However, this effect is again weaker compared to the increase in soot availability with engine speed. Overall, apart from particles size, the effects of engine conditions and EGR level on the velocity at which the particles are transferred to oil, are considerably weaker compared to the effects they have on the concentration of particles at the near-liner region. Therefore, it can be concluded that the distribution of particles close to the cylinder liner is the factor governing soot-in-oil deposition.

Variable			K_{th}	dT/dy	ν	$1/T_0$	$\mathbf{U_{th}}$
Particle Size	25 → 700	[nm]	↓↓	-	-	-	↓↓
EGR	0 → 35	[%]	↓	↓↓	↑	↑↑	↓
Engine Speed	2,000 → 2,500	[rpm]	-	↑	-	-	-
Engine Load	2 → 8	[bar]	↓	↑↑	↓	↓	↑

Table 5.1: Influence of particle size, engine conditions and EGR level on thermophoretic velocity and parameters governing the deposition velocity. Legend: (-) = not or weakly affected; (↑) moderate increase, <15%; (↑↑) strong increase, >15%; (↓) moderate decrease, <15%; (↓↓) strong decrease, >15%.

6 Rate of Soot-in-Oil Deposition

6.1 Introduction

Having calculated both the concentration and transfer mechanisms of soot particles in the regions of interest for deposition into oil in Chapters 4 and 5, the aim of this chapter is towards evaluating the rate of soot-in-oil deposition from both the liner and blow-by pathways. Results from the two pathways are compared in order to assess their relative importance. The influence of engine speed, engine load and EGR level on the deposition rates is also investigated, with both the In-cycle and Re-cycled sources of soot being taken into account. Results are also presented in terms of fraction of fuel converted into soot and deposited into oil.

In the first part of the chapter the amount of soot that ends up in the oil sump from deposition to the oil film on the cylinder liner is calculated. As not the entire liner is subjected to the scraping action of the piston rings, the fraction of liner subjected to scraping, and therefore of interest for soot accumulation in oil, has been determined. Finally, the rate of soot deposition in oil from this pathway is calculated.

In the second part of the chapter, the rate of soot-in-oil entrainment in the piston ring pack through blow-by gases is calculated. This required the determination of the mass of air escaping the combustion chamber towards the crankcase, blow-by. This, together with results from Chapter 4 (soot concentration in the piston crown-liner corner), allowed the calculation of the soot contained within blow-by gas entering the piston ring pack for deposition. As discussed in Chapter 5, it is assumed that all the particles carried by the blow-by gas passing through the piston ring pack towards the crankcase are deposited into oil. The final part of this chapter is concerned with validating the rates of transfer to oil obtained from the analytical deposition model presented in this thesis. Results are compared with the

typical deposition rate from a light-duty diesel engine and with the fraction of fuel in oil as soot. These were estimated in Chapter 3 from the 15 oil samples collected from light-duty diesel vehicles at different oil change intervals and analysed experimentally using TGA technique.

6.2 Amount of Soot-in-Oil via Deposition to the Oil Film on the Liner via Thermophoresis

The rate of soot-in-oil accumulation from deposition to the oil film on the cylinder liner depends upon three factors. Firstly, the amount of soot available in the near-liner region of the combustion chamber. Secondly, the degree of thermophoretic effect at the near liner, which according to what was presented in the previous chapter, is the only soot transfer mechanism present close to the wall, governing therefore the rate at which the available particles are deposited in the oil film. Finally, the third factor is the transfer of the oil film on the liner to the oil sump via the scraping action of the piston rings. The next section evaluates the swept liner, which represents the portion of liner which is subjected to the scraping action of the piston rings.

6.2.1 Swept Liner

The piston ring pack of light-duty diesel engines typically consist of three piston rings, schematically shown in Figure 6.1. The upper ring is a Top Compression Ring (TCR), commonly made of steel with a plain rectangular profile on the liner side. Its function is to seal the combustion chamber during high pressure conditions and to transfer heat from the piston to the cylinder liner. The second compression ring, named the wiper ring, made of cast iron, helps the TCR seal the combustion chamber as well as help the bottom ring, the Oil Control Ring (OCR), lubricates the liner during the upwards strokes and scraping off the oil film during the downward strokes. The main role of the OCR is to evenly distribute the oil onto the liner. The ring is perforated in the peripheral direction to facilitate the return of oil to the crankcase. The typical oil film left on the liner during the downstroke is between 5 and 10 μm thick [137]. The OCR does not contribute to the seal of the combustion chamber's gas.

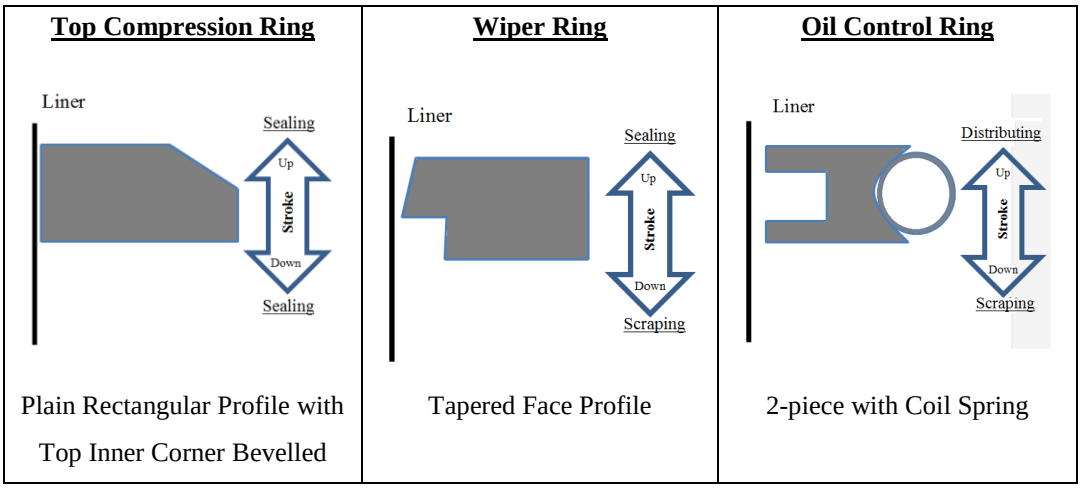

Figure 6.1: Schematic of the piston rings of the Ford Puma 2.0 L diesel engine used in this work as a model for the CFD simulations.

During the downstroke, the main roles of the piston rings are to seal the combustion chamber and to scrape oil off the liner in order to control oil consumption. The OCR is the first ring to encounter the large amount of oil left on the liner from the previous stroke. The Minimum Oil Film Thickness (MOFT) left behind is thinner due to its scraping action. The oil is mainly collected on the ring groove, where it is dragged through the peripherals holes by the blow-by gases into the crankcase. The second ring is fully flooded and it scrapes off the oil film left by the OCR, accumulating it on the third land. The MOFT is further reduced, confirming the scraping action of this ring. Finally, the top compression ring, due to its plain profile, does not scrap the oil left by the two previous rings. As a consequence, the MOFT value remains approximately the same as before.

During the upstroke, the TCR is the first ring to encounter the oil film left from the previous stroke. This passes under the ring without accumulating ahead of the ring. Under this condition, the MOFT remains the same as the one left from the previous downstroke. Gamble et al. [137] observed very little build up in front of the ring during only the changes of direction of the piston. If this happens, the oil accumulated on the first piston land in front of the TCR is considered lost through the exhausts via combustion, evaporation or inertia. The Second Ring, due to its shape, does not scrap any oil off the liner. Consequently, the MOFT left behind is considered to be the same as the TCR. The OCR encounters the oil left from the

second piston ring and the oil accumulated on the third land from the previous stroke. Its function during the upstroke is to supply oil to the liner and to evenly distribute it. The MOFT of the OCR is higher than that of the second ring.

Due to the rings' behaviour, not all the liner exposed to the in-cylinder gases is subjected to the scraping action of the rings and therefore contributing to soot-in-oil builds up. For instance, the oil film on the liner between cylinder head and top compression ring when the piston is at TDC (red band "a" from Figure 6.2) is never subjected to the scraping action of the rings. Therefore, this portion of liner does not contribute to soot-in-oil build up. Ma et al. [138] reported that the oil film in this region is not dragged back to the piston ring pack and it is, therefore, exhausted.

This is of particular interest as the soot concentration in the near-liner region evaluated using CFD, considered the entire liner exposed to the in-cylinder charge, and not only the swept liner subjected to recirculation. Furthermore, as discussed in Section 4.7, the CFD model did not include a crevice region. Therefore, the liner is exposed to the in-cylinder charge only above the piston head-liner corner. The top piston land, indicated by the orange portion in the right-hand side of Figure 6.2, is not considered in the calculations. As a consequence, the liner subjected to rings' scraping is exposed to the hot cylinder charge only when the piston has travelled a distance greater than the top piston land itself. The portion of liner exposed to the hot gas and subjected to the scraping action, named L_{exp}, is given by the difference between stroke and top piston land height.

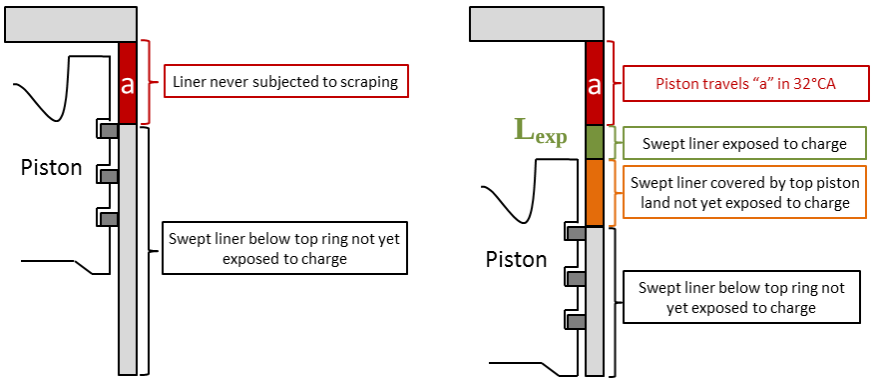

Figure 6.2: Schematic of the fraction of liner exposed to soot-laden cylinder gases subjected to the ring' scraping action.

According to the geometric characteristics of the engine and of the piston ring pack, L_{exp} is zero when the piston is between 32° BTDC and 32° ATDC. During these 64° CA, the soot deposited into the oil film at the liner does not contribute to soot build-up in the sump. This is of particular interest due to the fact that it is during this part of the cycle that the thermophoretic deposition velocity reaches its maximum values.

As the evaluation made using CFD assumed the amount of soot at the cylinder liner to be uniformly distributed along the liner exposed to the cylinder gases and changing only with time, it is necessary to calculate what fraction of the entire liner is subjected to the scraping action of the piston rings (f_{exp}). This is given by the ratio of L_{exp} and the entire liner exposed to the in-cylinder gases, as given by Equation 6.1.

$$f_{exp} = \begin{cases} 0 & Stroke \leq Top\ piston\ land \\ \dfrac{Stroke - Top\ piston\ land}{Stroke + Squish\ height} & Stroke > Top\ piston\ land \end{cases} \qquad 6.1$$

The variation of f_{exp} during the engine cycle is shown in Figure 6.3. Theoretically, the amount of soot-laden oil recirculated back to the oil sump could be reduced by increasing the top piston land height. However, this has a negative effect on oil consumption, as a higher amount of oil is left continuously exposed to the in-cylinder gases.

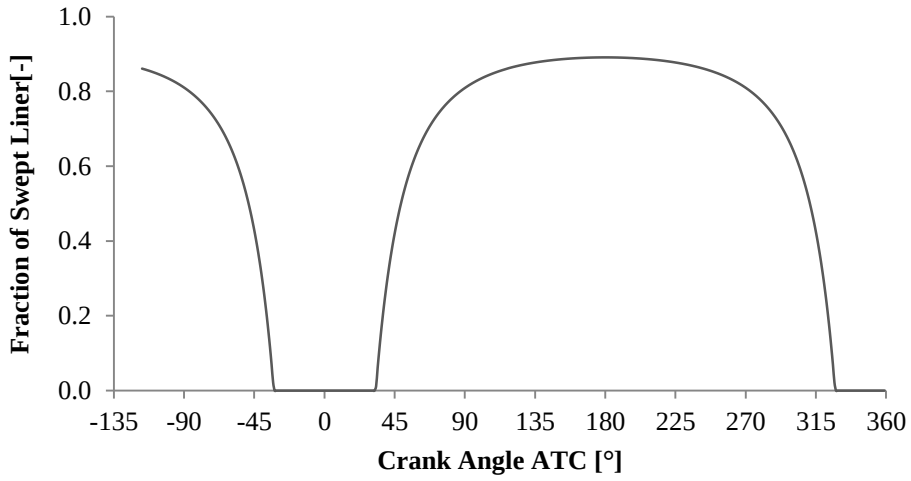

Figure 6.3: Fraction of swept liner exposed to the hot soot-laden in-cylinder gases contributing to soot deposition in oil during the engine cycle.

6.2.2 Rate of Soot Deposition at the Cylinder Liner

After having determined the concentration of soot at the near-wall liner, the degree of the thermophoretic effect and the fraction of liner which contributes to soot-in-oil builds up, the amount of soot deposited on the liner at a given time step can be determined. In this study, 1° CA was chosen as interval for the calculation. As two different engine speeds were investigated, the time step, dt, at every 1° CA changed accordingly:

$$dt = \frac{ds}{S_p} \tag{6.2}$$

In which ds, is the piston displacement at every1° CA, and S_p is the instantaneous piston velocity, given by Equations 6.3 and 6.4, respectively [11].

$$ds = a\ \cos d\vartheta + \sqrt{(l^2 - a^2 \sin^2 d\vartheta)} \tag{6.3}$$

$$S_p = \bar{S}_p \times \frac{\pi}{2}\left[1 + \frac{\cos\vartheta}{\sqrt{(l/a)^2 - \sin^2\vartheta}}\right] \tag{6.4}$$

Where a, is the crank radius, l the connecting rod length and $\bar{S}_p$ the mean piston velocity and ϑ is the crank radius angle.

The amount of soot deposited is calculated from the determination of a swept volume, and assuming that all of the soot within this is deposited. The assumption of neglecting re-entrainment of the deposited particles is valid due to the oil film that acts as a sticky-surface. The swept volume, as shown in Equation 6.5 is equal to the surface area of liner exposed to in-cylinder gas times the distance travelled by the particle at the thermophoretic velocity, L_{th}. The latter is calculated as the product between the thermophoretic velocity, U_{th}, and the time step, dt.

$$V_{swept}(\theta) = Area \cdot L_{th} = Area \cdot U_{th} \cdot dt \tag{6.5}$$

The ratio of the swept volume to the cell adjacent to the liner volume, V_{cell}, at each time step is:

$$f_{swept}(\theta) = \frac{V_{swept}}{V_{cell}} \tag{6.6}$$

This allowed the evaluation of the mass of soot contained in the swept volume and deposited on the liner at every time step, $m_{s,lin}$:

$$m_{s,lin}(\theta) = f_{swept} \cdot m_{s@liner} \quad 6.7$$

The term $m_{s@liner}$, representing the mass of soot available at the near-liner region, can be rewritten as in Equation 6.8 in order to show the contribution from both the In-cycle and Re-cycled sources of soot:

$$m_{s,lin}(\theta) = f_{swept} \cdot (m_{sInc@liner} + m_{sEGR@liner}) \quad 6.8$$

The mass of soot deposited in the liner actually contributing to soot-in-oil builds up, $m_{s,dep@lin}$, is then equal to the mass of soot deposited at the liner times the fraction of liner subjected to the scraping action of the piston rings, *fexp*:

$$m_{s,dep@lin}(\theta) = f_{exp} \cdot m_{s,lin} \quad 6.9$$

The term $m_{s,lin}$ was continuously adjusted in order to take into account the amount of soot deposited during previous steps. Finally, the amount of soot deposited into the oil film at the liner over the entire engine cycle is given by the integration of Equation 6.9 between IVC and the end of the exhaust stroke.

$$m_{dep} = \sum_{\theta=IVC}^{360^\circ} m_{dep}(\theta) \quad 6.10$$

The amount of soot calculated as in Equation 6.10 represents the contribution from a cylinder. The total engine contribution is then obtained by multiplying this value by the number of cylinders, which in this case is four.

6.3 Amount of Soot-in-Oil via Deposition in the Piston Ring Pack during Blow-by

Yasutomi et al. [139], schematised the oil flow in the piston ring pack as characterised by a relative small volume, short residential time and high temperatures. Results from Starks et al. [140] indicated that the oil residential time in the piston ring pack for a light-duty gasoline engine is approximately 60 seconds. Saville et al. [141] with a heavy-duty diesel engine reported a residential time three times higher than that seen in [140]. Direct comparison between the two results is difficult due to the different nature of the engines. The discrepancy may be due to the larger volume of the piston assembly for the heavy-duty engine, as well as to the higher in-cylinder pressure reached by the diesel engine.

The lubricant oil occupies approximately a quarter of the free volume between top compression ring and oil compression ring. Reported experimental data suggests that oil moves within the ring pack following different paths: axially, through the ring groove, through the ring end gaps, and circumferentially around the piston lands [142]. The axial displacement is determined by the inertial force generated by the reciprocating piston motion, with its magnitude governed by engine speed and volume of oil available [143]. In an experimental investigation, Thirouard et al. [144] observed that the groove-ring clearance was a major path for the oil to flow between piston lands. The process was mainly governed by the ring pumping action and by the lateral motion of the piston relative to the rings. The amount of oil available passing through the rings groove was governed by the ring squeezing action and by the vertical oil displacement caused by the inertial forces.

Finally, the oil flows through ring end gaps and circumferentially around piston lands is governed by the dragging action of the blow-by gases. Regarding the first path, Thirouard et al. [144] did not observe oil accumulation upstream of the gaps. Their results suggested that the oil, entering the gaps broke down into a mist due to the high fluid velocity, and was then deposited on the liner and piston land.

The oil is dragged circumferentially by the high blow-by gases velocity which generates a shear stress at the gas-lubricant interface [137]. Thirouard et al. [144]

experimentally observed that the velocity and direction of the circumferential oil displacement mainly depended on two factors: the relative position between consecutive ring end gaps and the magnitude and direction of the blow-by gases. The maximum oil velocity was achieved with the gaps located diametrically opposite to each other and the minimum with the gaps aligned. They also found that as blow-by gases were flowing in the direction of the crankcase, the oil was consequently moving towards the lower ring gap. On the other hand, when reverse blow-by was observed, the oil flow was also changing direction moving upwards, confirming the dependence of the oil motion on the blow-by gases.

Due to the interaction between oil and blow-by gas, as well as the relative large volume of oil available in piston ring pack volume, it has been assumed that all the soot carried by the blow-by gas is deposited into the oil in the piston ring pack. The assumption is justified by the high deposition rate observed by Tokura et al. [51]. As will be discussed in detail later on in Section 6.7, the relative contribution of deposition during blow-by to the overall soot-in-oil deposition is small. Therefore, any errors introduced by the above assumptions will have a small effect on the total rate of soot deposition calculated.

6.3.1 Blow-by Model

In order to determine the amount of soot entering the piston ring pack, and hence deposited, it is necessary to determine the mass of air escaping the combustion chamber into the crankcase, i.e. blow-by. Blow-by represents the major in-cylinder gas loss, and due to the gaps existing between the combustion chamber and crankcase volumes, it cannot be fully eliminated. It is well recognised that the gases escape the cylinder following three possible routes to reach the oil sump [138, 145-147]. The first, as illustrated in (*a)* from Figure 6.4, is through the clearance formed between piston ring and cylinder liner. The amount of blow-by in this direction is however limited by the oil film which acts to seal. A consistent amount of blow-by between liner and rings would cause the removal of this oil film, leading to an increase in wear [147]. The second flow path is between the flank of the ring and the ring groove, as shown in (*b)*. The gas flow in the first piston land is assumed to be a Couette flow, with a negligible pressure drop of 0.2%

[148]. Therefore, the pressure above the top compression ring is typically considered equal to the in-cylinder pressure. During most of the compression and expansion strokes, this is high enough to press the ring onto the lower groove flank limiting the amount of blow-by through this direction [147]. Finally, the third mechanism, (*c*), through the ring end gap, is generally recognised as the main path even at high levels of pressure. The gap section available for the blow-by gases to pass through the ring increases at high pressure as the rings expanded towards the liner [149].

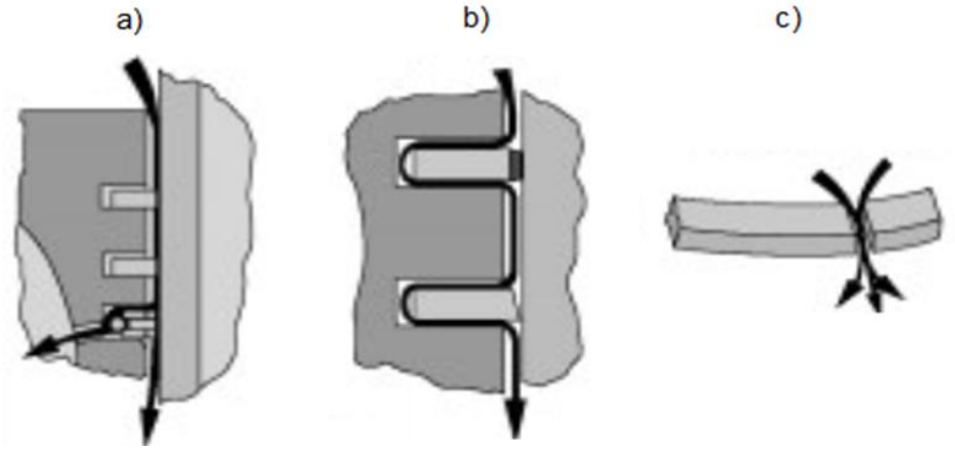

Figure 6.4:Schematic of Blow-by paths: a) between piston ring and cylinder; b) between piston ring and groove side; c) through the ring gap [145].

Accordingly, blow-by in this work is studied by considering the end ring gaps as the only possible passage for the gas. The amount of gas escaping the combustion chamber is quantified using a two-ring compressible flow model, similar to that used by Munro [50]. The gas passage is treated as a number of volumes connected by orifices, as illustrated in Figure 6.5. During the entire cycle, the rings are assumed to be located on the lower groove flank.

The oil control ring is neglected in the calculation as its main function is to evenly distribute the oil in the piston ring pack rather than sealing the volume. Within each volume, gas temperature and pressure are assumed to be constant. Due to the large surface area to volume ratio, the gas temperature is considered to be cooled to the liner temperature, here assumed 410 K [26]. The pressure in the third land,

region (*3*) from Figure 6.5, is considered to be the same as the crankcase pressure, while in the top land, region (*1*) is assumed to be the in-cylinder pressure.

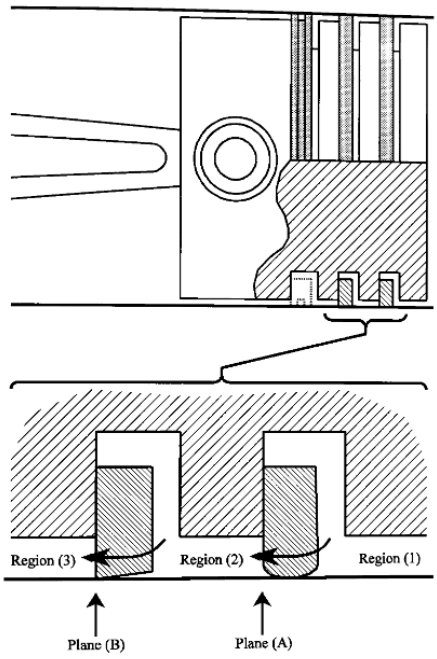

Figure 6.5: Schematic of two-ring compressible flow Blow-by model.

The mass flow rate from region *1* to region *2*, $\dot{m}_{BB}$, is calculated from the compressible gas flow through a restriction equation. For subsonic flow the mass flow rate is given by Equation 6.11:

$$\dot{m}_{BB} = \frac{C_d A_o \, p_u}{\sqrt{R_g \, T_g}} \left(\frac{p_o}{p_u}\right)^{\frac{1}{\gamma}} \sqrt{\frac{2\gamma}{\gamma - 1}\left[1 - \left(\frac{p_o}{p_u}\right)^{\frac{\gamma-1}{\gamma}}\right]} \qquad 6.11$$

When the ratio between the downstream, p_o and upstream pressures, p_u, is:

$$\frac{p_0}{p_u} \leq \left(\frac{2}{\gamma + 1}\right)^{\frac{\gamma}{\gamma-1}} \qquad 6.12$$

The flow is choked and the mass flow rate is then calculated as:

$$\dot{m_{BB}} = \frac{C_d\, A_o\, p_u}{\sqrt{R_g\, T_g}} \sqrt{\gamma} \left(\frac{2}{\gamma+1}\right)^{\frac{\gamma-1}{2(\gamma-1)}} \qquad 6.13$$

With C_d the orifice discharge coefficient, A_o the orifice area [m^2], R_g the specific gas constant [J/(kg K)] and T_g the gas temperature assumed to be equal to the liner temperature (410 K).

The product ($C_d \cdot A_o$) is referred to as the effective blow-by area. Pugh [150], using a DI diesel engine having the same piston ring pack as that used as a model in this work, evaluated the blow-by area under firing conditions by matching the estimated blow-by gas to that measured over a complete cycle. The actual blow-by was measured with a Mass Air Flow (MAF) sensor. He reported an effective blow-by area of 4.1 x 10^{-8} m^2. This value is here used for the calculations and it is kept constant throughout the calculations.

The upstream, p_u, and downstream, p_0, pressures are defined as the higher and lower pressures, respectively. Therefore, they change during the cycle depending on which is the larger between the in-cylinder pressure and the second piston land pressure. The pressure in the second piston land as a function of the crank angle, p_2, assuming no changes in gas temperature is calculated as:

$$p_{2(n+1)} = p_{2(n)} \frac{m_{2(n)} + (\dot{m}_{BB} - \dot{m}_{CC})dt}{m_{2(n)}} \qquad 6.14$$

With:

$p_{2(n+1)}$ = Pressure in the second piston land at step (n+1) [Pa]
$p_{2(n)}$ = Pressure in the second piston land at step (n) [Pa]
$m_{2(n)}$ = Mass of gas in the second piston land at step (n) [kg]
$\dot{m}_{BB}$ = Mass flow rate across TCR during the step [kg/s]
$\dot{m}_{CC}$ = Mass flow rate across second compression ring during the step [kg/s]
dt = Time interval between steps (n) and (n+1) [s]

The mass flow rate between the second piston land and the crankcase, $\dot{m}_{CC}$, is calculated using the same equations used for $\dot{m}_{BB}$. The initial mass in the second

piston land is calculated from the ideal gas law by assuming p_2 to be at the arithmetic mean of the cylinder and crankcase pressures. The inter-ring volume was measured including the space above and behind the second compression ring. These were measured from the liner and piston dimensions of the Ford 2.0 litre DI diesel engine used as a model in this thesis.

The in-cylinder and second land pressures, and the instantaneous mass of blow-by gases passing through the TCR, are shown in Figure 6.6 and Figure 6.7 for engine condition Case 1d from Table 4.3, respectively. As the in-cylinder pressure (p_{cyl}) rises during the compression stroke, the inter-ring pressure (p_2) starts increasing. During this period the gas is flowing from the combustion chamber to the piston ring pack. Continuing in the stroke, p_2 keeps increasing remaining however, much lower than p_{cyl}. The pressure in the second piston land reaches its peak approximately 20° crank angle degrees after the in-cylinder pressure peak. This lag is due to the fact that the ring end gap restricts the flow, lowering the pressure and delaying the response to the combustion chamber variations. The rapid in-cylinder pressure drop during the expansion stroke associated to the slow response of the pressure in the second piston land, leads to a situation where p_2 becomes higher than p_{cyl}. A similar behaviour is described by Thirouard and Tian [144]. With p_2 higher than p_{cyl}, the gas changes direction, flowing back from the second land to the combustion chamber, a period referred to as reverse blow-by. This occurs approximately at 50° ATDC, and it is shown in Figure 6.7 by the negative values of blow-by mass. This implies that the Re-cycled soot particles (available throughout the engine cycle) can enter the piston ring pack and deposit in oil only between the compression stroke and the first period of the expansion stroke. On the other hand, the In-cycle particles are available only after the combustion process and after they reach the piston head-liner bottom corner. As this occurs only approximately at 20° ATDC, the period available for these particles for entering the piston ring pack is limited to approximately 30° CA.

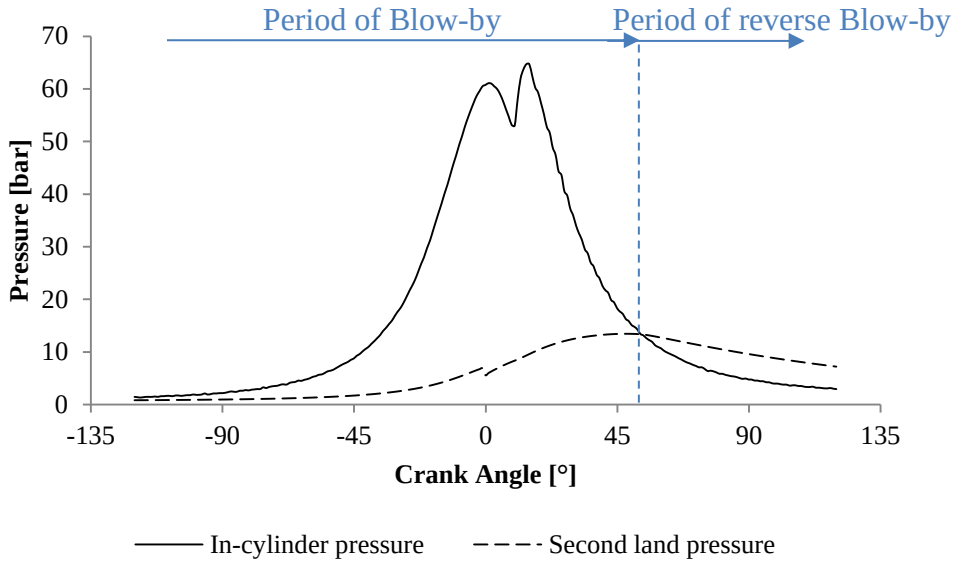

Figure 6.6: In-cylinder (solid line) and second piston land (dotted line) pressures during the engine cycle. Engine conditions of 2,000 rpm, 2 bar BMEP and 35.1% EGR (Case 1d from Table 4.3).

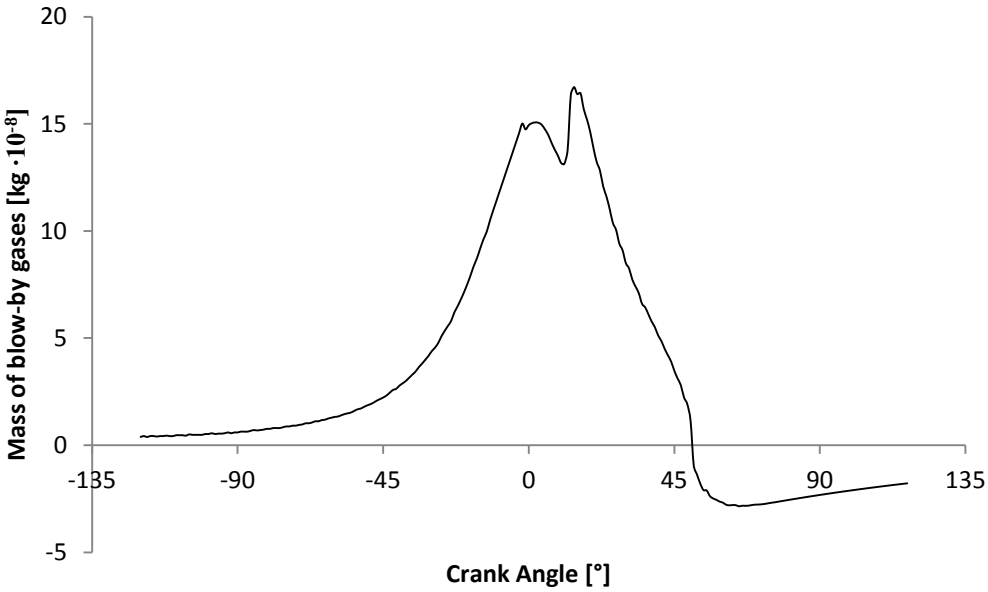

Figure 6.7: Instantaneous blow-by mass through the TCR gap. Engine conditions of 2,000 rpm, 2 bar BMEP and 35.1% EGR (Case 1d from Table 4.3).

In Figure 6.8 the amount of blow-by over the entire engine cycle is shown as a percentage of the intake air volume for all the engine conditions investigated in this work. Values represent different engine load and speed conditions, at a constant value of EGR. The percentage of blow-by is between 1.0 and 1.4% of the

intake mass. The percentage is found to decrease as engine speed is increased. This is due to the fact that at high speeds the time available for the gases to escape the combustion chamber is reduced. The effects of EGR on blow-by were found to be negligible and therefore have not be shown.

The influence of engine load is difficult to observe from Figure 6.8 as the load has effects on both the mass of air inducted in the cylinder and the blow-by rate. Furthermore, the in-cylinder pressure increase with engine load is counteracted by the increase in pressure of the gas in the second piston land. The effects of engine load on blow-by are more evident in Figure 6.9, where it is shown the cumulative value of blow-by mass over the engine cycle. As engine load increased, more air is inducted in the combustion chamber. This also increased the in-cylinder pressure, consequently rising the pressure difference between combustion chamber and crankcase, which according to Equations 6.11 and 6.13, causes the cumulative blow-by to increase.

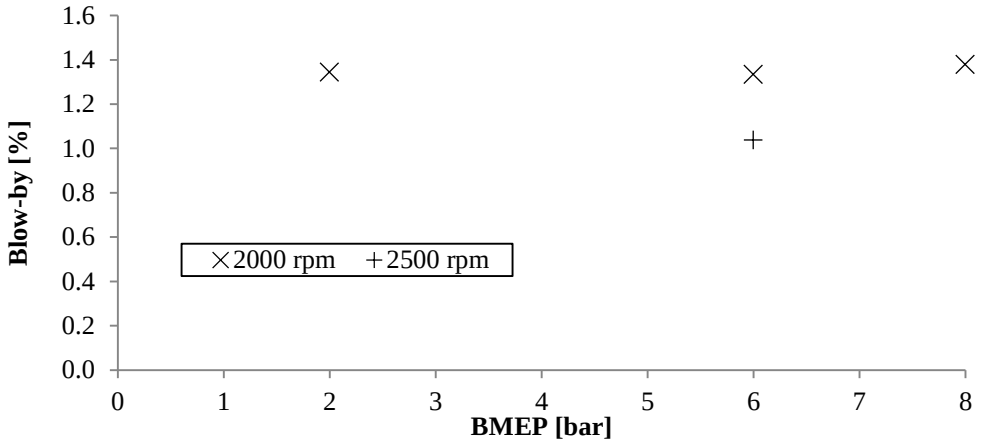

Figure 6.8: Ratio of blow-by gases as a percentage of the in-cylinder air mass.

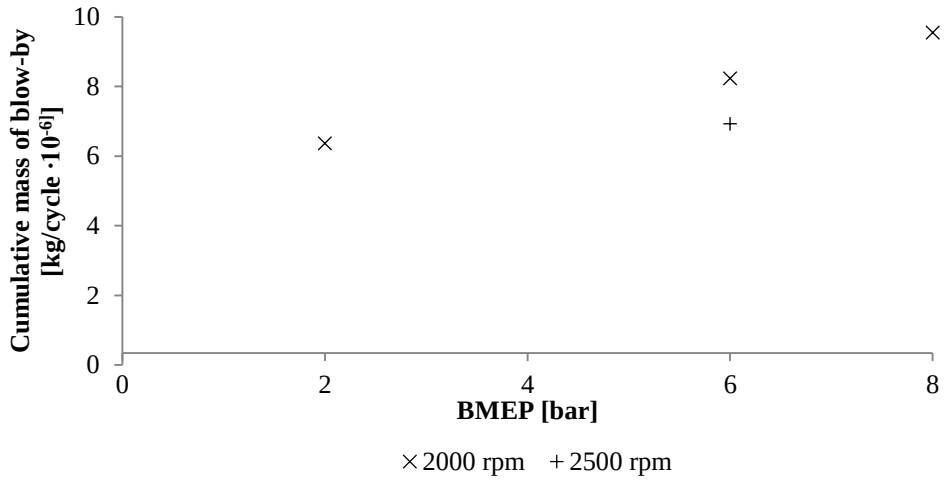

Figure 6.9: Cumulative mass of blow-by over the entire engine cycle for engine conditions from Table 4.3.

6.3.2 Rate of Soot Deposition in the Piston Ring Pack during Blow-by

The amount of soot entering the piston ring pack during blow-by over an engine cycle, $m_{s,BB}$, is determined as in Equation 6.15.

$$m_{s,BB} = \sum_{\theta=IVC}^{360^\circ} m_{s,BB}(\theta) \qquad 6.15$$

The instantaneous amount, m_{s_BB} (ϑ), is calculated at every 1° CA. $m_{s,BB}$ (ϑ) can be rewritten as in Equation 6.16:

$$m_{s,BB}(\theta) = \frac{f_{m_{BB}}}{f_{V_{Bottom}}} \cdot m_{s,bottom} \qquad 6.16$$

Where $m_{s,bottom}$, is the mass of soot at the piston head-liner corner, previously evaluated in Chapter 4 with the aid of CFD simulations. It includes the contribution from both the In-cycle and Re-cycled sources of soot. The term f_{mBB} represents the fraction of blow-by gases escaping the combustion chamber at every 1°CA, evaluated as the ratio of blow-by gas mass to the in-cylinder charge mass. The term $f_{Vbottom}$ is the volume considered by the CFD simulation for the evaluation of $m_{s,Bottom}$, divided by the total in-cylinder volume, previously shown in Figure 4.23. Assuming the combustion chamber to be an homogenous reactor [48], i.e. uniform gas density, the ratio between f_{mBB} and $f_{Vbottom}$ represents the fraction of CFD volume used to evaluate $m_{s.bottom}$ involved with the blow-by

process. Therefore, the product given in Equation 6.16 represents the mass of soot entering the piston ring pack carried within the blow-by gases at each ϑ interval, and deposited to oil in the piston ring pack.

6.4 Overall Rate of Soot Deposition in Oil

The rate of soot deposition in oil for the sixteen cases investigated in this thesis is shown in Figure 6.10 and Figure 6.11. These include the contribution from both liner and blow-by pathways, as well as In-cycle and Re-cycled sources of soot. Results are presented with the EGR level on the x-axis, and as a function of engine load and speed, respectively. On the y-axes, the rate of deposition is given both in terms of mass over time and as a percentage in weight of soot into oil after 100 hours. The latter has been estimated by assuming an oil capacity of 4700g and neglecting oil consumption. Overall, the amount of soot deposited for all the engine conditions, varies between 2.7 mg/h (0.006 wt%/100h) and 340 mg/h (0.726 w%t/100h), for a no EGR, low engine load condition and a high EGR, high engine load condition, respectively.

As expected from what has been presented so far, the rate of soot deposition strongly increases with engine load and EGR level. Engine speed has a weaker influence compared to the other two variables. As engine load is increased from 2 to 8 bar BMEP the amount of soot deposited in oil increases up to an order of magnitude, with values at 8 bar between 15 and 20 times larger than at 2 bar. This is mainly due to the greater amount of fuel injected per cycle, as well as to the higher in-cylinder gas temperature which promotes the formation of soot particles. As the EGR level is increased from 0 to 35%, the amount of soot deposited into oil increases at rates similar to those observed with engine load, with values up to 20 times larger. The effects of EGR on the amount of soot in oil is further discussed in the next section of this chapter, where the relative contribution of the In-cycle and Re-cycled sources of soot is discussed. At high engine speeds the turbulent level within the combustion chamber increases, enhancing the transport of particles towards the liner and the piston head-liner corner regions, increasing

consequently the amount of soot available for deposition. Theoretically, as engine speed increases, the time available for deposition within a cycle decreases; in Figure 6.11 this is masked by plotting the results as a function of time rather than cycle.

Between $1.2 \cdot 10^{-4}$ and $6.3 \cdot 10^{-3}$% of fuel ends up in oil as soot particles, with an average value of $2.1 \cdot 10^{-3}$% over the sixteen cases. The percentage increases as the EGR level increased. This is due to the fact that as EGR increases, the amount of fuel remains constant while the equivalent fuel-air ratio increases due to the greater proportion of exhaust gases recirculated. These results are useful in inferring the amount of soot deposited into oil from values of fuel injected. In fact, the latter is a common parameter measured during engine tests, unlike the measurement of the amount of soot-in-oil which typically requires extraction of oil from the oil sump followed by a sample preparation and analysis with techniques such as TGA or FTIR.

The amount of soot deposited in oil represents between 1.4 and 5.4% of the in-cylinder soot emitted at EVO (taken from CFD results and listed in Table 4.3), with an average value of 2.9% over the sixteen cases. These percentages do not correlate with engine load, speed or EGR level, confirming results from Chapter 4 in which it was discussed that the amount of soot at the near-wall region is not correlated to the spatial averaged in-cylinder amount of soot. A similar result was reported by Dahlen [72].

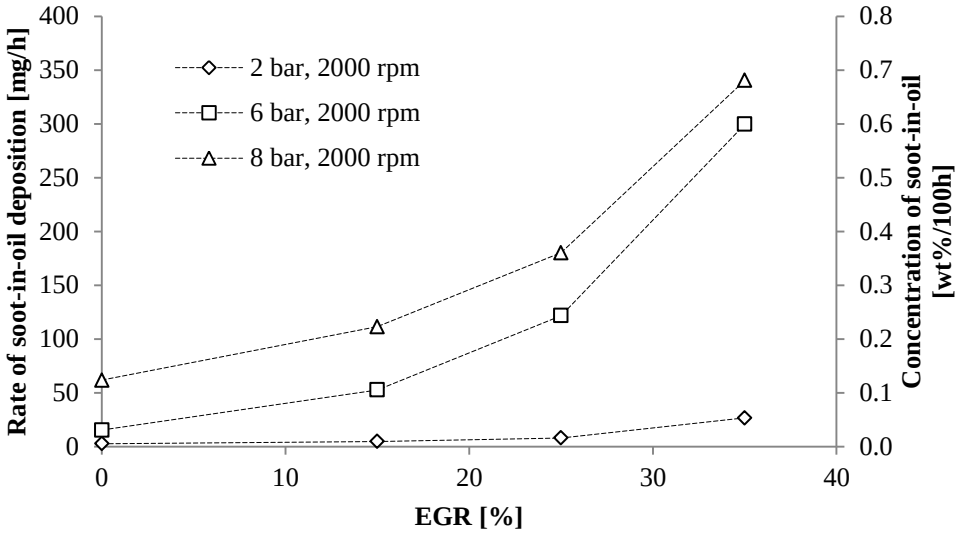

Figure 6.10: Rate of soot deposition in oil from both transfer pathways as a function of engine load and EGR, at a constant speed of 2,000 rpm, and concentration of soot-in-oil after 100h.

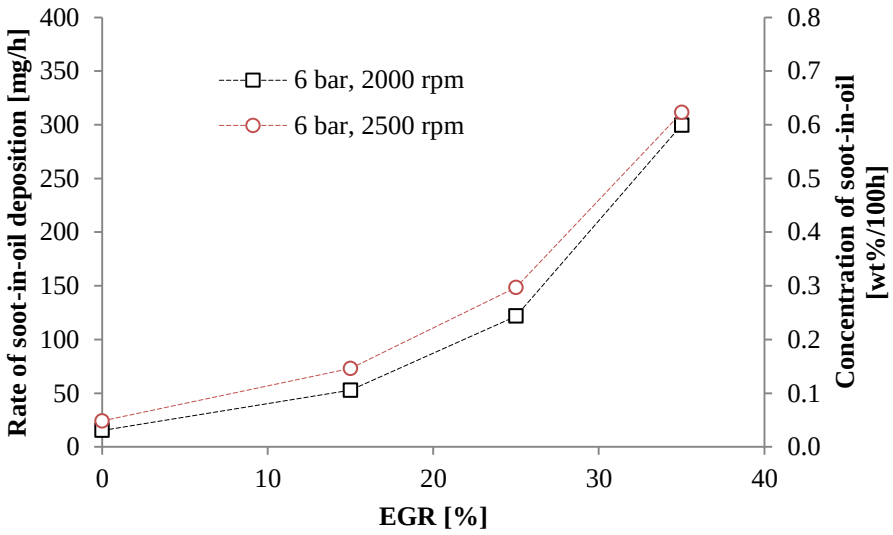

Figure 6.11: Rate of soot deposition in oil from both transfer pathways as a function of engine speed and EGR, at a constant load of 6 bar BMEP, and concentration of soot-in-oil after 100h.

The results analysed so far do not allow, however, to distinguish between the relative contributions to the total soot-in-oil deposition rate. Four different sources of deposition can be identified: 1) In-cycle soot deposited at liner during the closed part of the cycle, from IVC to EVO; 2) In-cycle soot deposited at liner post-EVO (expansion stroke after EVO and exhaust stroke); 3) Re-cycled soot deposited at liner during the entire cycle (intake, compression, expansion and exhaust strokes); 4) Blow-by. These four sources are discussed in the next section of this chapter. It is worth mentioning that this is the first time these have been investigated computationally to account for soot transfer to engine oil, with only contribution "1)" being considered in the literature to date [4, 5, 72].

6.4.1 Relative Contributions to Soot-in-Oil

The contribution of each individual source of soot-in-oil deposition during an engine cycle is shown in Figure 6.12, representing Case 2b, at 2,000 rpm, 6 bar BMEP and 15% EGR.

During the compression stroke only the Re-cycled source of soot is present within the combustion chamber as the In-cycle source has not yet been produced. Deposition during the compression stroke occurs both via blow-by and thermophoresis. The latter occurs only from 60° BTDC as before deposition via thermophoresis is not taking place due to the gas temperature being lower than the liner temperature. From 32° BTDC to 32° ATDC the soot deposited at the liner does not contribute to soot build up as the portion of liner subjected to the scraping action of the piston rings is not yet exposed to the hot soot-laden combusted gases. Deposition during these 64°CA occurs only via blow-by. When EGR is implemented, the deposition during the compression stroke contributes for approximate 15% of the total deposition.

The In-cycle source reaches the liner only approximately at 20°ATDC, but deposition starts only after the scraped portion of the liner is again exposed to the in-cylinder charge. During the expansion stroke, the temperature gradient which controls the thermophoretic deposition velocity, drops significantly compared to its peak value achieved near TDC. However, the rate of soot deposition is still high for two reasons: firstly, as the piston moves downwards the surface area for

deposition increases, and secondly, the drop in gas pressures increases both the kinematic viscosity and the thermophoretic constant, partially counteracting the temperature gradient effect. The drop in in-cylinder pressure also causes the deposition via blow-by to end as no soot-laden gases are flowing from the combustion chamber to the crankcase. This occurs approximately at 50° ATDC, and from this crank angle onwards, deposition occurs only at the cylinder liner.

At EVO, a large amount of soot is exhausted from the cylinder during the blow-down process. The loss of soot particles continues via the piston displacement during the exhaust stroke. In Chapter 4, the amount of soot during these two processes was estimated as proportional to the gas loss during the blow-down and displacement processes. Results for this engine condition indicate that, overall the soot deposited after EVO accounts for approximately 13% of the total amount of soot deposited in oil. Despite the high amount of soot loss after EVO, this large value is justified by the large surface of liner available for deposition from after EVO until the end of the exhaust stroke.

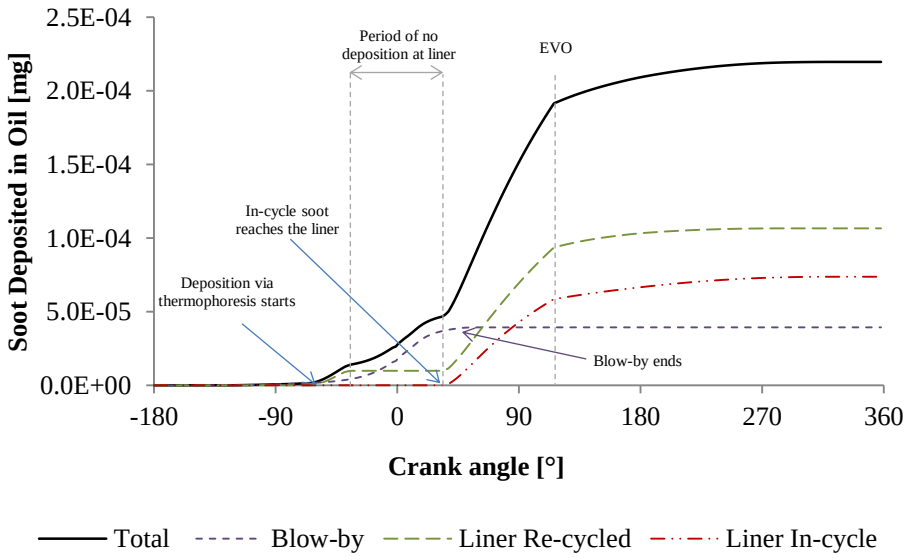

Figure 6.12: Amount of soot deposited in oil during the entire engine cycle, for the four contributions investigated in this work.

The relative importance of the four sources of soot-in-oil deposition is summarised in Figure 6.13 for all the engine conditions investigated. Each point from Figure 6.10 and Figure 6.11 is here represented by a column in which the four contributors are shown.

Overall, deposition in the piston ring pack during blow-by is found to be a minor contributor for soot-in-oil; it varies between 0 and 20% of the total soot deposited. The 0% value is obtained when there are no exhausted gases recirculated back in the combustion chamber. This is due to the fact that, as presented in Chapter 4, the availability of the In-cycle source of soot at the piston head-liner corner is negligible. This is in agreement with other authors' results who studied blow-by considering the In-cycle source only [3-5]. The contribution of blow-by increases as the EGR level increases. This is due to the fact that the particles recirculated back enter the combustion chamber uniformly distributed with the in-cylinder charge. Contribution during blow-by is also found to decrease with engine speed. This is mainly due to the fact that as engine speed increases, the amount of gas escaping the combustion chamber towards the crankcase decreases due to the shorter engine cycle period.

Deposition on the oil film at the liner via thermophoresis is the dominant pathway for all the engine conditions investigated. Results in Figure 6.13 allow the evaluation of the contribution from both the In-cycle and Re-cycled source of soot. As EGR is increased, the contribution of the Re-cycled source increases faster than that of the In-cycle source. This is explained as follows: as the Re-cycled particles re-enter the combustion chamber uniformly distributed, its availability at the near-liner is governed by the level of EGR and by the amount of in-cylinder soot emitted at EVO from the preceding cycle. On the other hand, the availability of near-liner In-cycle particles is weakly correlated to the soot at EVO. It mainly depends on the convective transport of the formed particles from the bulk region to the liner. According to the results presented in Sections 4.4 and 4.6, as EGR level increases, the in-cylinder soot at EVO increases faster than that at the liner. The contribution of the Re-cycled becomes the larger contributor for EGR levels of approximately 15-20% depending on the engine condition. However, for the

highest engine load condition, i.e. 8 bar BMEP, the contribution of the In-cycle source is larger than the Re-cycled for the entire range of EGR levels investigated. This is due to the high rates of oxidation encountered by the Re-cycled source at the high temperature and pressure environment, summarised in Table 4.4.

Finally, comparing the Cases at 6 bar BMEP, 2,000 and 2,500 rpm, it is shown that the relative contribution of the In-cycle source is greater for the high engine speed case. This is due to the larger turbulent level of the charge which enhances transport of particles from the bulk to the liner region.

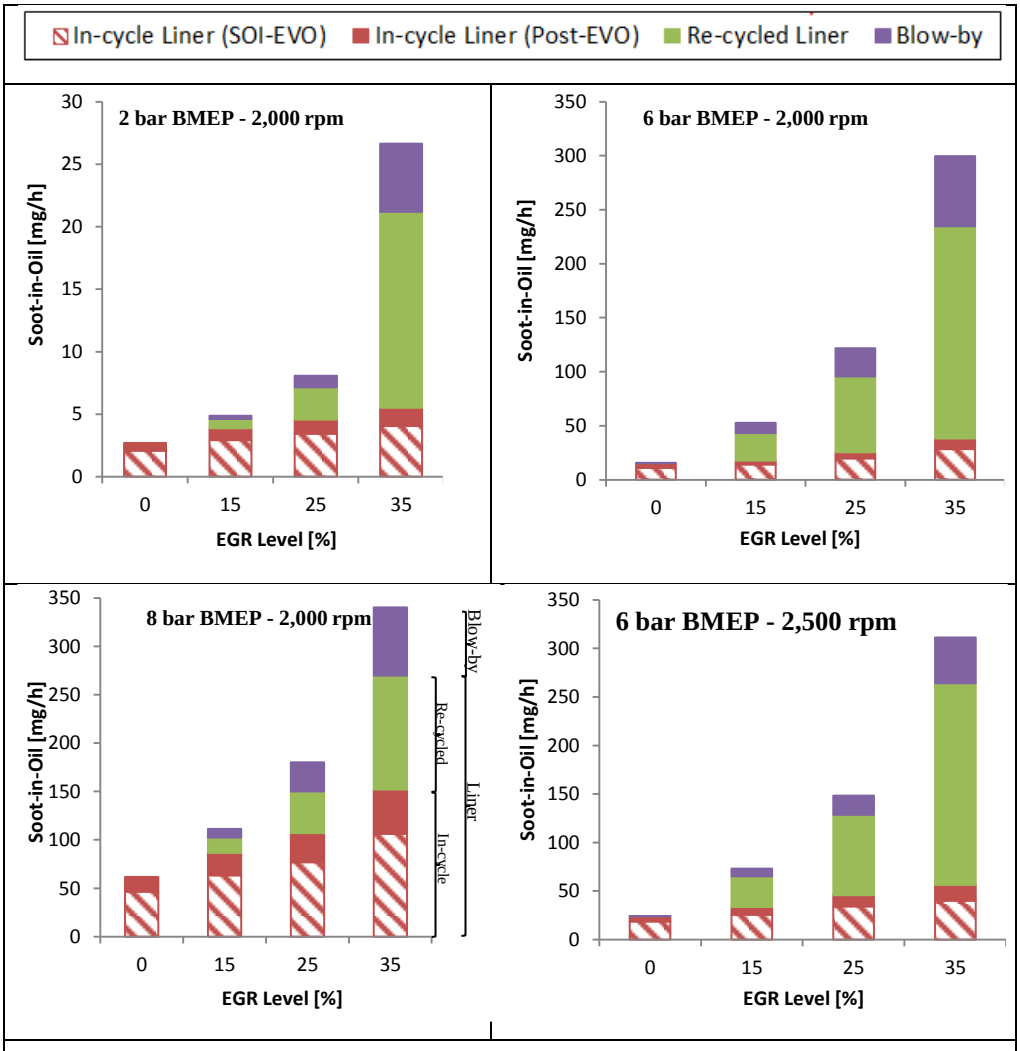

Figure 6.13: Soot rate of deposition evaluated at different EGR levels examining the relative importance of transport of soot by thermophoresis at the liner from In-cycle (SOI to EVO and Post-EVO) and Re-cycled sources and by Blow-by gas.

Overall, the evaluation of the amount of soot-in-oil by only considering the soot formed during the combustion process and entrained into oil from SOI to EVO causes an underestimation of between 20 and 75%. The smallest value is obtained when the level of EGR is 0%, and it is solely due to the deposition during the post-EVO period of the cycle. On the other hand, as EGR increases, the contribution during the compression stroke from the Re-cycled particles is found to play an important role.

6.5 Comparison against Experimental Results

A direct validation of the proposed soot-in-oil deposition model was not possible as the engine used as a model for the CFD simulations was not available at the time of the investigation. Instead, results are compared with typical light-duty diesel engine soot-in-oil deposition rate. This was obtained in Chapter 3 by experimentally measuring the amount of soot-in-oil from the fifteen oil samples collected at different oil change intervals.

A direct comparison between experimental and computed results was not possible due to the different nature of the two investigations. Experimental rates of depositions were obtained from used oil sample collected during regular oil services in the Nottingham area. Information such as oil mileage and vehicle characteristics, together with the results from the TGA investigation allowed estimating a rate of deposition from several light-duty diesel engines. Although details about engine conditions of these oil samples were not available, results are representative of real-world driving conditions. Furthermore, the trend over the 15 samples tested indicated that the amount of soot-in-oil grows fairly linearly with oil mileage, providing robustness to the calculated rates of deposition. On the other hand, computational results are obtained at specific engine conditions. Although the engine conditions modelled can be representative of real world driving conditions, it is not possible to know which of these engine conditions is used throughout the typical distance covered by the vehicles from where the oil samples were extracted. The comparison is, therefore, between the ranges of rates

of soot deposition rather than the actual values obtained from each of the methodology approaches. For the computational study, two sets of results are considered and compared: firstly, those obtained with the model commonly found in literature which considered only deposition of the In-cycle source between SOI and EVO, here named as *Old model*. Secondly, the results from the new model presented here which included the deposition of the Re-cycled particles and extended the period of deposition to the entire engine cycle, named *New model*. Two different approaches have been used for the comparison. First, in terms of rate of deposition [mg/h], and second in terms of fraction of fuel converted into soot and deposited in oil as soot [g_{soot}/g_{fuel}]. In Figure 6.14 and Table 6.1 results are given in terms of rates of deposition. On the left and right-hand sides of Figure 6.14, TGA results are compared with those obtained from the *Old* and *New* models, respectively. Typically, the maximum level of EGR is governed by the equivalent fuel ratio. According to the threshold limit of 0.8 suggested by Heywood [11], only Case 3d (2,000 rpm, 8 bar BMEP and 35%) exceeds this value, with also the two cases at 6 bar BMEP and 35% EGR (Cases 2d and 4d) close to this limit. On the other hand, engine conditions without EGR are also not realistic, as recent engines constantly recirculate exhaust gas in order to limit NO_x emissions. In Figure 6.14, all the values of EGR are given for completeness, although the region of major interest is between 15 and 25% EGR. These are the only two limits reported in Table 6.1.

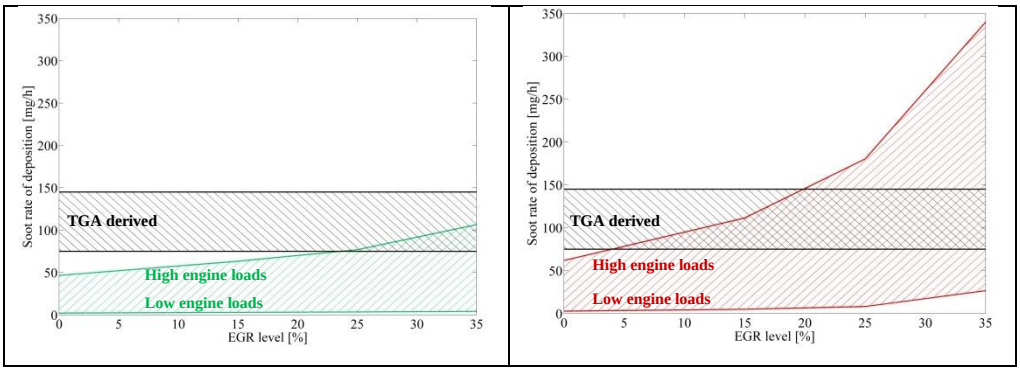

Figure 6.14: Old deposition model (left hand side, green region) and new deposition model (right hand side, red region), compared against TGA derived rates of deposition during urban and extra-urban combined driving condition (black regions).

Method	Assumptions	EGR [%]	Range of Soot Rates of Deposition [mg/h]
TGA	1 wt%; combined driving conditions	-	70-140
Old Model	In-cycle, SOI-EVO (low load-high load)	15	3-63
		25	4-77
New Model	In-cycle & Re-cycled, entire engine cycle (low load- high load)	15	5-102
		25	7-150

Table 6.1: Comparison between modelled and experimental rates of soot deposition.

It appears clear from the above results that the *Old model* under-predicts the typical rate of soot depositions of a typical diesel engine for almost all the engine conditions studied in this work, including those at high engine loads. Only the deposition rate of Case 3c (2,000 rpm, 8 bar BMEP and 25% EGR), typical of a medium-high engine load condition, is higher than the lower limit derived from diesel vehicles, with a value of 77 mg/h. Regarding the *New model*, only Case 1 and the two 0% conditions at 6 bar BMEP were below the lower limit diesel vehicles range. All the other engine conditions were within or above the suggested range of soot deposition into oil. This suggests that although a more direct comparison would be necessary in order to further validate the model, the new proposed approach shows that there is the need to improve the typical deposition models.

The need to include the Re-cycled source of soot and extending the deposition analysis to the entire engine cycle, is also shown from the comparison between fractions of fuel in oil as soot, summarised in Table 6.2.

Although both the *Old* and *New* models failed to match the experimentally derived results, results from the *New* model are approximately 2-3 times higher than those from the *Old* model, and considerably closer to the TGA-derived. Furthermore, results at 35% EGR, not reported in Table 6.2, are within the TGA-measured region.

Method	Assumptions	EGR [%]	Percentage of fuel entrained into oil [%·10^{-3}]
TGA	1 wt%; combined driving conditions	-	4 – 8
Old Model	In-cycle, SOI-EVO	15	0.1 – 0.9
		25	0.2 – 1.3
New Model	In-cycle & Re-cycled, entire engine cycle	15	0.3 – 1.9
		25	0.4 – 3.1

Table 6.2: Comparison between modelled and experimental fractions of fuel deposited into oil as soot particles.

6.6 Discussion and Conclusions

Results according to the existing deposition model (In-cycle source from SOI to EVO only), show that when EGR is increased from 0 to 35%, the rate of soot-in-oil deposition increases up to two times. Differences from other authors' results who used the same model are within 10 % [3-5]. All these results, however, underestimate the rate of deposition obtained from the TGA investigation and used in this work as benchmark values. Moreover, Dennis et al. [80] and Nagai et al. [57] reported that when EGR is increased from 0 to 25%, engine wear rates increased between 4 and 10 times. The only consideration of the In-cycle source fails to justify the increase in wear with EGR observed by these authors.

The new model presented in this thesis also includes the Re-cycled particles. A limitation of the current method is that the contribution of the Re-cycled particles is obtained by post-processing CFD results, without actually modelling or measuring the amount of particles recirculated. Although for future works an experimental approach or a modification to the CFD model would be ideal, the approach used in this work allowed demonstrating the importance and contribution of this source of soot and also permitted to study the two sources separately. Considering both the In-cycle and Re-cycled sources, the amount of

soot-in-oil increases by up to twenty times when EGR is increased from 0 to 35%. The re-cycled soot for high levels of EGR levels resulted the larger contributor.

A further development to the existing model is the analysis of deposition extended to the entire engine cycle. This arose mainly from two observations made during the first stages of this work: first is that Re-cycled particles are available throughout the engine cycle including the period before SOI. Second, it was observed that the instantaneous rate of deposition reaches its highest at EVO, Figure 6.12. This is due to both the larger surface of oil film exposed to the hot combusted gas and to the availability of In-cycle particles which increases during the expansion stroke driven by the turbulent environment in the combustion chamber. Therefore, limiting the analysis from SOI to EVO, may have underestimated the amount of soot deposited during an engine cycle. Results confirmed it, with deposition outside the SOI-EVO period of up to 30% of total amount of soot-in-oil.

Although blow-by gas passing the rings is recognised as a potential soot transfer pathway, its contribution is considered to be negligible [3-5]. This is confirmed from the results obtained by considering only the In-cycle source. This is because the concentration of particles at the piston crown-liner corner is over an order of magnitude smaller compared to the spatial-averaged concentration. However, the contribution of this pathway is not negligible anymore when EGR is used. This is due to the fact that the Re-cycled particles are considered to be homogeneously distributed having had sufficient time to mix with the charge. Results indicated that for a high level of EGR, although deposition at the liner is still the most important pathway, the contribution from blow-by can represent up to 20% of the total amount of soot deposited into oil.

The importance of considering the Re-cycled particles and of extending the model to the entire engine cycle is confirmed from the comparison with the TGA-related results. In fact, the rate of deposition with the existing model underestimated those experimentally derived for almost all the engine conditions modelled. Instead, the new model was able to match the experimentally derived results. The agreement between the two results is in some way impressive due to the different methods

followed to estimate the rates of deposition. On the other hand, results in terms of fraction of fuel entrained into oil as soot underestimate those derived from TGA. Although values from the new model presented here are considerably closer if compared with those obtained with the existing model. The discrepancy between the different comparisons may be due to the different assumptions used for calculating the two TGA-derived results. The NEDC cycle was used to obtain reference values such as vehicle speed for the rate of deposition and fuel consumption for the fraction of fuel in oil as soot. While the former was found to be representative of real world vehicle speed around the Nottingham area [88], the latter parameter is well recognised to underestimate real-world fuel consumptions [87], with the consequence that the fuel-soot ratio estimated in Section 3.2.3 may overestimate real values. For future work, the use of a test engine similar to that used for the CFD simulation will allow a better comparison between theoretical and experimental results.

The rate of deposition as a function of the other engine conditions investigated in this work, engine speed and engine load were also calculated. As expected, the amount of soot-in-oil drastically increases with engine load, while it is less influenced by engine speed.

7 Discussion and Conclusions

7.1 Discussion

The work reported in this thesis is concerned with studying the mechanisms by which soot is transferred to the lubricating oil in light-duty diesel engines. Engine speed, load and EGR level were the parameters studied during the investigation using a combination of computational and analytical tools. Other variables that may influence the transfer, such as fuel injection parameters, air swirl and top piston land height were kept fixed as constant.

Particular interest was given to the potential role of EGR on the transfer mechanisms and on the rate of soot-in-oil deposition. Typically, the effects of EGR on soot-in-oil build-up are studied by considering its detrimental effects on the formation process during the combustion event. However, initial results indicated that this effect only, cannot justify the drastic increase in engine wear with EGR reported in the literature [57]. Therefore, the focus was also given to the potential effects of the particles re-circulated in the combustion chamber during the induction stroke with the EGR gas. Comparison of the findings with experimental results obtained with TGA provided evident robustness that neglecting the EGR Re-cycled soot will underestimate the amount of soot transferred into bulk oil.

The typical concentration of soot-in-oil of light-duty diesel engine vehicles, measured with TGA, is on average 1.0 wt% after 15,000 km. Furthermore, results indicated that despite the difference in vehicle models and potential driving conditions, soot-in-oil concentration increased fairly linearly with oil mileage. A similar relationship soot concentration-mileage was also obtained by Lockwood [52]. However, a direct comparison with the actual soot-in-oil concentration was not possible as this study was relative to heavy-duty diesel engines.

Soot concentration of approximately 3 wt% is reported as threshold value before engine wear and oil viscosity increase to limits intolerable for the engine life. According to the results obtained in this work, at the time of the oil drain, all the samples investigated were below the suggested margin of 3 wt%. Car manufactures normally recommend the oil to be changed annually or once the vehicle has reached a certain mileage, up to 30,000 km per year, whichever comes first. According to the findings, if changing the oil every year appears to be sustainable for the quality of the lubricant oil, extending the oil mileage up to the values suggested by manufacture recommendation does not appear to be achievable, with some of the samples tested that may reach potential values of between 3 and 4 wt%.

The oil samples tested were collected from engines which conformed to Euro IV and V legislations. The analysis conducted on the fifteen oil samples, indicated that the concentrations of soot-in-oil between the two Euro standards are similar, with differences between Euro IV and V legislations of within 10%. This is in contrast to the drastic reduction in PM tailpipe emission imposed between the two standards. As the amount of soot-in-oil strongly depends on in-cylinder soot concentrations and distribution, this suggests that in order to comply with the Euro V standard, the automotive industry mainly acted downstream of the combustion chamber, via aftertreatment systems, such as the DPF.

At the time of the TGA investigation, vehicles meeting Euro VI legislation were not yet available on the market. The current Euro VI legislation has seen a further reduction in NO_x emissions compared to previous standards. The introduction of aftertreatments such as the SCR or the LNT systems for complying with the new NO_x limits may open to the opportunity for calibrating engines towards higher engine-out NO_x. This may be achieved by limiting or not requiring EGR, with consequential improvement in terms of both fuel economy and soot formation and entrainment into oil. However, the impact of these strategies on soot-in-oil concentrations could not be assessed.

The same fifteen oil samples were tested in order to measure the typical particle size distribution of soot particles entrained into oil. The large number of samples

analysed, and the typical polydispersed particle distribution of soot particles, suggested the author to use a relatively novel method, NTA, instead of more traditional techniques such as TEM and DLS. Details of the advantages of NTA over TEM and DLS were discussed in Section 3.3. The particle size distributions of the samples were found to not correlate with either the oil mileage or soot concentrations. This suggests that the lubricant oil at the end of the typical service period is able to avoid particle agglomeration in the oil sump, with the anti-dispersant oil additives still coping with the reported amounts of soot in oil.

Sizing results showed an average particle size of 155 nm, with 90% of the particles smaller than 236 nm. Particles larger than 400 nm were only 1% of the entire population. Particles larger than 1 μm were not found in any of the samples. This indicated a gap between the maximum particle size detected, and the typical mesh size of common oil filters equipped in diesel engine oils, i.e., above 5 μm. As a result, oil filters may fail to trap soot particles entrained into oil.

The engine used as a model for the CFD simulations is a light-duty diesel engine which conformed to Euro IV legislation. TGA results indicated that differences in soot-in-oil concentrations between Euro IV and V engines, strongly depending on in-cylinder soot amount and distribution, were limited. This suggests that the engine used for the simulations was able to represent the state of art at the time of the investigation. Main in-cylinder differences between the two Euro Standards would be the injection strategies and EGR levels used to limit engine-out NO_x emissions. These are parameters that can be adjusted with the CFD.

The pre-existing CFD model, calibrated against experimental values during previous works undertaken at the University of Nottingham [101], had limitations for not including a crevice region, not considering the soot particles re-entering with EGR gas, and for being restricted to the closed part of the cycle, i.e. from IVC to EVO.

The crevice region is of interest for determining the availability of the In-cycle particles for deposition in the piston ring pack through blow-by. The availability of these particles was instead studied at the piston crown-liner corner region. This

will overestimate the actual availability in the crevice volume. As results showed that the concentration at the crown-liner corner was negligible, it can be concluded that the inclusion of a crevice region is of minor importance for the deposition of soot-in-oil. Similar results were obtained by other authors [3-5]. As the EGR Re-cycled particles are assumed to be homogeneously distributed within the combustion chamber, the amount entering the piston ring pack is mainly dependent on the blow-by rate rather than on the actual location at which these are monitored.

As discussed in Chapter 4, the CFD code takes into account the EGR level by adjusting the intake gas composition. This allowed the CFD to evaluate the effects of EGR on the soot produced during the combustion process, the In-cycle source. The Re-cycled source was instead studied analytically by post-processing soot values at EVO from the previous cycle and by calculating the oxidation rates using the same models and constants as for the CFD simulation. The oxidation process is analytically evaluated using the in-cylinder bulk gas temperature. This may underestimate oxidation in the piston bowl region where the combustion process takes place and higher local temperatures are achieved. However, the objective was to calculate the Re-cycled amount at the near-wall region, where the gas temperature is lower and can be assumed to be equal to the bulk gas temperature.

The IVO-IVC period, where the Re-cycled particles enter the combustion chamber mixed with the in-cylinder charge, is not included in the CFD simulations. However, during this interval neither transfer via thermophoresis or blow-by in the piston ring pack has yet to be initiated. As a result, the interval IVO-IVC is of no interest for the transfer of soot-in-oil.

The scenario is different during the other part of the cycle and not included in the CFD model, the post-EVO period. At EVO, a large fraction of the oil film on the liner is exposed to the soot-laden hot gas and the in-cylinder gas temperature is still considerably higher than the liner temperature, therefore promoting the deposition via thermophoresis. Deposition is calculated by assuming that loss of particles during the blow-down and displacement exhaust processes is

proportional to the loss of in-cylinder gas mass. This is based on the assumptions that the in-cylinder pressure distribution is uniform and that thermophoresis is still the dominant transport mechanism in the near-wall region, despite the gas flowing outside the combustion chamber. This represents the major knowledge gap of the deposition model presented in this work. Despite the uncertainties of the analysis undertaken during the post-EVO, results showed that deposition occurring during this period could play an important role in the rate of soot accumulation in oil.

For all the engine conditions investigated in this work, soot transfer to oil during blow-by is found to be a minor contributor compared to deposition at the cylinder liner. However, at high EGR levels its importance increases due to the larger fraction of soot particles Re-cycled. The contribution of the particles produced from the combustion process is instead negligible. At high values of EGR, deposition during blow-by represents up to 20% of the total deposition to bulk oil. Furthermore, as engine speed is reduced from 2,500 to 2,000 rpm, the contribution of blow-by increased by 15%. This is a direct consequence of the higher percentage of blow-by gas that escapes the combustion chamber at low engine speed. Although not investigated in this work, during idling conditions due to the low engine speed (around 800 rpm) and high EGR levels (up to 50%), deposition during blow-by may represent a large contributor to soot-in-oil. Similarly, in heavy-duty diesel engines, which typically run at lower engine speeds, deposition during blow-by could be more important than for light-duty diesel engines when high rates of EGR are applied.

As discussed in Chapter 4, EGR systems in light-duty diesel engines are commonly high-pressure loop types, in which the exhaust gas are extracted prior the turbocharger turbine without passing through any after-treatment systems. The re-introduction of the soot particles, from a “tailpipe emissions” point of view is not of particular interest as most of them are oxidised prior EVO. However, findings from this work highlighted that from an “oil” point of view these Re-cycled particles can significantly increase the amount of soot-in-oil. This problem could be partially overcome by using a LP-EGR loop system. In the past, one of the main reason limiting the application of this type of EGR was that the

turbocharger compressor would have been subjected to soot deposit formation [98]. However, with the introduction of the DPF, the exhaust gas, extracted downstream the turbocharger turbine and the particle filter are essentially soot-free. The attraction towards this system is increased by its beneficial effects on fuel consumption [98]. However, as discussed in Chapter 4, another limiting parameter of this system is its poor response to transient operations, and in particular at decreasing engine load [151]. To partially overcome this, another potential solution that could be beneficial to soot-in-oil concentration could be the use of hybrid EGR systems, where the high-pressure and low-pressure loops are combined.

7.2 Future Work

The TGA investigation should be extended to new diesel engines meeting Euro VI legislation. This will allow establishing if the new after-treatment technologies such as SCR and NSC systems have led towards engine calibrations which promote NO_x engine-out emissions, via less/no EGR, with direct consequences to soot-in-oil concentrations.

The analytical and computational findings have highlighted the role of EGR in promoting soot-in-oil rates of deposition. Of particular importance is the role of the Re-cycled particles. These however, were evaluated by post-processing CFD results. Thus, the CFD should include the contribution of the Re-cycled particles, allowing for a study of the spatial distribution and oxidation process of these particles.

Furthermore, the present CFD model is limited to the closed part of the cycle, from IVC to EVO. The possibility of soot transfer to oil film at the liner during the post-EVO period of the cycle was discussed based on post-processing CFD data at EVO. As results indicated that this period could be a significant contributor to soot-in-oil, simulations should be extended to include soot amount and distribution during the exhaust stroke. In order to do this, a new code

including valve computational and the effects of the exhaust gas flow would become necessary.

7.3 Conclusions

- The percentage in weight of soot entrained into oil of cars and light commercial diesel vehicles, measured via TGA, is on average 1 wt% after 15,000 km. The concentration of soot into lubricant at the time of the oil change interval was found to be below the car manufacturing recommended limits [24].
- Oil samples collected from engines meeting Euro IV and V legislations showed very similar concentrations of soot-in-oil, with differences within 10%. This indicates that there is no correlation between soot-in-oil values and PM tailpipe values.
- The average size of the soot-in-oil agglomerates is found to be 150 nm, with a standard deviation of 60 nm. Particles smaller than 100 nm represent 10% of the entire population. Only 1% of the agglomerates are larger than 400 nm, and no particles larger than 1μm were found in any of the samples tested.
- Agglomerates size distribution is found not to be correlated with oil mileage, soot-in-oil concentration, or with emission standards legislation.
- Transfer of soot through blow-by in the piston ring pack contributes for a minor fraction, < 20% of the total rate of soot accumulation in oil. Re-cycled particles are the only source of particles, with the contribution from the In-cycle being negligible for all the engine conditions and EGR levels investigated.
- The fraction of particles deposited through this pathway is also found to decrease as engine speed increases and to be weakly correlated to engine load.

- Deposition in the oil film on the cylinder liner via thermophoresis is the dominant soot transfer mechanism for all the engine conditions and EGR levels investigated in this work.
- Soot transfer to the oil film on the cylinder liner via thermophoresis accounts for > 80% of the entire amount of soot-in-oil. Rates of deposition increase with engine speed, engine load and EGR level. Engine speed has only a weak influence, with variation between the 2,000 and 2,500 rpm cases within 3%. Engine load has instead a strong influence, with a raise of soot accumulation by a factor of 13 as engine load is increased from 2 to 8 bar BMEP.
- The sources of soot accumulated in the lubricating oil are both the soot produced In-cycle during the combustion process and the soot Re-cycled with the EGR gas. The latter becomes the larger contributor for levels of EGR higher than 15-20%.
- As the Re-cycled particles are introduced during the induction stroke, entrainment into oil occurs during the compression, expansion and exhaust strokes. Deposition during the compression stroke, and post-EVO periods accounts for approximately 30% of the total soot-in-oil deposition.

8 References

1. La Rocca, A., Di Liberto G., Shayler P. J., Parmenter, C. D. J., Fay M. W., *Application of nanoparticle tracking analysis platform for the measurement of soot-in-oil agglomerates from automotive engines.* Tribology International, 2014. **70**: p. 142-147.

2. La Rocca, A., Di Liberto, G. , Shayler, P. J. , Parmenter, C., Fay, M. W., *A novel diagnostic tool for measuring soot agglomerates size distribution in used automotive lubricant oils.* SAE Int. J. Fuels Lub., 2014. **7**(1): p. 301-306.

3. Tan, S., M. , Ng, H., K., Gan, S., *Computational Study of Soot Entrainment via Thermophoretic Deposition and Crevice Flow in a Diesel Engine.* Lecture Notes in Electrical Engineering, 2013. **190**: p. 951-963.

4. Tan, S.M., Ng, K. H., Gan, S., *CFD Modelling of Soot Entrainment Via Thermophoretic Deposition and Crevice Flow in a Diesel Engine.* Journal of Aerosol Science, 2013. **66**: p. 83-95.

5. Tan, S.M., Ng, K. H., Gan, S., *Computational Study of Crevice Soot Entrainment in a Diesel Engine.* Applied Energy, 2013. **102**: p. 898-907.

6. Ryason, P.R., Hansen, T. P, *Voluminosity of soot aggregates: a means of characterizing soot-laden oils.* SAE paper, 1991. **912343**.

7. Batko, M.A., Florkowski, D. W., Devlin, M. T., Li, S., Eggerding, D. W., Lam, W. Y., McDonnel, T. F., Jao, T., *Low temperature theological properties of aged crankcase oils.* SAE paper, 2000. **2000-01-2943**.

8. Green, D.A., Lewis, R., *The Effects of Soot-Contaminated Engine Oil on Wear and Friction: a Review.* IMechE, 2008. **222**(D): p. 1669-1689.

9. Talbot, L., Cheng, R. K., Schefer, R.W., Willis, D.R., *Thermophoresis of particles in a heated boundary layer.* J. Fluid Mech., 1980. **101**(4): p. 737-758.

10. https://www.gov.uk/government/statistical-data-sets/veh02-licensed-cars#table-veh0255. 2013.

11. Heywood, J.B., *Internal combustion engine fundamentals,* ed. McGraw.-Hill Company. 1988.

12. Clague, A.D.H., Donnet, J. B., Wang, T. K., & Peng, J. C. M., *A Comparison of Diesel Engine Soot with Carbon Black.* Carbon, 1999. **37**: p. 1553-1565.

13. Eastwood, P., *Particulate Emissions from Vehicles*, ed. Wiley 2008.

14. Piock, W., Hoffmann, G., Berndorfer, A., Salemi, P., et al., *Strategies Towards Meeting Future Particulate Matter Emission Requirements in Homogeneous Gasoline Direct Injection Engines.* SAE International. **2011-01-1212**.

15. La Rocca, A., Bonatesta, F., Fay, M. W. and Campanella, F., *Characterisation of Soot in Oil from a Gasoline Direct Injection Engine using Transmission Electron Microscopy*. tribology International, 2015. **86**: p. 77-84.

16. Tzamkiozis, T., Ntziachristos, L., Samaras, Z., *Diesel Passenger Car PM Emissions: From Euro 1 to Euro 4 with Particle Filter*. Atmospheric Environment 2010. **44**: p. 909-916.

17. http://www.smmt.co.uk/industry-topics/emissions/car-emissions-testing-in-the-uk/euro-6-what-is-it/. *Euro 6: What is it?* Accessed March 2016.

18. Fiebig, M., Wiartalla, A., Holderbaum, B., Kiesow, S., *Particulate Emissions from Diesel Engines: Correlation between Engine Technology and Emissions.* Journal of Occupational Medicine and Toxicology, 2014. **9**: p. 1-18.

19. Agarwal, D., Singh, K. S., Agarwal, K. A., *Effect of Exhaust Gas Recirculation (EGR) on performance, emissions, deposits and durability of a constant speed compression ignition engine.* Applied Energy, 2011. **88**: p. 2900-2907.

20. Ladommatos, N., Balian, R., Horrocks, R., Cooper, L., *The Effect of Exhaust Gas Recirculation on Combustion and NOx Emissions in a High-Speed Direct-Injection Diesel Engine.* SAE International, 1996. **960840**.

21. Richards, K.J., Subramaniam, M. N., Reitz, R. D., Lai, M. C., et al., *Modeling the Effects of EGR and Injection Pressure on Emissions in a High-Speed Direct-Injection Diesel Engine* SAE International, 2001. **2001-01-1004**.

22. Song, B.-H., Choi, Y.-H., *Investigation of Variations of Lubricating Oil Diluted by Post-Injected Fuel for the Regeneration of CDPF and its Effects on Engine Wear*. Journal of Mechanical Science and Technology, 2008. **22**: p. 2526-2533.

23. Sanchez, F.P., Bandivadekar, A., German, J., *Estimated Cost of Emission Reduction Technologies for Light-Duty Vehicles.* The International Council on Clean Transportation, 2012.

24. Miyahara, M., Watanabe, Y., Naitoh, Y., Hosonuma, K., et al. , *Investigation into Extending Diesel Engine Oil Drain Interval (Part 1) - Oil Drain Interval Extension by Increasing Efficiency of Filtering Soot in Lubricating Oil.* SAE International, 1991. **912339**.

25. La Rocca, A., Di Liberto G., Shayler P. J., Fay M. W. , *The nanostructure of soot-in-oil particles and agglomerates from an automotive diesel engine.* Tribology International 2013. **61**: p. 80-87.

26. Ng, H.K., *The Simulation of combustion in diesel engines using Kiva-3v on a PC platform*. 2003, Ph.D Thesis, University of Nottingham.

27. Kittelson, D.B., *Engines and Nanoparticles: a Review.* Journal of Aerosol Science, 1988. **29**: p. 575-588.

28. Fairbanks, J.W., *Diesel engines vs. spark ignition gasoline engines - which is greener?* Emissions reduction workshop, 2003.

29. Amann, C.A., Siegla, D. C., *Diesel Particulates-What They Are and Why.* Aerosol Science Technology, 1982. **1**: p. 73-101.

30. Esangbedo, C., Boehman, A. L., Perez, J. M., *Characteristics of Diesel Engine Soot that lead to Excessive Oil Thickening* Tribology International, 2011. **47**: p. 194-203.

31. Tree, D.R., Svensson, K. i>, , *Soot processes in compression ignition engines.* . Progress in Energy and Combustion Science, 2007. **33**: p. 272-309.

32. Haynes, B.S., H. G. Wagner, *Soot formation.* Prog. Energy Combust., 1981. **7**: p. 229-273.

33. Dederichs, A.S., *Flamelet Modelling of Soot Formation in Diffusion Flames*. 2004, Ph.D. Thesis, Lund Institute of Technology. p. 174 pages.

34. Graham, S.C., Homer, J. B., Rosenfeld, J. L. J., *The Formation and Coagulation of Soot Aerosols Generated by the Pyrolysis of Aromatic Hydrocarbons.* Proceeding of Royal Society of London, 1975. **A344**.

35. Xi, J., Zhong, B.-J., *Soot in diesel combustion systems.* Chem. Eng. Technol., 2006. **29**(6): p. 665-673.

36. Wersborg, B.L., Howard, J. B., Williams, G. C., *Physical mechanisms in carbon formation in flames.* Combust. Inst., 1973. **14**: p. 929-940.

37. Sabin, K., Bandin, M., Prieto, G., Sarmiento, F., *Fractal Aggregates in Tennis Ball Systems.* Physics Education, 2009. **44**(5): p. 499-502.

38. Dec, J.E., *A conceptual Model of DI Diesel Combustion Based on Laser-Sheet Imaging.* SAE Paper, 1997. **970873**.

39. Bonatesta, F., La Rocca, A., Shayler, P. J., Wahab, E., *The Influence of Swirl Ratio on Soot Quantity and Distribution in the Cylinder of a Diesel Engine.* Proceedings of the European Combustion Meeting 2007, 2007: p. 1-6.

40. Keeler, B., *Constraints on the operation of a diesel engine in partially-premixed combustion mode*. 2009, Ph.D., University of Nottingham.

41. Nabi, M.N., Zare, A., Farhad, M. H., Md, M. R., et al. , *Influence of Fuel-Borne Oxygen on European Stationary Cycle: Diesel Engine Performance and Emissions with a Special Emphasis on Particulate and NO emissions.* Energy Conversion and Management, 2016. **127**: p. 187-198.

42. Nishida, K., Gao, J. M., Zhang, Y., *Spray and Mixture Properties of Evaporating Fuel Spray Injected by Hole-Type Direct Injection Diesel Injector* International Journal of Engine Research, 2008. **9**(4).

43. Yun, H., Sellnau, M., Milovanovic, N., Zuelch, S., *Development of Premixed Low-Temperature Diesel Combustion in a HSDI Diesel Engine* SAE International, 2008. **2008-01-0639**.

44. Ng, H.K., Shayler, P. J., Willcock, M., *Investigations of Pollutant Formation and Emissions from HPCR Diesel Engines.* Proceedings of the FISITA 2006 World Automotive Congress, 2006.

45. Hsu, B.D., *Practical Diesel-Engine Combustion Analysis* SAE International Book. 2002.

46. Tsolakis, A., Megaritis, A., Wyszynski, M. L. Theinnoi, K., *Engine Performance and Emissions of a Diesel Engine Operating on Diesel-RME Blends with EGR.* Energy, 2007. **32**(11): p. 2072-2080.

47. Rajkumar, S., Sudarshan, G., *Influence of Engine Speed on Mixing and Emission Characteristic of Multiple-Injection Common Rail Direct Injection Engine.* Applied Mechanics and Materials, 2015. **787**(702-706).

48. Kittelson, D.B., Ambs, J. L., Hadjkacem, H., *Particulate Emissions from Diesel Engines: Influence of In-Cylinder Surface.* SAE International, 1990(900645): p. 1-16.

49. Suhre, B.R., Foster, D. E., *In-Cylinder Soot Deposition Rates due to Thermophoresis in a Direct Injection Diesel Engine.* SAE International, 1992(921629): p. 35-48.

50. Munro, R., *Blow-By in Relation to Piston and Ring Features.* SAE International, 1981. **810932**.

51. Tokura, N., Terasaka, K., Yasuhara, S., *Process through which Soot Intermixes into Lubricating Oil of a Diesel Engine with Exhaust Gas Recirculation.* SAE International, 1982. **820082**.

52. Lockwood, F.E., Zhang, Z. G., Choi, S. U. S., Yu, W., *Effect of Soot Loading on the Thermal Characteristics of Diesel Engine Oils.* SAE International, 2001. **2001-01-1714**.

53. Gopalakrishnan, V., Zukoski, C. F., *Viscosity of hard-sphere suspensions: can we go lower?* Industrial and Engineering Chemistry Research 2006. **45**: p. 6906-6914.

54. Green, D.A., Lewis, R., *Effect of Soot on Oil Properties and Wear of Engine Components.* Journal of Physic, 2007. **40**: p. 5488-5501.

55. Taylor, R.I., Mainwaring, R., Mortier, R. M., *Engine Lubricant Trends since 1990.* Proc. IMechE Part J: Engineering Tribology, 2005. **219**: p. 331-346.

56. Liu, C., Nemoto, S., Ogano, S., *Effect of Soot Properties in Diesel Engine Oils on Frictional Characteristics.* Tribology Transactions, 2003. **46**(1): p. 12-18.

57. Nagai, I., Endo, H., Nakamura, H., Yano, H., *Soot and valve train wear in passenger car diesel engines.* SAE paper, 1983. **831757**.

58. Rounds, F.G., *Carbon: cause of diesel engine wear?* SAE paper, 1977. **770829**.

59. Olomolehin, Y., Kapadia, R., Spikes, H. , *Antagonistic Interaction of Antiwear Additives and Carbon Black.* Tribology Letters 2009. **37**(1): p. 37-49.

60. Ratoi, M., Spikes, H. A, *The influence of soot and dispersant on ZDDP film thickness and friction.* Lubric. Sci., 2004. **17**(1): p. 25-43.

61. Corso, S.A., R., *The effect of diesel soot on reactivity of oil additives and valve train materials.* SAE International, 1984. **841369**.

62. Li, S., Csontos, A. A., Gable, B. M., Passut, C. A., Jao, T., *Wear in Cummins M-11/EGR Test Engines.* SAE paper, 2002. **2002-01-1672**.

63. Berbezier, I., Martin, J. M., Kapsa, P., *The role of carbon in lubricated mild wear.* Tribology International, 1986. **19**(3): p. 115-122.

64. Green, D.A., Leqis, R., Dwyer-Joyce, R. S., *The wear effects and mechanisms of soot contaminated automotive lubricants.* Engineering tribology, 2006. **Proc. IMechE**(J).

65. Kuo , C.C., Passut, C. A., Jao. T., Csontos, A. A., Howe, J. M., *Wear Mechanism in Cummins M-11 High-Soot Diesel Test Engines* SAE International, 1998. **981372**.

66. International, A., *Standard Test Method of Cummins M11 EGR Test*, in *D6975-04*. 2010.

67. Groff, W.P., *Evaluation and Qualification of Gasoline and Diesel Engine Lubricants, .* Southwest Research Institute, Texas, 1997.

68. Andrews, G.E., Abdelhalim, S., Williams, P. T., *The Influence of Lubricating Oil Age on Emissions from an IDI Diesel.* SAE International, 1993. **931003**: p. 1-17.

69. Walsh, D.P., *Oil Analysis 101.* Orbit, 2005. **5**: p. 25-50.

70. Bredin, A., Larcher, A. V., Mullins, B. J., *Thermogravimetric analysis of carbon black and engine soot - Towards a more robust oil analysis method.* Tribology International, 2011. **44**: p. 1642-1650.

71. Uy, D., Ford, A. M., Jayne, T> D., O'Neill E. A., et al., *Characterization of Gasoline Soot and Comparison to Diesel Soot: Morphology, Chemistry, and Wear*. Tribology International, 2014. **80**: p. 198-209.

72. Dahlen, L., *On Applied CFD and Model Development in Combustion Systems Development for DI Diesel Engines: Prediction of Soot Mediated Oil Thickening*. 2002, Ph.D. Thesis, Royal Institute of Technology, Stockholm, Sweden.

73. McGeehan, J.A., Fontana, B. J., *Effect of Soot on Piston Deposits and Crankcase Oils - Infrared Spectrometric Technique for Analyzing Soot.* SAE International, 1980. **801368**.

74. Su, D.S., Jentoft, R. E., Muller, J.-O., Rothe, D., Jacob, E., et al., *Microstructure and Oxidation Behaviour of Euro IV Diesel Engine Soot: a Comparative Study with Synthetic Model Soot Substances.* Catalysis Today, 2004. **90**: p. 127-132.

75. Kawamura, M., Ishiguro, T., Morimoto, H., *Electron Microscopic Observation of Soots in Used Diesel Engine Oils.* Lubrication Engineering, 1987. **43**: p. 269-280.

76. Dragovic, R., *Sizing and Phenotyping of Cellular Vescicles using Nanoparticle Tracking Analysis* Nanomedicine, 2011. **7**(780-788).

77. Filipe, V., Hawe, A., Jiskoot, W., *Critical Evaluation of Nanoparticle Tracking Analysis (NTA) by NanoSight for the Measurement of Nanoparticles and Protein Aggregates.* Pharmaceutical Research, 2010. **27**(5): p. 796-810.

78. Lapuerta, M., Martos, F. J., Herreros, J., M., *Effect of Engine Operating Conditions on the Size of Primary Particles Composing Diesel Soot Agglomerates* Aerosol Science, 2007: p. 455-466.

79. Mathis, U.M., M., Kaegi, R., *Influence of diesel engine combustion parameters on primary soot particle diameter.* Environ. Sci. Technol. , 2005. **39**(1887-1892).

80. Dennis, A.J., Garner, C. P., Taylor, D. H. C., *The Effect of EGR on Diesel Engine Wear.* SAE International, 1999. **1999-01-0839**.

81. http://www.dft.gov.uk/vca/fcb/new-car-fuel-consump.asp. 2013.

82. Sharma, N.O., Pahalagedara, L., Joshi, A., Suib, S. L., *Experimental Study of Carbon Black and Diesel Engine Soot Oxidation Kinetics Using Thermogravimetric Analysis.* Energy and Fuels, 2012. **26**: p. 5613-5625.

83. http://www.astm.org/Standards/D5967.htm. *Standard Test Method for Evaluation of Diesel Engine Oils in T-8 Diesel Engine*. D5967 2013.

84. http://www.cars-data.com/en. 2016.

85. Naitoh, Y., Hosonuma, K., Tamura, K., Miyahara, Watanabe, Y., *Investigation into Extending Diesel Engine Oil Drain Interval (Part 2) - Development of Long Drain Diesel Engine Oil Having Low Soot Dispersancy*. SAE International, 1991. **912340**.

86. Barlow, T.J., Latham, S., McCrae, I. S., Boulter, P.G., *A Reference Book of Driving Cycles for Use in the Measurement of Road Vehicle Emissions*, in *Published project PPR354*, T. Limited, Editor. 2009.

87. Mock, P., German. J., Bandivadekar, A., et al. , *From Laboratory to Road.* ICCT White Paper, May 2013.

88. Council, N.C., *Nottinghamshire Local Transport Plan 2011-2026*. 2011.

89. Transport, D.f., *Travel Time Measures for Local 'A' Roads, England: April 2015 to March 2016*. 2016.

90. https://www.dieselnet.com/standards/eu/fuel_reference.php. [cited March 2016.

91. Malloy, A., Carr, B., *Nanoparticle Tracking Analysis - The Halo System* Particle & Particle Systems Characterization, 2006. **23**(2): p. 197-204.

92. Dymond, J.H., *Viscosity of Selected Liquid n-Alkanes*. J. Phys. Chem. Ref. Data, 1994. **23**(1): p. 41-53.

93. http://nanobio.physics.ucsb.edu/pdfs/equipment/Nanosight%20NTA2.1%20software%20manual.pdf. *NanoSight NTA 2.1 Analytical Software*. 2010.

94. Catanese, A., *Emission Characterization and Cylinder Pressure Information for Applications in the Electronic Engine Management of Diesel Engines*, in *Engines Research Group*. 2006, Ph.D. Thesis, University of Nottingham.

95. Rogers, G.F.C., Mayhew, Y. R., *Thermodynamic and Transport Properties of Fluids*, ed.Blackwell Publishing 1995.

96. Abd-Alla, G.H., *Using Exhaust Gas Recirculation in Internal Combustion Engines: a Review.* Energy Conversion and Management, 2002. **43**: p. 1027-1042.

97. Kim, H., Sung, N., *Multidimensional Engine Modeling: NO and Soot Emissions in a Diesel Engine with Exhaust Gas Recirculation.* KSME International Journal, 2001. **15**(8): p. 1196-1204.

98. Zheng, M., Reader, G. T., Hawley, G. J., *Diesel engine exhaust gas recirculation-a review on advanced and novel concepts.* Energy Convers Manage 2004. **45**: p. 883-900.

99. Hoard, J., Abarham, M., Styles, D., Giuliano, J. M., et al., *Diesel EGR Cooler Fouling* SAE International, 2008. **2008-01-2475**.

100. Reifarth, S., *EGR-Systems for Diesel Engines*, in *Department of Machine Design*. 2010: Royal Institute of Technology.

101. Mahmood, W.M.F.W., La Rocca, A., Shayler, P. J. , *Predicted Paths of Soot Particles in the Cylinders of a Direct Injection Diesel Engine.* SAE International, 2012. **2012-01-0148**.

102. Mahmood, W.M.F.W., *Computational Studies of Soot Paths to Cylinder Wall Layers of a Direct Injection Diesel Engine*. 2011, Ph.D. Thesis, University Of Nottingham.

103. T-3, G., *Kiva-3v Source Code.* New Mexico: Los Alamos National Laboratory, 1998.

104. Amsden, A.A., *Kiva-3v: A KIVA Program with Block-Structured Mesh for Complex Geometries.* Los Alamos National Laboratory, 1993. **LA-12503-MS**.

105. Varnavas, C.A., Assanis, D. N., *The effects of Spray, Mixing and Combustion Model Parameters on KIVA-II Predictions.* Sae Paper, 1991. **911785**.

106. Amsden, A.A., Ramshaw, J.D., O'Rourke, P.J.. Dukowicz, J.K, *Kiva: A Computer Program for Two- and Three-Dimensional Fluid Flows with Chemical*

Reactions and Fuel Sprays. Los Alamos National Laboratory, 1985. **LA-10245-MS**.

107. Amsden, A.A., O'Rourke, P.J., Butler, T.D. , *KIVA-II - A Computer Program for Chemically Reactive Flow with Sprays.* Los Alamos National Laboratory, 1989. **LA-11560-MS**.

108. O'Rourke, P.J., Amsden, A. A. , *The TAB Method for Numerical Calculation of Spray Droplet Break-up.* Sae Paper, 1987. **872089**.

109. Patterson, M.A., Kong, S.-C., Hampson, G. J., Reitz, R. D., *Modeling the Effects of Fuel Injection Characteristics on Diesel Engine Soot and NOx Emissions.* SAE International, 1994. **940523**.

110. Ladommatos, N., Song, H., Zhao, H., *Measurements and predictions of diesel soot oxidation rates.* IMechE216, 2002: p. 677-689.

111. Hiroyasu, H., Nishida, K., *Simplified Three-Dimensional Modeling of Mixture Formation and Combustion in a D.I. Diesel Engine.* SAE International, 1989. **890269**.

112. Kim, H., Sung, N., *Combustion and Emission Modelling for a Direct Injection Diesel Engine.* SAE International, 2004. **2004-01-0104**.

113. Nagle, J., Strickland-Constable, R. F., *Oxidation of Carbon between 1000-2000 °C.* Proceedings of the 5th Carbon Conference, 1962. **1**: p. 154-164.

114. Roth, P.V.G., S., *High Temperature Oxidation of Soot Particles by O, OH, and NO.* Turbulence and Molecular Processes in Combustion 1993. **Elsevier, Amsterdam**

115. Wagner, R.B., Green, J. B., Storey, J. M., Daw, C. S. , *Extending Exhaust Gas Recirculation Limits in Diesel Engines.* Oak Ridge National Laboratory, June 2000: p. 1-10.

116. Abarham, M., Hoard, J., Assanis, D., Styles, D. et al., *Numerical Modeling and Experimental Investigations of EGR Cooler Fouling in a Diesel Engine.* SAE International 2009. **2009-04-20**.

117. Ewing, D., Ismail, B., Cotton, J. S., Chang, J.-S., *Characterization of the Soot Deposition Profiles in Diesel Engine Exhaust Gas Recirculation (EGR) Cooling Devices Using a Digital Neutron Radiography Imaging Technique.* SAE International, 2004. **2004-01-1433**.

118. Epstein, N., *Elements of Particle Deposition onto Nonporous Solid Surfaces Parallel to Suspension Flows.* Experimental Thermal and Fluid Science, 1997. **14**: p. 323-334.

119. Lepperhoff, G., Houben, M., *Mechanisms of Deposit Formation in IC Engines and Heat Exchangers.* SAE International, 1993. **931032**.

120. Knauer, M., Carrara, M., Rothe, D., Niessner, R., Ivleva, N. P., *Changes in Structure and Reactivity of Soot during Oxidation and Gasification by Oxygen, Studied by Micro-Raman Spectroscopy and Temperature Programmed Oxidation.* Aerosol Science and Technology, 2009. **43**: p. 1-8.

121. Woodward, *A Second-Law Analysis of Air-Standard Diesel-Turbocharger-Bottoming Cycles.* Proc. IMechE 1993. **207**: p. 107-114.

122. Lyford-Pike, E.J., Heywood, J. B., *Thermal boundary layer thickness in the cylinder of a spark-ignition engine.* International Journal of Heat and Mass Transfer, 1984. **27**(10): p. 1873-1878.

123. Tree, D.R., Dec, J. E., *Extinction Measurements of In-Cylinder Soot Deposition in a Heavy-Duty DI Diesel Engine.* SAE International, 2001. **2001-01-1296**.

124. Wells, A.C., Chamberlain, A.C., *Transport of small particles to vertical surfaces.* British Journal of Applied Physics, 1967. **18**: p. 1793-1799.

125. Friedlander, S.K., Johnstone, H. F., *Deposition of suspended particles from turbulent gas streams.* Industrial and engineering chemistry, 1957. **49**(7): p. 1150-1156.

126. Tyndall, J., *Scientific Addresses* New Haven, Conn., C. C. Chatfield & Co., 1870. **5**.

127. Waldmann, L.Z., Schmitt, K. H., *In: C. N. Davies (Ed.).* Aerosol Science, 1966.

128. Epstein, P.S., *On the Resistance Experienced By Spheres in Their Motion Through Gases.* Physical Review, 1924. **23**(2): p. 710-733.

129. Incropera, F.P., , DeWitt, D. P., *Introduction to Heat Transfer*. 2006: Wiley, 5th Ed.

130. Brock, J.R., *On the Theory of Thermal Forces Acting on Aerosol Particles* Journal of Colloid Science, 1962. **17**(8): p. 768-780.

131. Rosner, D.E., Khalil, F. Y., *Particle Morphology - and Knudsen Transition-Effects on Thermophoretically Dominated Total Mass Deposition Rates from "Coagulation-Aged Aerosol Population.* Journal of Aerosol Science, 2000. **31**(3).

132. Mansouri, S.H., Heywood, J. B., Radhakrishnan, K., *Divided-Chamber Diesel Engine, Part I: a Cycle Simulation Which Predict Performance and Emissions.* SAE International, 1982. **820273**.

133. Borgnakke, C., Arpaci, V. S., Tabaczynski, R. J., *A Model for the Instantaneous Heat Transfer and Turbulence in a Spark Ignition Engine.* SAE International, 1980. **800287**.

134. Annand, W.J.D., *Heat Transfer in the Cylinder of Reciprocating Internal Combustion Engines.* Proc. IMechE, 1963. **177**.

135. Woschni, G., *A Universally Applicable Equation for the Instantaneous Heat Transfer Coefficient in the Internal Combustion Engine.* SAE International, 1964. **670931**.

136. Perry, R.H., Green, D. W., *Perry's Chemical Engineers' Handbook*, ed. M.G.H. Professional. 2008.

137. Gamble, R.J., Priest, M., Taylor, C. M., *Detailed analysis of oil transport in the piston assembly of a gasoline engine.* Tribology Letters, 2003. **14**(2): p. 147-156.

138. Ma, Z., *Oil Transport Analysis of a Cylinder Deactivation.* SAE International, 2010. **2010-01-1098**.

139. Yasutomi, S., Maeda, Y., Maeda, T., *Kinetic approach to engine oil. 1. Analysis of lubricant transport and degradation in engine system.* . Industrial & Engineering Chemistry Product Research and Development, 1981. **20**(3): p. 530-536.

140. Stark, M.S., Gamble, R. J., Hammond, C. J., Gillespie, H. M., Lindsay Smith, J. R., Nagatomi, E., Priest, M., Taylor, C. M., R. I., Taylor, Waddington, D. J., *Measurement of Lubricant Flow in a Gasoline Engine.* Tribology Letters, 2005. **19**(3): p. 163-168.

141. Saville, S.B., Gainey, F. D., *A study of lubricant condition in the piston ring zone of single-cylinder diesel engines under typical operating conditions.* SAE International, 1989. **881589**.

142. Yilmaz, E., Tian, T., Wong, V. W., Heywood, J. B., *The contribution of different oil consumption sources to total oil consumption in a spark ignition engine.* SAE International, 2004. **2004-01-2909**.

143. Usui, M., Murayama, K., Oogake, K., Yoshida, H., *Study of oil flow surrounding piston rings and visualization observation.* SAE International, 2008. **2008-01-0795**.

144. Thirouard, B., Tian T., *Oil transport in the piston ring pack (Part I): identification and characterization of the main oil transport routes and mechanisms.* SAE International, 2003(200030345).

145. Ebner, W., H., Jaschek, A., O., *The importance of Blow-by measurements, measuring equipment and implementation.* SAE International, 1998.

146. Rao, V.K., Gardiner, D. P., Bardon, M. F., *Effects of gas leakage and crevices on cold starting of engines.* SAE Technical Paper, 1994(940078): p. 15-20.

147. Ruddy, B.L., Dowson, D., Economou, P. N., *The Prediction of Gas Pressures within the Ring Packs of Large Bore Diesel Engines.* Journal of Mechanical Engineering Science, 1981. **23**(6): p. 295-304.

148. Namazian, M., *Studies of combustion and crevice gas motion in a flow-visualization spark-ignition engine*. 1981, Ph.D. Thesis, Massachusetts Institute of Technology.

149. Ra, Y., Reitx, R. D., *Effects of piston crevice flows and lubricant oil vaporization on diesel engine deposits.* SAE International. **2006-01-1149**.

150. Pugh, G.J., *The analysis of heat release in the investigation of split-main fuel injection in a diesel engine*. 2004, Ph.D. Thesis, University of Nottingham.

151. Reifarth, S., Angtrom, H.-E., *Transient EGR in a High-Speed DI Diesel Engine for a set of different EGR-routings.* SAE International, 2010. **2010-01-1271**.